



Invited review

# Multi-scale numerical simulation of fluidized beds: Model applicability assessment



Shuai Wang<sup>a</sup>, Chenshu Hu<sup>a</sup>, Kun Luo<sup>a,b,\*</sup>, Jiahui Yu<sup>a</sup>, Jianren Fan<sup>a,b</sup>

<sup>a</sup> State Key Laboratory of Clean Energy Utilization, Zhejiang University, Hangzhou, 310027, China

<sup>b</sup> Shanghai Institute for Advanced Study of Zhejiang University, Shanghai, 200120, China

## ARTICLE INFO

### Article history:

Received 12 September 2022

Received in revised form

22 November 2022

Accepted 23 November 2022

Available online 2 December 2022

### Keywords:

Fluidized bed

Dense gas-solid flows

Multi-scale numerical methods

Drag model

Inter-particle collisions

## ABSTRACT

In the past few decades, multi-scale numerical methods have been developed to model dense gas-solid flow in fluidized beds with different resolutions, accuracies, and efficiencies. However, ambiguity needs to be clarified in the multi-scale numerical simulation of fluidized beds: (i) the selection of the sub-models, parameters, and numerical resolution; (ii) the multivariate coupling of operating conditions, bed configurations, polydispersity, and additional forces. Accordingly, a state-of-the-art review is performed to assess the applicability of multi-scale numerical methods in predicting dense gas-solid flow in fluidized beds at specific fluidization regimes (e.g., bubbling fluidization region, fast fluidization regime), with a focus on the inter-particle collision models, inter-phase interaction models, collision parameters, and polydispersity effect. A mutual restriction exists between resolution and efficiency. Higher-resolution methods need more computational resources and thus are suitable for smaller-scale simulations to provide a database for closure development. Lower-resolution methods require fewer computational resources and thus underpin large-scale simulations to explore macro-scale phenomena. Model validations need to be further conducted under multiple flow conditions and comprehensive metrics (e.g., velocity profiles at different heights, bubbles, or cluster characteristics) for further improvement of the applicability of each numerical method.

© 2022 Chinese Society of Particuology and Institute of Process Engineering, Chinese Academy of Sciences. Published by Elsevier B.V. This is an open access article under the CC BY-NC-ND license (<http://creativecommons.org/licenses/by-nc-nd/4.0/>).

## 1. Introduction

A fluidized bed is a complex dense gas-solid system in which frequent particle collisions and intense gas-solid mixing interconnect at the particle scale. Besides, mesoscale structures (e.g., bubbles and clusters evolution) significantly influence macroscale bed hydrodynamics (e.g., pressure drop). The crucial operating parameters include superficial gas velocity, operating pressure, bed temperature, solid properties, and geometric configuration. Changing operating parameters leads to the transition of fluidization regimes. Two dimensionless numbers, i.e., Reynolds number ( $Re_p$ ) and Archimedes number ( $Ar$ ) are commonly used to characterize fluidization regimes (Fig. 1), which include bubbling fluidization, fast fluidization, pneumatic transport, and spouting regimes (Bi & Grace, 1995; Kunii & Levenspiel, 2013). In the past

few decades, many experimental efforts have been made to study such dense gas-solid systems. However, the experimental measurements have intrinsic limitations due to harsh operating conditions and high costs.

Numerical simulation provides a cost-effective alternative to investigate multi-phase flow and multi-physics processes in fluidized beds. As shown in Fig. 2, numerical simulation has been increasingly applied to study dense gas-solid flow in fluidized beds. It is noted that the percentage of the simulation work has rapidly risen to more than 30% in the total studies of fluidized beds in recent years.

Multi-scale numerical methods exist for modelling dense gas-solid flow in fluidized beds at different efficiencies and resolutions. As shown in Fig. 3, these methods can be identified by the treatment of gas and solid phases, and the interaction between them. Based on Navier-Stokes equations and Lattice Boltzmann equations, the gas phase can be described by direct numerical simulation (DNS) and local averaging methods in which the gas turbulence is described by large-eddy simulation (LES) or Reynolds-averaging Navier-Stokes (RANS). Based on the Eulerian

\* Corresponding author. State Key Laboratory of Clean Energy Utilization, Zhejiang University, Hangzhou, 310027, China.

E-mail address: [zjulk@zju.edu.cn](mailto:zjulk@zju.edu.cn) (K. Luo).

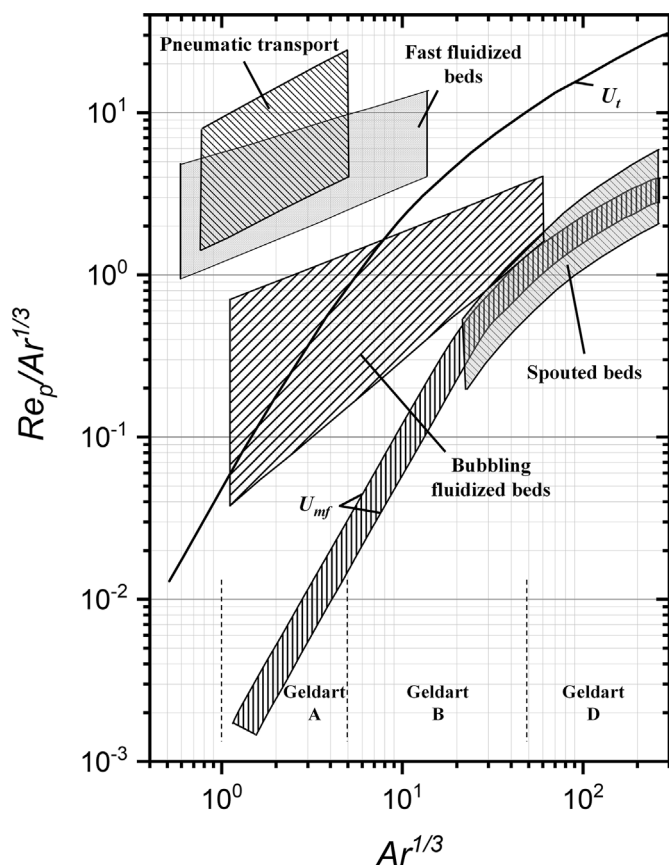


Fig. 1. Schematic diagram of fluidization regimes. Reproduced from Kunii and Levenspiel (2013).

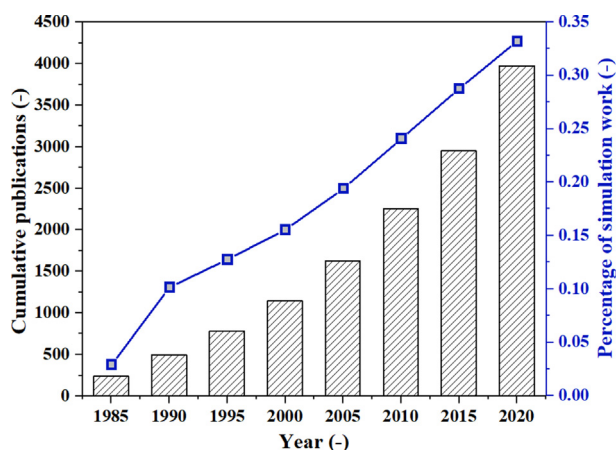


Fig. 2. The trend of the number of publications relevant to the simulation of dense gas-solid flow in fluidized beds (Source = Scopus; Keyword = “dense gas-solid flow” or “particulate flow” and “fluidized bed” and “particles”) and the percentage of simulation work (Keyword = simulation or modelling).

and Lagrangian frameworks, the solid phase is respectively assumed as a continuum and dispersed particles. Compared with continuum methods such as the two-fluid model (TFM), the discrete element method (DEM) has the intrinsic capability of describing the kinematics of each particle. The coarse-grained method (CGM) minimises computational costs by lumping several real particles with identical properties into a numerical parcel. Gas-solid interactions related to mass, momentum, and

energy exchanges are commonly described by particle-resolved methods or empirical models. The former method directly obtains interactions via calculating detailed information in the gas-solid interface while the latter needs several closure models on drag force, heat and mass transfer, and chemical reactions.

Although multi-scale numerical methods have been increasingly applied to simulate fluidized beds, challenges still exist for model selection. On the one hand, a proper choice of model parameters plays a vital role in successfully simulating fluidized beds. On the other hand, a fluidized bed involves the multivariate coupling of operating conditions, bed configurations, polydispersity, additional forces, etc. It lacks a review to elucidate which model and the related parameters are applicable for modelling fluidized beds at a specific fluidization condition. To fulfil the knowledge gap, this article delivers a state-of-the-art review of the applicability assessment of multi-scale numerical methods in modelling fluidized beds under different fluidization conditions. The current review is structured as follows: section 2 gives mathematical models. Specifically, the governing equations of the fluid and solid phases are given in sections 2.1 and 2.2, respectively. Sub-models for the inter-phase momentum exchanges, inter-particle collisions, and multi-physics processes are given in sections 2.3, 2.4, and 2.5, respectively. After then, section 3 presents a comprehensive applicability assessment of multi-scale numerical methods in modelling fluidized beds at specific fluidization conditions. The conclusion is drawn in the final section.

## 2. Computational framework

The existing numerical methods for modelling dense gas-solid flow can be categorized into different groups based on the grid resolution. Different resolution leads to distinct accuracy. The similarity of the words “resolution” and “accuracy” is that they both reflect the model’s capability in simulating gas-solid flow. However, the resolution refers to the calculation procedure of the gas-solid flow, e.g., different grid resolutions (i.e., fine grids, coarse grids, medium grids). The accuracy refers to the calculation results by different resolutions, i.e., a higher resolution gives rise to higher accuracy, and vice versa. Besides, higher-resolution methods need more computational resources and thus are suitable for smaller-scale simulations to provide a database for closure development. Lower-resolution methods require fewer computational resources and thus underpin large-scale simulations to explore macro-scale phenomena. A specified method can be employed considering the balance between the resolution and efficiency.

As shown in Fig. 4, the multi-scale numerical methods have been generally classified into three groups, particle-resolved direct numerical simulation (PR-DNS), computational fluid dynamics-discrete element method (CFD-DEM), two-fluid method (TFM), as widely accepted in the previous literature (Baltussen et al., 2018; Sundaresan et al., 2018; Tenneti & Subramaniam, 2014). For the micro-scale simulation corresponding to the PR-DNS approach, the flow dynamics around each particle are fully resolved, where the no-slip constraint is satisfied. Hence the drag force, heat transfer, mass transfer, and chemical reactions can be accurately described. The non-uniform distribution of solid properties, such as density, temperature, and species inside or on the surface can be captured. For the macro-scale simulation corresponding to the TFM approach, the gas and solid phases are assumed to be interpenetrating media. Inter-particle collisions are simplified by a kinetic theory of granular flow (KTGF) while inter-phase interactions are described by empirical correlations. This approach can only obtain cell-averaged information for both gas and solid phases. In contrast, for the simulation between the micro-scale and macro-scale scenarios, i.e., CFD-DEM, the trajectory of each particle is

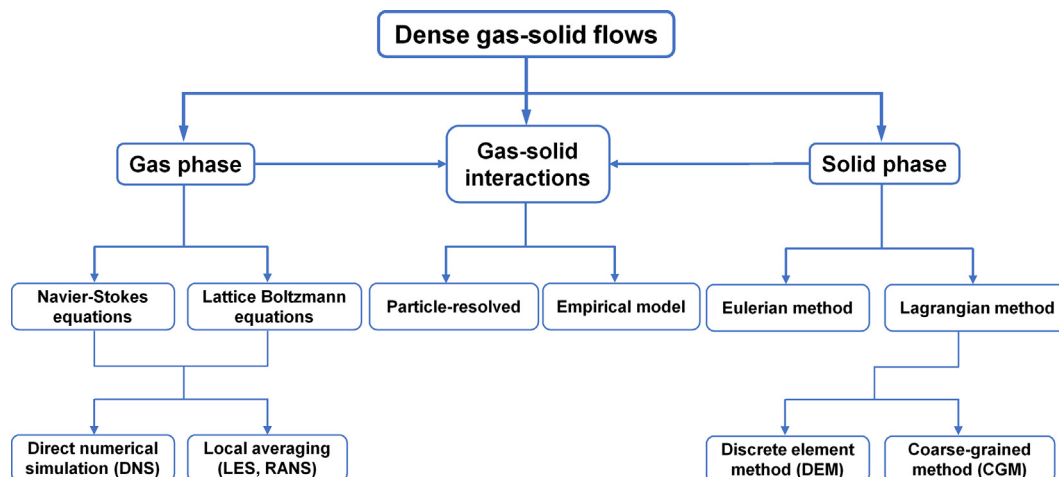


Fig. 3. Numerical methods for modelling dense gas-solid flow.

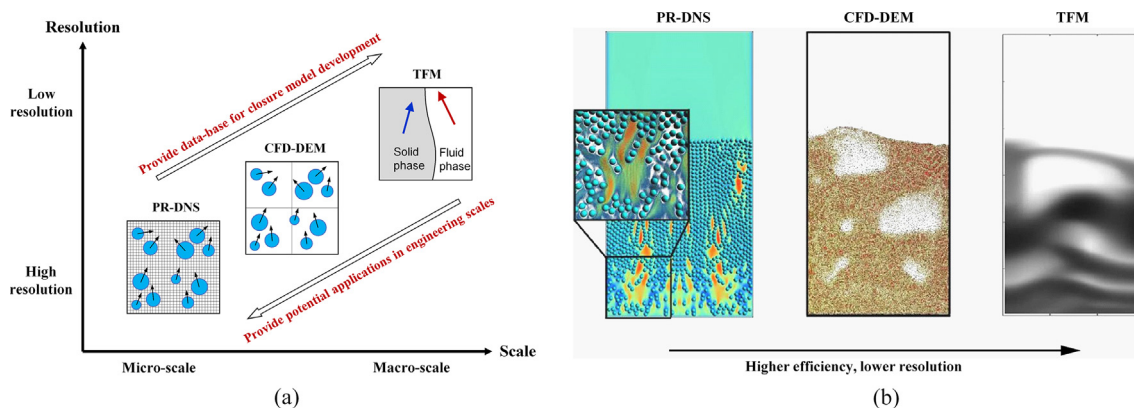


Fig. 4. Illustration of multi-scale numerical methods for modelling dense gas-solid flow, including particle-resolved direct numerical (PR-DNS), computational fluid dynamics-discrete element method (CFD-DEM), and two-fluid model (TFM): (a) multi-scale numerical methods; (b) multi-scale numerical simulations (reproduced from Baltussen et al. (2018)).

tracked, and inter-particle collisions are solved. This approach can obtain cell-averaged information for the gas phase but particle-based information for the solid phase. When a coarse-grained treatment is introduced to the CFD-DEM, the coarse-grained CFD-DEM (CG-DEM) is obtained, in which several real particles with the same properties are lumped into a parcel to reduce particle number and the resultant computational costs. When a solid stress model is introduced to the CG-DEM, the multi-phase particle-in-cell (MP-PIC) or dense discrete phase method (DDPM) is gained, in which the inter-particle collisions are further simplified and modelled.

More attention should be paid to the so-called “CFD-DEM” frequently encountered in the literature. As shown in Fig. 5, CFD-DEM can also be divided into resolved CFD-DEM, semi-resolved

CFD-DEM, and unresolved CFD-DEM (Hager, 2014; Wang et al., 2019), dependent on the grid size-to-particle diameter ratio ( $\Delta/d_p$ ). The resolved CFD-DEM targets modelling gas-solid flow with  $\Delta/d_p < 1/10$ , which means the flow dynamics around each particle are fully resolved. The resolved CFD-DEM is also termed PR-DNS when simulating gas-solid fluidized beds. The unresolved CFD-DEM aims to model gas-solid flow with  $\Delta/d_p > 3$ , which means the inter-phase interactions are solved by empirical correlations. The unresolved CFD-DEM is commonly termed CFD-DEM when simulating gas-solid fluidized beds. Recently, Wang et al. (2019) developed a semi-resolved CFD-DEM, which bridges the simulation gap between the resolved CFD-DEM and unresolved CFD-DEM. The main idea is to correct the relative velocity between the particle and fluid

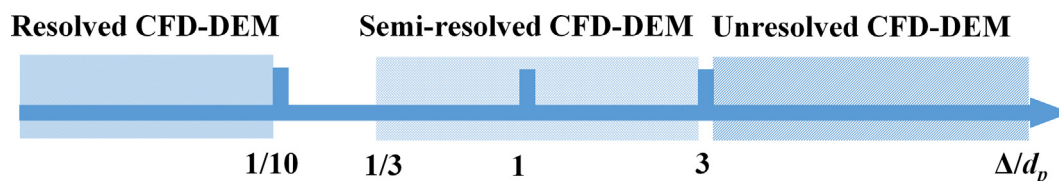


Fig. 5. Applicable regions of the grid size-to-particle diameter ratio ( $\Delta/d_p$ ) for resolved CFD-DEM, semi-resolved CFD-DEM, and unresolved CFD-DEM. Reproduced from Wang et al. (2019).

phase by kernel approximation to obtain a more accurate drag force. This method has been extended to heat transfer and various chemical engineering processes (Wang & Liu, 2020; Zhu et al., 2022). Similarly, the semi-resolved CFD-DEM was also realized by a smoothing operation by solving a diffusion equation for each transferred quantity (e.g., the inter-phase coupling force) (Capecelatro & Desjardins, 2013a; Radl et al., 2015; Sun & Xiao, 2015). As the development of the semi-resolved CFD-DEM is still underway and needs more verifications and validations for fluidized bed applications, a detailed discussion of this method is not included in the present review. For brevity, the resolved CFD-DEM corresponds to the “PR-DNS” while the unresolved CFD-DEM corresponds to the “CFD-DEM” in this review.

## 2.1. Equations of fluid phase

### 2.1.1. Navier-Stokes equations

Two categories of equations are commonly used to solve the fluid phase, i.e., Navier-Stokes equations and Lattice Boltzmann equations. In the Navier-Stokes equations, the conservation of mass, momentum, energy, and species for the fluid phase is given by:

$$\frac{\partial(\epsilon_f \rho_f)}{\partial t} + \nabla \cdot (\epsilon_f \rho_f \mathbf{u}_f) = R_f \quad (1)$$

$$\frac{\partial(\epsilon_f \rho_f \mathbf{u}_f)}{\partial t} + \nabla \cdot (\epsilon_f \rho_f \mathbf{u}_f \mathbf{u}_f) = -\epsilon_f \nabla p_f - \mathbf{F}_{fp} + \rho_f \epsilon_f \mathbf{g} + \nabla \cdot (\epsilon_f \boldsymbol{\tau}_f) + \mathbf{I}_{pf} \quad (2)$$

$$\frac{\partial(\rho_f \epsilon_f C_{p,f} T_f)}{\partial t} + \nabla \cdot (\rho_f \epsilon_f \mathbf{u}_f C_{p,f} T_f) = \nabla \cdot (\epsilon_f k_f \nabla T_f) - Q_{fp} + \Delta H_{rf} \quad (3)$$

$$\frac{\partial(\rho_f \epsilon_f Y_{fk})}{\partial t} + \nabla \cdot (\rho_f \epsilon_f \mathbf{u}_f Y_{fk}) = \nabla \cdot (\rho_f \epsilon_f D_{fk} \nabla Y_{fk}) + R_{fk} \quad (4)$$

where  $\epsilon_f$  is the fluid volume fraction.  $R_f$ ,  $\Delta H_{rf}$ ,  $I_{pf}$ , and  $R_{fk}$  are the source terms of mass, momentum, energy, and species, respectively.  $\mathbf{F}_{fp}$  and  $Q_{fp}$  are the interphase momentum and energy exchanges, respectively.  $\boldsymbol{\tau}_f$  is the fluid shear stress.  $D_{fk}$  is the diffusion coefficient of  $k$ th fluid species.  $\epsilon_f$  equals one except at the particle boundary in the PR-DNS while it is calculated based on the local solid concentration in the other methods.

### 2.1.2. Lattice Boltzmann equations

Lattice Boltzmann method (LBM) has drawn increasing attention due to its parallel efficiency and implementation simplicity. The widely used lattice Boltzmann Bhatnagar-Gross-Krook (LBGK) model is given by:

$$f_i(\mathbf{x} + \mathbf{e}_i dt, t + dt) - f_i(\mathbf{x}, t) = -\frac{1}{\tau} (1 - \beta(\epsilon_s, \tau)) (f_i(\mathbf{x}, t) - f_i^{eq}(\rho, \mathbf{u})) + \beta(\epsilon_s, \tau) \Omega_i^s \quad (5)$$

$$f_i^{eq}(\rho, \mathbf{u}) = \omega_i \rho \left( 1 + \frac{\mathbf{e}_i \cdot \mathbf{u}}{C_s^2} + \frac{(\mathbf{e}_i \cdot \mathbf{u})^2}{2C_s^4} - \frac{\mathbf{u}^2}{2C_s^2} \right) \quad (6)$$

$$\beta(\epsilon_s, \tau) = \frac{\epsilon_s(\tau - 0.5)}{1 - \epsilon_s + (\tau - 0.5)} \quad (7)$$

$$\Omega_i^s = f_{-i}(\mathbf{x}, t) - f_i(\mathbf{x}, t) + f_i^{eq}(\rho, \mathbf{U}_s) - f_i^{eq}(\rho, \mathbf{u}) \quad (8)$$

where  $f_i^{eq}(\mathbf{x}, t)$  is the equilibrium distribution function.  $\beta(\epsilon_s, \tau)$  is the weighting function.  $\Omega_i^s$  is the additional collision term for solid obstacles.

## 2.2. Equations of solid phase

### 2.2.1. Lagrangian description

In the CFD-DEM, particle dynamics is governed by Newton's law of motion. The changes in mass, velocity, temperature, and species are individually tracked as follows:

$$\frac{dm_i}{dt} = R_i \quad (9)$$

$$m_i \frac{d\mathbf{v}_i}{dt} = m_i \mathbf{g} + \mathbf{f}_{d,i} + \mathbf{f}_{p,i} + \mathbf{f}_{c,i} + \mathbf{f}_{add,i} \quad (10)$$

$$I_i \frac{d\boldsymbol{\omega}_i}{dt} = \mathbf{M}_t + \mathbf{M}_r \quad (11)$$

$$m_i C_{p,i} \frac{dT_{p,i}}{dt} = q_{fp,i} + q_{pp,i} + q_{r,i} + \Delta H \quad (12)$$

$$\frac{dm_i Y_{i,k}}{dt} = R_{i,k} \quad (13)$$

where  $R_i$  is the mass source term due to chemical reactions.  $\mathbf{f}_{d,i}$ ,  $\mathbf{f}_{p,i}$ , and  $\mathbf{f}_{c,i}$  are drag force, pressure gradient force, and collision force, respectively.  $\mathbf{f}_{add,i}$  is the additional force, including the cohesive force, lift force, electrostatic force, etc.  $I_i$  is the moment of inertia.  $\mathbf{M}_t$  is the torque from the tangential collision and  $\mathbf{M}_r$  is the torque from the rolling friction.  $q_{fp,i}$ ,  $q_{pp,i}$ ,  $q_{r,i}$  and  $\Delta H$  are the heat transfer due to convection, conduction, radiation, and chemical reactions, respectively.  $R_{i,k}$  is the species source term due to chemical reactions. The CG-DEM uses the coarse-grained particle (i.e., parcel) to represent a certain number of real particles. The underlying assumption is that particles in a parcel with the same properties (e.g., density, velocity, temperature, and species). This leads to a remarkable decrease in particle number and computational costs. Generally, the parcel follows similar rules as the particle-based method as listed in Eqs. 9–13.

### 2.2.2. Eulerian description

In the Eulerian framework, the solid phase is solved similarly to the fluid phase. The conservation equations of the solid phase can be given as:

$$\frac{\partial(\epsilon_{sm} \rho_{sm})}{\partial t} + \nabla \cdot (\epsilon_{sm} \rho_{sm} \mathbf{u}_{sm}) = R_{sm} \quad (14)$$

$$\frac{\partial(\epsilon_{sm} \rho_{sm} \mathbf{u}_{sm})}{\partial t} + \nabla \cdot (\epsilon_{sm} \rho_{sm} \mathbf{u}_{sm} \mathbf{u}_{sm}) = -\epsilon_{sm} \nabla p_f + \nabla \cdot \boldsymbol{\tau}_s + \sum_{l=1, l \neq m}^M \beta_{slm} (\mathbf{u}_{sl} - \mathbf{u}_{sm}) + \rho_{sm} \epsilon_{sm} \mathbf{g} + \beta_{fsm} (\mathbf{u}_g - \mathbf{u}_{sm}) \quad (15)$$

$$\frac{\partial(\rho_{sm}\varepsilon_{sm}C_{psm}T_{sm})}{\partial t} + \nabla \cdot (\rho_{sm}\varepsilon_{sm}\mathbf{u}_{sm}C_{psm}T_{sm}) = \nabla \cdot [\varepsilon_{sm}k_{sm}\nabla T_{sm}] + Q_{fp} + \Delta H_{rsm} \quad (16)$$

$$\frac{\partial(\rho_{sm}\varepsilon_{sm}Y_{smk})}{\partial t} + \nabla \cdot (\rho_{sm}\varepsilon_{sm}\mathbf{u}_{smk}Y_{smk}) = \nabla \cdot (\rho_f\varepsilon_f D_{smk}\nabla Y_{fk}) + R_{smk} \quad (17)$$

where  $\beta_{slm}$  is the momentum exchange coefficient between  $l^{\text{th}}$  and  $m^{\text{th}}$  solid phase.  $\beta_{fsm}$  is the interphase momentum exchange coefficient for the solid phase  $m$ .

### 2.3. Inter-phase interaction model

#### 2.3.1. Particle-resolved method

Several numerical strategies have been proposed to accurately resolve gas-solid interactions. In general, the PR-DNS requires a computational grid much smaller than the particle diameter. It is impractical to use a body-fitted mesh to cope with the moving boundary of particles. Methods based on a fixed Cartesian mesh are more computationally efficient but require additional techniques to solve the fluid-solid boundary. In previous studies, the immersed boundary method (IBM) (Uhlmann, 2005) has been frequently adopted in the PR-DNS. Several branches, such as direct-forcing and ghost-cell immersed boundary methods (Tseng & Ferziger, 2003; Uhlmann, 2005), have been proposed and applied in many studies of particle-laden flow (Luo et al., 2016, 2017; Luo, Wang, et al., 2017; Uhlmann & Chouippe, 2017). The direct-forcing immersed boundary method is implemented as follows:

$$\mathbf{f}(\mathbf{x}) = \int_{\Omega} \mathbf{F}_k(\mathbf{x}_k) \cdot \delta(\mathbf{x} - \mathbf{x}_k) d\mathbf{x}_k \quad (18)$$

where  $\Omega$  denotes the computation domain,  $\mathbf{x}$  is the position of the Eulerian mesh,  $\mathbf{x}_k$  is the position of the Lagrangian point constituting the immersed boundary.  $\delta(\mathbf{x} - \mathbf{x}_k)$  is the Dirac delta function.  $\mathbf{F}_k(\mathbf{x}_k)$  is the force exerted on the Lagrangian point  $\mathbf{x}_k$ . To ensure that the no-slip boundary condition is satisfied at the particle surface, a force  $\mathbf{F}_k(\mathbf{x}_k)$  is imposed on the Lagrangian point. Based on the momentum equation, one can get:

$$\mathbf{f} = \frac{\partial \mathbf{u}}{\partial t} + \mathbf{u} \cdot \nabla \mathbf{u} + \nabla p - \frac{1}{Re} \nabla^2 \mathbf{u} = \frac{\mathbf{u}^{n+1} - \mathbf{u}^n}{\Delta t} - \mathbf{rhs} \quad (19)$$

where  $\mathbf{rhs} = -(\mathbf{u} \cdot \nabla \mathbf{u} + \nabla p - \frac{1}{Re} \nabla^2 \mathbf{u})$ . For the Lagrangian point  $\mathbf{x}_k$  at the immersed boundary, the force is:

$$\mathbf{F}_k(\mathbf{x}_k) = \frac{\mathbf{u}_k^{n+1} - \mathbf{u}_k^n}{\Delta t} - \mathbf{rhs}_k = \frac{\mathbf{u}_k^{n+1} - \hat{\mathbf{u}}_k}{\Delta t} + \frac{\hat{\mathbf{u}}_k - \mathbf{u}_k^n}{\Delta t} - \mathbf{rhs}_k \quad (20)$$

where  $\hat{\mathbf{u}}_k$  is the intermediate velocity which satisfies the momentum equation without external force:

$$\frac{\hat{\mathbf{u}}_k - \mathbf{u}_k^n}{\Delta t} - \mathbf{rhs}_k = 0 \quad (21)$$

Then the force exerted on the Lagrangian point at the immersed boundary is given by:

$$\mathbf{F}_k(\mathbf{x}_k) = \frac{\mathbf{u}_k^{n+1} - \hat{\mathbf{u}}_k}{\Delta t} = \frac{\mathbf{u}_L - \hat{\mathbf{u}}_k}{\Delta t} \quad (22)$$

where  $\mathbf{u}_L$  is the desired velocity on position  $\mathbf{x}_k$  at the next time step, noted as:

$$\mathbf{u}_L = \mathbf{u}_p + \boldsymbol{\omega}_p \times (\mathbf{x}_k - \mathbf{x}_c) \quad (23)$$

However, the desired velocity at  $(n+1)$  time level  $\mathbf{u}_L^{n+1}$  is unknown. A first-order explicit scheme using  $\mathbf{u}_L^n$  is applied. To improve accuracy, a multi-direct forcing strategy can be used (Wang et al., 2008). The total hydrodynamic force  $\mathbf{F}_{fp}$  and torque  $T_{fp}$  acting on the particle can be integrated as:

$$\mathbf{F}_{fp} = - \int_1^N \mathbf{F}_k(\mathbf{x}_k) d\mathbf{x}_k \quad (24)$$

$$\mathbf{T}_{fp} = - \int_1^N (\mathbf{x}_k - \mathbf{x}_c) \mathbf{F}_k(\mathbf{x}_k) d\mathbf{x}_k \quad (25)$$

#### 2.3.2. Empirical models

Empirical correlations need to be employed to calculate the interphase momentum exchange for unresolved methods (i.e., CFD-DEM, TFM and CGM). When modelling gas-solid fluidized beds, the drag force  $\mathbf{f}_{d,i}$  and pressure gradient force  $\mathbf{f}_{p,i}$  are commonly considered (Zhu et al., 2007). For the TFM, the calculation of interphase momentum exchange is embodied in Eq. (15). In the CFD-DEM, these forces are given by:

$$\mathbf{f}_{d,i} = \frac{V_{p,i}\beta}{\varepsilon_s} (\mathbf{u}_{f,i} - \mathbf{v}_{p,i}) \quad (26)$$

$$\mathbf{f}_{p,i} = -V_{p,i}\nabla p_f \quad (27)$$

where  $V_{p,i}$  is the particle volume and  $\beta$  is the interphase momentum exchange coefficient. The drag force highly affects the prediction accuracy. Various drag correlations have been available in the open literature, derived from experiments (Ergun, 1952; Syamlal & O'Brien, 1988; Wen, 1966) or DNS simulations (Beetstra et al., 2007a; Hill et al., 2001; Tenneti et al., 2011). The applicability of different drag models will be assessed in the following sections.

In the CGM, the particle volume  $V_p$  should be replaced by the parcel volume  $V_{cgp,i}$ :

$$V_{cgp,i} = W_p V_{p,i} \quad (28)$$

where  $W_p$  is the coarse-grain ratio, representing the number of particles in a parcel.

### 2.4. Inter-particle collision model

#### 2.4.1. Discrete element method

Under the Lagrangian framework, different models have been proposed to describe inter-particle collisions, such as the discrete element method (DEM) and direct simulation Monte Carlo (DSMC). Among these models, the DEM is the most used one. Specifically, two contact models based on the DEM framework have been developed, i.e., the hard-sphere contact model (Campbell & Brennen, 1985) and the soft-sphere contact model (Cundall & Strack, 1979). The former features an event-driven scheme, which

resolves the event of binary inter-particle collisions at a specific time instant. As a result, the hard-sphere contact model fails to predict particulate flow with high solid concentration. In contrast, the soft-sphere contact model with a time-driven scheme can handle multiple inter-particle collisions as time proceeds, which is more suitable to model dense gas-solid flow. The soft-sphere contact model is given by:

$$\mathbf{f}_{c,ij} = \mathbf{f}_{cn,ij} + \mathbf{f}_{ct,ij} \quad (29)$$

$$\mathbf{f}_{cn,ij} = -k_{n,ij}\delta_{n,ij}\mathbf{n}_{ij} - \eta_{n,ij}(\mathbf{v}_{r,ij} \cdot \mathbf{n}_{ij})\mathbf{n}_{ij} \quad (30)$$

$$\mathbf{f}_{ct,ij} = \min\left\{ \left| -k_{t,ij}\delta_{t,ij}\mathbf{t}_{ij} - \eta_{t,ij}[(\mathbf{v}_{r,ij} \cdot \mathbf{t}_{ij})\mathbf{t}_{ij} + (\boldsymbol{\omega}_i \times \mathbf{r}_i - \boldsymbol{\omega}_j \times \mathbf{r}_j)] \right|, \mu\mathbf{f}_{cn,ij} \right\} \quad (31)$$

where subscripts  $n$  and  $t$  represent the normal and tangential directions, respectively.  $\mathbf{n}_{ij}$  and  $\mathbf{t}_{ij}$  are the unit vectors.  $k_{n,ij}$  and  $k_{t,ij}$  are the stiffness coefficients,  $\delta_{n,ij}$  and  $\delta_{t,ij}$  are overlap displacements,  $\eta_{n,ij}$  and  $\eta_{t,ij}$  are the damping coefficients.  $\mathbf{v}_{r,ij}$  is the relative velocity and  $\mu$  is the friction coefficient. Moreover, the damping coefficient is related to the restitution coefficient. For instance, in the linear spring-dashpot (LSD) model, the damping coefficients are defined as:

$$\eta_{n,ij} = \frac{2\sqrt{m_{eff}k_{n,ij}}|\ln e_{n,ij}|}{\sqrt{\pi^2 + \ln^2 e_{n,ij}}} \quad (32)$$

$$\eta_{t,ij} = \frac{2\sqrt{m_{eff}k_{t,ij}}|\ln e_{t,ij}|}{\sqrt{\pi^2 + \ln^2 e_{t,ij}}} \quad (33)$$

where  $e_{n,ij}$  and  $e_{t,ij}$  are restitution coefficients.  $m_{eff} (= \frac{m_i m_j}{m_i + m_j})$  is the effective mass of particle  $i$  and particle  $j$ , wherein  $m_i$  and  $m_j$  are the mass of particle  $i$  and particle  $j$ , respectively.

Many rolling friction models have been proposed under distinct collision conditions. These models may be classified into four categories: (a) directional constant torque models; (b) viscous models; (c) elastic-plastic spring-dashpot models; and (d) contact-independent models (Ai et al., 2011). These rolling friction models and their formula are summarized in Table 1, among which the directional constant torque model (also Model A) is most applied in the simulation of dense gas-solid flow in fluidized beds (Goniva et al., 2012; Yang et al., 2016a).

#### 2.4.2. Two-fluid model

In the TFM, the inter-particle collisions are considered through the solid stress tensor, i.e., the solid pressure and solid viscosity. Solid stress is commonly described by the kinetic theory of granular flow (KTGF) (Ding & Gidaspow, 1990). Based on this theory, various constitutive equations for solid stress have been proposed (Gidaspow, 1994; Lun et al., 1984; Srivastava & Sundaresan, 2003). According to Agrawal et al. (2001), the solid stress tensor  $\boldsymbol{\tau}_s$  can be calculated as:

$$\boldsymbol{\tau}_s = -[P_{sm} + \eta\mu_b(\nabla \cdot \mathbf{u}_{sm})]\mathbf{I} + \mu_{sm} \left\{ \left[ \nabla \mathbf{u}_{sm} + (\nabla \mathbf{u}_{sm})^T \right] - \frac{2}{3}(\nabla \cdot \mathbf{u}_{sm})\mathbf{I} \right\} \quad (34)$$

where  $P_{sm}$  is the solid pressure,  $\eta$  is a function of particle restitution coefficient,  $\mu_{sm}$  is the shear viscosity, and  $\mu_b$  is the bulk viscosity.

Compared with the DEM, many simplifications and assumptions are employed to derive the KTGF models, which limits the TFM universality. For example, the classical KTGF model often assumes the granular flow as frictionless particles and neglects the rotational movements (Wu et al., 2019). Besides, most KTGF models are derived from monodisperse systems. To overcome these issues, efforts have been made to develop the KTGF model considering the realistic particle collisions, which will be discussed in the following section.

#### 2.4.3. Coarse-grained method

According to the treatment of inter-particle collisions, the coarse-grained method (CGM) can be further divided into two categories. The first one is the CG-DEM (Lu et al., 2016), in which several real particles are lumped into a numerical parcel to reduce particle number and the inter-particle collisions are resolved. Lu et al. (2016) claimed that corrections to collision parameters are required to ensure consistency between the parcel-based and particle-based systems.

The inter-parcel interactions can also be described in a continuum-based way in two existing approaches, i.e., MP-PIC (Snider, 2001) and DDPM (Popoff & Braun, 2007). In the former, the collision force is modelled by:

$$\mathbf{f}_{c,i} = -\frac{V_{p,i}}{\varepsilon_s} \nabla \tau_p \quad (35)$$

where  $\tau_p$  is the solid normal stress, calculated based on the Eulerian grid to account for the inter-particle collisions. The solid normal stress plays a vital role in preventing particles from over-packing. The stress model proposed by Harris and Crighton (1994) is commonly used:

$$\tau_p = \frac{P_s \varepsilon_s^\beta}{\max[\varepsilon_{s,cp} - \varepsilon_s, \gamma(1 - \varepsilon_s)]} \quad (36)$$

where  $P_s$  is a constant with the unit of pressure,  $\beta$  is a constant with a recommended range of 2–5.  $\varepsilon_{s,cp}$  is the solid volume fraction at the close packing status.

In the DDPM, the collision force is modelled by:

$$\mathbf{f}_{c,i} = -\frac{V_{p,i}}{\varepsilon_s} \nabla \boldsymbol{\tau}_s \quad (37)$$

where  $\boldsymbol{\tau}_s$  is the solid stress tensor, calculated based on the KTGF theory.

### 2.5. Multi-physics models

Additional models are commonly implemented into the multi-scale numerical methods to consider the effect of multi-physics processes in fluidized bed applications. For brevity, only the implementation of multi-physics models in the CFD-DEM framework is presented.

#### 2.5.1. Chemical reactions

Chemical engineering processes commonly involve significant chemical reactions, e.g., evaporation, pyrolysis, gasification, combustion, etc. To model these reactions, the corresponding reaction kinetics should be implemented into the CFD and DEM frameworks. A first-order Arrhenius law is commonly adopted to describe homogeneous reactions on the CFD side:

$$k = A_0 \exp(-E/RT) \quad (38)$$

**Table 1**  
Typical rolling friction models in the literature (Ai et al., 2011).

Category	Formulation	Remarks
Models Type A: Directional constant torque models	$M_r = -\frac{\omega_{rel}}{ \omega_{rel} } \mu_r R_r F_n$ $\omega_{rel} = \omega_i - \omega_j$	<ul style="list-style-type: none"> <li>The model applies a constant torque in pairs on each pair of particles in contact.</li> <li>The direction of the torque is against the relative rotation between the two contact entities.</li> </ul>
Models Type B: Viscous models	$M_r = -\mu_r R_r F_n (\omega_i r_i - \omega_j r_j)$	<ul style="list-style-type: none"> <li>The magnitude is related to the angular velocity.</li> <li>The term in the brackets represents the relative translational velocity at the contact between two particles due to relative rotation.</li> </ul>
Models Type C: Elastic-plastic spring-dashpot models	$M_r = M_r^k + M_r^d$ $\Delta M_r^k = -\frac{\mu_r R_r F_n}{\theta_r^m} \Delta \theta_r$ $M_{r,t+\Delta t}^d = \begin{cases} -C_r \dot{\theta}_r & \text{if }  M_{r,t+\Delta t}^k  \leq M_r^m \\ -f C_r \dot{\theta}_r & \text{if }  M_{r,t+\Delta t}^k  = M_r^m \end{cases}$	<ul style="list-style-type: none"> <li>The model consists of two components: a mechanical spring torque and a viscous damping torque.</li> <li>The mechanical spring torque is dependent on the relative rotation between the two contracting entities.</li> <li>Including the rolling back curve that makes it suitable to be applied in cyclic rolling problems.</li> <li>The viscous damping torque is assumed to be dependent on the relative rolling angular velocity between the two particles in contact and the damping constant.</li> </ul>
Models Type D: Contact-independent models	None	<ul style="list-style-type: none"> <li>The model is dependent on the total rotation or rotational velocity of a particle instead of the relative rotation or rotational velocity of a pair of particles in contact.</li> <li>The model leads to different torques being applied to each of the two particles in contact, thus violating equilibrium.</li> </ul>

where  $A_0$  is the pre-exponential factor.  $E$  is the activation energy.  $R$  is the universal gas constant.

In contrast, the heterogeneous reactions may be controlled by additional effects. For example, char combustion is dominated by both reaction resistance and diffusion resistance, with the reaction rate given by Syamlal and Bissett (1992):

$$\frac{dm_p}{dt} = \frac{-\varepsilon_s V_p P_{O_2}}{2d_p (1/k_f + 1/k_a + 1/k_r)} MW_{O_2} \quad (39)$$

where  $1/k_f$  is the film diffusion resistance,  $1/k_a$  is the ash diffusion resistance, and  $1/k_r$  is the surface reaction resistance. Moreover, during the thermochemical conversion, the particle continuously varies its density and size. The particle shrinkage models (Gomez-Barea & Leckner, 2010) are commonly used to account for this effect.

### 2.5.2. Additional forces

Cohesive force widely exists in dense gas-solid flow with different types, e.g., liquid bridge, electrostatic, and Van der Waals forces. The liquid bridge force needs to be considered during the contact between wet particles, which consists of the capillary force and viscous force. According to Mikami et al. (1998), the capillary force between particles is given by:

$$f_{cap} = \pi \gamma_{st} r_p \left[ \exp\left(A \frac{h}{r_p} + B\right) + C \right] \quad (40)$$

$$A = -1.1 \left(\frac{V}{r_p^3}\right)^{0.53} \quad (41)$$

$$B = \left(-0.34 \ln\left(\frac{V}{r_p^3}\right) - 0.96\right) \beta^2 - 0.019 \ln\left(\frac{V}{r_p^3}\right) + 0.48 \quad (42)$$

$$C = 0.0042 \ln\left(\frac{V}{r_p^3}\right) + 0.078 \quad (43)$$

where  $h$  is the separation distance,  $V$  is the liquid volume,  $r_p$  is the particle radius, and  $\beta$  is the contact angle of the liquid with the particle.

The viscous force results from the relative movement of the particles with the liquid bridge, which can be calculated as (Adams, 1987):

$$f_{vis,n} = 6\pi \mu_l r_p v_{r,n} \frac{r_p}{h} \quad (44)$$

$$f_{vis,t} = 6\pi \mu_l r_p v_{r,t} \left(\frac{8}{15} \ln \frac{r_p}{h} + 0.9588\right) \quad (45)$$

where  $\mu_l$  is the liquid viscosity.  $v_{r,n}$  and  $v_{r,t}$  are the relative velocities in the normal and tangential directions, respectively.

The Van der Waals interaction between particles originating from the intermolecular forces is significant for fine particles, which is given by:

$$f_{vdw} = \frac{A' r_p}{12h^2} \quad (46)$$

where  $A'$  is the Hamaker constant. Note that this equation cannot be applied directly to particles in close contact. Two modified models are proposed, i.e., Johnson-Kendall-Robert (JKR) model (Johnson et al., 1971) and the Derjaguin, Muller and Toporov (DMT) model (Derjaguin et al., 1975), in which the former is suitable for particles with higher surface energy and the latter is applicable for particles with lower surface energy and smaller size.

The pressure difference on the opposite side of a specific particle induced by the velocity shear gradient leads to the lift force. The lift force is first described by Saffman (1965) for creeping flow ( $Re_p \ll 1$ ) with a linear shear velocity profile. Loth and Dorgan (2009) demonstrated the lift force was difficult to model because many physical factors contribute to lift generation, and they proposed two primary mechanisms, i.e., vorticity in the gas phase and particle rotation. The Saffman lift force is given by (Zhu et al., 2007):

$$\mathbf{f}_{Saffman,i} = 1.615 d_i^2 (\rho_f \mu_f)^{1/2} |\boldsymbol{\omega}_f|^{-1/2} [(\mathbf{u}_f - \mathbf{v}_i) \times \boldsymbol{\omega}_f] \quad (47)$$

where  $\omega_f$  is the vorticity of the fluid phase. The work from Saffman was then extended by McLaughlin (1991) and Mei (1992) to limit the restriction of  $Re_p \ll Re_\omega^{1/2}$ , which applied to the above formulation. Loth and Dorgan (2009) discussed further and proposed the following equation valid up to  $Re_p = 50$ , including the contribution from particle rotation on the lift force:

$$C_L = J^* \frac{12.92}{\pi} \sqrt{\frac{\omega^*}{Re_p}} + Q_{p,eq}^* C_{L,\Omega}^* \quad (48)$$

where  $\omega^*$  and  $Q_p^*$  are related to the vorticity and particle angular velocity, respectively. Thus, this lift force is calculated as follows (Smuts, 2015):

$$\mathbf{f}_{Mei,i} = 0.125\pi d_i^2 \rho_f C_L \left| \mathbf{u}_f - \mathbf{v}_i \right| \left[ \left( \mathbf{u}_f - \mathbf{v}_i \right) \times \frac{\boldsymbol{\omega}}{|\boldsymbol{\omega}|} \right] \quad (49)$$

As the lift force is induced by the velocity gradient on the particle, this force will be larger for the particle with a larger size. Comparing the ratio of the Saffman lift force to the Stokes drag force for simple shear flows, it is accepted that the former is negligible at very small shear rates, or very low  $Re_p$  (Johnson, 2016). However, the lift force will be significant for the scenario where the slip velocity is large with high shear rates, such as the wall boundary layer for the turbulent bubbly flows (Hager, 2014).

Moreover, the charged particles are often encountered in fluidized beds and the electrostatic force between two charged particles is given by:

$$\mathbf{f}_{e,ij} = \frac{q_i q_j}{4\pi\epsilon_0 S^2} \quad (50)$$

where  $q_i$  and  $q_j$  are particle charges.  $\epsilon_0$  is the vacuum permittivity.  $S$  is the distance between two particles.

### 3. Applicability assessment

Although numerical simulation can provide detailed information on gas-solid hydrodynamics, it is still challenging to model multi-scale fluidized beds accurately and efficiently. The validity of the model should be confirmed by comparing it with experimental data or analytical solutions. On the other hand, the validation benefits the further improvement of numerical models. Moreover, the selection of sub-models, including the drag model and collision model, significantly affects the simulation results. Thus, the applicability of multi-scale numerical methods and sub-models are assessed in the following sections.

#### 3.1. Applicability of different methods

This section focuses on the applicability of multi-scale numerical methods in modelling gas-solid flow in fluidized beds under different fluidization conditions (e.g., fluidization regime, particle classification).

##### 3.1.1. Model validations in the BFB

Table 2 lists several model validations towards gas-solid flow in BFBs. Only a few studies using the PR-DNS are reported due to high computational costs. For example, Luo et al. (2016) simulated a lab-scale BFB within 9,240 particles, and the predicted solid velocity agreed well with the experimental data. Tang et al. (2016) compared the PR-DNS results with the experimental data in a BFB within 5,000 particles, and good agreement about the granular temperature was obtained. Nevertheless, as indicated in Table 2,

the PR-DNS seems to underpredict the solid volumetric flux and bed expansion height (Tang et al., 2016). The discrepancy may stem from the selection of simulation time, boundary conditions, numerical algorithms, and collisional parameters. Moreover, the grid resolution that each particle covers only five grids is relatively low.

The CFD-DEM has been validated against various BFB experiments. For the BFB within coarse particles (i.e., Geldart Group B and D), the CFD-DEM can generally capture crucial gas-solid characteristics. Commonly, time-averaged statistics such as voidage profiles, velocity profiles, and bed expansion heights are used for model validation. However, discrepancies still exist between the simulation results and experimental data. For example, Muller et al. (2008) demonstrated that considerable deviations appeared in the lateral profiles of velocity and voidage at higher bed heights and near walls. The improvement by tuning the drag model to validate this experiment is still unsatisfactory (Agrawal et al., 2018; Stanly & Shoen, 2018). Fig. 6 shows the comparison of PR-DNS, CFD-DEM, and experimental results by Luo et al. (2016). The PR-DNS reasonably predicts the solid velocity at the bed heights of 15 mm and 25 mm, but it underestimates the velocity at the bed height of 35 mm. In contrast, the CFD-DEM fails to reproduce the solid velocity at all heights and near walls. They demonstrated that such a difference between the PR-DNS and CFD-DEM was attributed to the drag force calculation, where the prevailing drag models tended to underestimate the drag force. This viewpoint was also convinced by Kriebitzsch et al. (2013) and Third et al. (2016). The inherent issue of the CFD-DEM exists in calculating the interphase momentum exchange, which will be further discussed in the following section. Liu and van Wachem (2019) validated the CFD-DEM with experimental data in a BFB, and good agreement between the prediction and experimental data was achieved regarding the solid vertical velocity and minimum fluidization velocity. However, the predicted solid horizontal velocity, solid velocity fluctuations, and granular temperature deviate significantly from the experimental data. Thus, it is necessary to validate the CFD-DEM more comprehensively.

In the BFB, bubbles dominate flow patterns, indicating the significance of conducting model validation regarding bubble dynamics. Specifically, the CFD-DEM is quantitatively validated with experimental measurements regarding bubble size and bubble velocity (Liu & van Wachem, 2019; Lu et al., 2015; Pepiot & Desjardins, 2012). A good agreement was achieved in terms of the bubble size. However, the deviation appeared in predicting the bubble rising velocity (Liu & van Wachem, 2019), which may be attributed to the neglect of bubble interactions (e.g., coalescence, breakage). Wu et al. (2016) demonstrated that the pulsed fluidized bed can be an excellent benchmark for model validation as it has the regular bubble evolution. They found that the CFD-DEM simulation could reproduce the bubble patterns in the pulsed fluidized bed both qualitatively and quantitatively (Wu et al., 2016, 2017).

Only a few CFD-DEM simulations focused on the BFB within fine particles (i.e., Geldart Group A) partly due to high computational costs. Besides, the cohesive force becomes more significant compared with other forces for fine particles. However, the role of the cohesive force is still an open issue. Wang, Chao, and Jakobsen (2010) simulated a BFB within 75  $\mu\text{m}$  fluid catalytic cracking (FCC) particles and found that the cohesive force insignificantly affected bed hydrodynamics. However, Galvin and Benyahia (2014) showed that the cohesive force should be considered to correctly capture crucial phenomena such as pressure overshoot and hysteresis in the non-bubbling regime. Via simulating a BFB within 60  $\mu\text{m}$  glass particles, Kobayashi et al. (2013) demonstrated that the cohesive force was necessary to be implemented to obtain reasonable flow patterns. Li, Wang, et al. (2017) simulated gas-solid flow in two BFBs

**Table 2**  
Validations of multi-scale methods in simulating BFBs.

Authors	Year	Method	Geldart Group	Bed geometry	Experiment	Comparison results
Luo et al. (2016)	2016	PR-DNS	B-D	Pseudo-2D	Muller et al. (2008)	(1) $V_{sy}$ : +
Tang et al. (2016)	2016	PR-DNS	D	Pseudo-2D	Tang et al. (2016)	(1) $G_s$ : ±; (2) $\theta_s$ : +; (3) Solid motion: ±; (4) Pressure fluctuation: ±
Muller et al. (2008)	2008	CFD-DEM	B-D	Pseudo-2D	Muller et al. (2008)	(1) $V_{sy}$ : ±; (2) $\theta_s$ : ±
Yang, Padding, Buist, and et al. (2017)	2017	CFD-DEM	D	Pseudo-2D/3D	Yang, Padding, Buist, and et al. (2017)	(1) $V_{sy}$ : +; (2) $G_s$ : +; (3) $\epsilon_s$ : ±
Goldschmidt et al. (2004)	2004	CFD-DEM	D	Pseudo-2D	Goldschmidt et al. (2004)	(1) $\epsilon_s$ : ±; (2) Bed expansion dynamics:
Liu and van Wachem (2019)	2019	CFD-DEM	D	Pseudo-2D	Gopalan et al. (2016)	(1) $U_{mf}$ : +; (2) $V_{sy}$ : +; (3) $V_{sx}$ : -; (4) $V_{sy,rms}$ : ±; (5) $V_{sx,rms}$ : -; (6) $D_{bub}$ : ±; (7) $U_{bub}$ : -; (8) $\theta_s$ :
Wu et al. (2017)	2017	CFD-DEM	B	Pseudo-2D	Wu et al. (2017)	(1) $D_{bub}$ : +; (2) Wavelength: +
Li, Wang, et al. (2017)	2017	CFD-DEM	A	Pseudo-2D	Li, Wang, et al. (2017)	(1) $D_{bub}$ : ±; (2) $U_{bub}$ (as a function of $D_{bub}$ ): +; (3) Visualization: ±
Bakshi, Altantzis, et al. (2018)	2018	TFM	B	Pseudo-2D	Bakshi, Altantzis, et al. (2018)	(1) Bubble fraction: +; (2) $D_{bub}$ : ±
Acosta-Iborra et al. (2011)	2011	TFM	B	3D	Acosta-Iborra et al. (2011)	(1) Bubble pattern: ±; (2) $D_{bub}$ (as a function of frequency): ±
Verma et al. (2014)	2014	TFM	B	3D	Verma et al. (2014)	(1) Solid circulation time: ±
Gao et al. (2018)	2018	TFM	A	3D	Dubrawski et al. (2013)	(1) Pressure signal: +; (2) $L_{bub}$ : +; (3) $U_{bub}$ : +; (4) $N_{bub}$ : ±; (5) $D_{bub}$ : ±
Liang et al. (2014)	2014	MP-PIC	B	Pseudo-2D	Hernandez-jimenez et al. (2011)	(1) LLDPE particle (1) $D_{bub}$ : +; (2) $\epsilon_f$ : ±; (3) $U_{bub}$ : ±
Lu, Benyahia, and Li (2017)	2017	MP-PIC/CG-DEM	D	Pseudo-2D	Gopalan et al. (2016)	Alumina particle (1) $D_{bub}$ : ±; (2) $\epsilon_f$ : +; (3) $U_{bub}$ : ±
Song et al. (2018)	2018	MP-PIC	A	2D	Zhu et al. (2008)	Glass particle (1) $D_{bub}$ : ±; (2) $\epsilon_f$ : +; (3) $U_{bub}$ : ±
Ostermeier et al. (2019)	2019	DDPM	B	2D	Ostermeier et al. (2019)	(1) $\epsilon_f$ : +; (2) Bed expansion height: +
Sakai et al. (2014)	2014	CG-DEM	B	3D	Sakai et al. (2014)	(1) $V_{sy}$ : ±; (2) Bubble possibility: -
						MP-PIC (1) Pressure signal: ±; (2) $V_{sy}$ : -; (3) $V_{sx}$ : -; (4) $\theta_s$ : -
						CG-DEM (1) Pressure signal: ±; (2) $V_{sy}$ : +; (3) $V_{sx}$ : -; (4) $\theta_s$ : -

$V_{sx}$  solid horizontal velocity,  $V_{sy}$  solid vertical velocity,  $V_{sx,rms}$  RMS (root mean square) of solid horizontal velocity,  $V_{sx,rms}$  RMS of solid horizontal velocity,  $G_s$  solid flux,  $\epsilon_f$  gas volume fraction;  $\epsilon_s$  solid volume fraction;  $\theta_s$  granular temperature,  $D_{bub}$  bubble size,  $U_{bub}$  bubble rising velocity,  $L_{bub}$  bubble pierce length,  $N_{bub}$  bubble frequency,  $U_{mf}$  minimum fluidization velocity,  $\Delta p$  pressure drop, LLDPE low linear density polyethylene, TFM two-fluid model.  
+ good, ± acceptable, - poor.

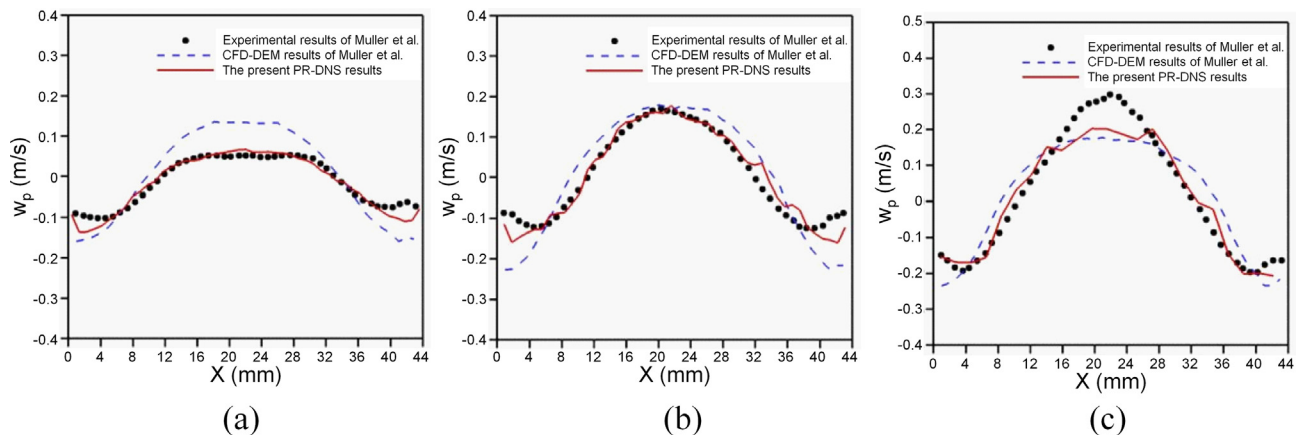


**Fig. 6.** Comparison of the time-averaged solid vertical velocity among the PR-DNS results, CFD-DEM results, and experimental data at different heights (a)  $Z = 15$  mm; (b)  $Z = 25$  mm; (c)  $Z = 35$  mm. Reproduced from Luo et al. (2016).

within Geldart Group A particles. For the FCC particles (148  $\mu\text{m}$ ), the cohesive force showed a modest effect on bubble dynamics, but the simulation using non-cohesive particles failed to reproduce particle agglomerations observed in the experiment. For sorbent particles (100  $\mu\text{m}$ ), the cohesive force should be considered to reasonably predict the flow pattern. One reason for the above-mentioned contradiction is that the influence of cohesion depends on the particle properties (e.g., size, density, and roughness). Hence,

further experimental measurements and numerical simulations are needed on this topic.

Many model validations on the TFM simulation of gas-solid flow in BFBs have been reported. Compared with the CFD-DEM, the TFM relies more on the proper selection of sub-models and model parameters (Wu et al., 2019). For the BFB within coarse particles, the TFM can predict reasonable bed hydrodynamics. Bakshi, Altantzis, et al. (2018) simulated gas-solid flow in a pseudo-two-dimensional (2D) fluidized bed and compared simulation results

with experimental data regarding bubble characteristics and solid circulation time. They demonstrated that the three-dimensional (3D) simulations showed better agreement with experimental data as compared with the 2D simulations. Acosta-Iborra et al. (2011) reported a model validation towards gas-solid flow in a 3D cylindrical BFB. The accuracy of the TFM was assessed, including the velocity, frequency, and equivalent diameter of bubbles. Verma et al. (2014) investigated the bubble behaviours in a cylindrical BFB by experimental measurements and TFM simulations. Good agreement was achieved for three types of Geldart Group B particles.

However, several studies suggested that the TFM results showed significant discrepancies from the experimental measurements. Wu et al. (2016) found that the standard TFM could not correctly reproduce the hexagonal bubble morphology observed in the experiment. It might be attributed to the limitation of the 2D geometrical configuration adopted in the simulation. As pointed out by Bakshi, Altantzis, et al. (2018), the 2D simulation failed to reproduce gas-solid hydrodynamics in BFBs and the 3D simulation needed to be carried out. However, the 3D TFM simulation of pseudo-2D BFBs is still challenging. Yang, Padding, Buist, and et al. (2017) compared the simulation using a standard TFM and a novel TFM considering the particle rotation effect in pseudo-2D and 3D BFBs. As shown in Fig. 7, in the pseudo-2D BFB, the solid velocity and flux predicted by the standard TFM deviate significantly from the experimental data while the novel TFM provides a satisfactory prediction. In the 3D BFB, both TFMs gave reasonable results. Thus, it is necessary to use the state-of-the-art TFM (e.g., KTGF for rough spheres) when modelling pseudo-2D BFBs.

Controversy also appears regarding the role of cohesive force in the TFM simulation of BFBs within fine particles. It was noticed that the standard TFM largely overestimated bed expansion (Mckeen & Pugsley, 2003; Zimmermann & Taghipour, 2005). Zimmermann and Taghipour (2005) gained a bed expansion deviation of 100% by TFM simulations but approximately 20% by experiments. The TFM failed to predict gas-solid flow in BFBs within Geldart Group A particles, owing to the existence of heterogeneous structures, i.e., agglomerates or clusters. The formation of heterogeneous structures is related to the inter-particle cohesive force, which is not considered in the standard TFM (Mckeen & Pugsley, 2003; Van Wachem & Sasic, 2008). Wang et al. (2011) demonstrated that it might be due to insufficient resolution in spatial and temporal scales. The high-resolution simulation with fine grids and small time steps could overcome this issue. However, Li et al. (2016) demonstrated that fine grids could improve the prediction, but the bed expansion height was still overpredicted by the TFM simulation. Similar findings were evidenced by Sande and Ray (2014). To improve the prediction accuracy of the TFM in simulating BFBs within fine particles, the effect of heterogeneous structures should be considered. Essentially, the formation of heterogeneous structures varies from gas-solid interactions. Hence, efforts have been made to develop new drag models that can accurately describe the interphase momentum exchange for fine particles.

The drag models can be mainly divided into two categories, i.e., the drag model suitable for homogeneous systems and the one feasible for heterogeneous systems. The former includes the drag models proposed by Ergun and Orning (1949), Wen (1966), Gidaspow (1994), Hill et al. (2001), Rong et al. (2013), etc, which are derived from gas-solid flow in absence of heterogeneous structures. In contrast, the energy-minimization multi-scale (EMMS) drag model is the first one proposed considering heterogeneous structures (i.e., clusters) in the CFB riser, which treats the sub-grid flow structure as a dense phase and dilute phase to correct the drag force (Li & Kwauk, 1994; Yang et al., 2003). It was then extended to BFBs

by replacing clusters with bubbles (Shi et al., 2011). Gao et al. (2018) assessed different drag models for the TFM simulation of fluidized beds within Geldart Group A particles. They demonstrated that the EMMS drag model provided a better agreement with the experimental data than the conventional drag models (e.g., the Gidaspow drag model). Nevertheless, most validations of the TFM for gas-solid flow in BFBs within fine particles were focused on limited metrics, i.e., the bubbling expansion height and voidage profiles. Hence, comprehensive model validations need to be conducted to further examine the accuracy of the TFM.

The applicability of the MP-PIC in predicting hydrodynamics in BFBs is still in controversy. Liang et al. (2014) found that the MP-PIC could not capture the bubble coalescence in a BFB within Geldart Group B particles and it predicted a homogenous gas-solid distribution in the lateral direction. Lu, Benyahia, and Li (2017) simulated gas-solid flow in a BFB within Geldart Group D particles, and they also compared the CFD-DEM, CG-DEM, and MP-PIC results, as shown in Fig. 8. The CFD-DEM and CG-DEM give reasonable prediction regarding the solid vertical velocity and the results from the MP-PIC severely deviates from the experimental data (Gopalan et al., 2016). Nevertheless, several studies showed that the MP-PIC could reasonably reproduce gas-solid hydrodynamics in BFBs within fine particles (Feng et al., 2018; Karimipour & Pugsley, 2012; Song et al., 2018). These simulations also observed the homogeneous distribution of time-averaged variables in the lateral direction, indicating that it was difficult for the MP-PIC to predict BFBs within heterogeneous structures. In the MP-PIC, the solid pressure (i.e., normal stress) model from Harris and Crighton (1994) is commonly used while the solid shear stress accounting for translational motion, collision, and Coulomb friction is usually neglected. Hence, the incapability of the MP-PIC in modelling gas-solid flow in BFBs is attributed to the solid stress model. Verma and Padding (2020) improved the solid stress model and velocity update method in the traditional MP-PIC. The shear solid stress from Srivastava and Sundaresan (2003) was implemented, and the trilinear interpolation and mapping schemes were used. Based on the same benchmark reported by Lu, Benyahia, and Li (2017), the newly developed MP-PIC agreed well with the CFD-DEM results and experimental data (Gopalan et al., 2016).

The validation of the DDPM regarding dense gas-solid flow in BFBs has been seldom reported in the open literature. Cloete et al. (2011) simulated a large-scale BFB and gave an acceptable prediction of pressure drop. Ostermeier et al. (2019) demonstrated that although the DDPM gave the pressure drop and bed expansion height similar to the TFM, it could not reliably reproduce flow patterns. Using CFD-DEM results as benchmarks, Chen and Wang (2014) evaluated different numerical methods for predicting impinging gas-solid flow. They demonstrated that the TFM failed to predict the particle trajectory crossing effect while the DDPM failed to predict the cases of jets merging, as shown in Fig. 9.

The CG-DEM shows an accurate prediction of dense gas-solid flow in BFBs. Sakai et al. (2014) demonstrated that the CG-DEM gave a reasonable prediction of bed height and pressure drop in a BFB within Geldart Group B particles, consistent with the CFD-DEM results. Liu et al. (2013) validated the CG-DEM towards a BFB within Geldart Group B particles and gained a good prediction of bubble characteristics. Lu, Benyahia, and Li (2017) comprehensively assessed the accuracy of different methods in a BFB within Geldart Group D particles and demonstrated that the CG-DEM predicted reasonable gas-solid hydrodynamics. Hu, Luo, Wang, and et al. (2019a, 2019b) compared the CG-DEM simulations with the experimental data under different superficial gas velocities and a good agreement was achieved in terms of the solid vertical velocity.

In summary, the higher-resolution methods can better predict gas-solid hydrodynamics in BFBs with less model tuning. Based on

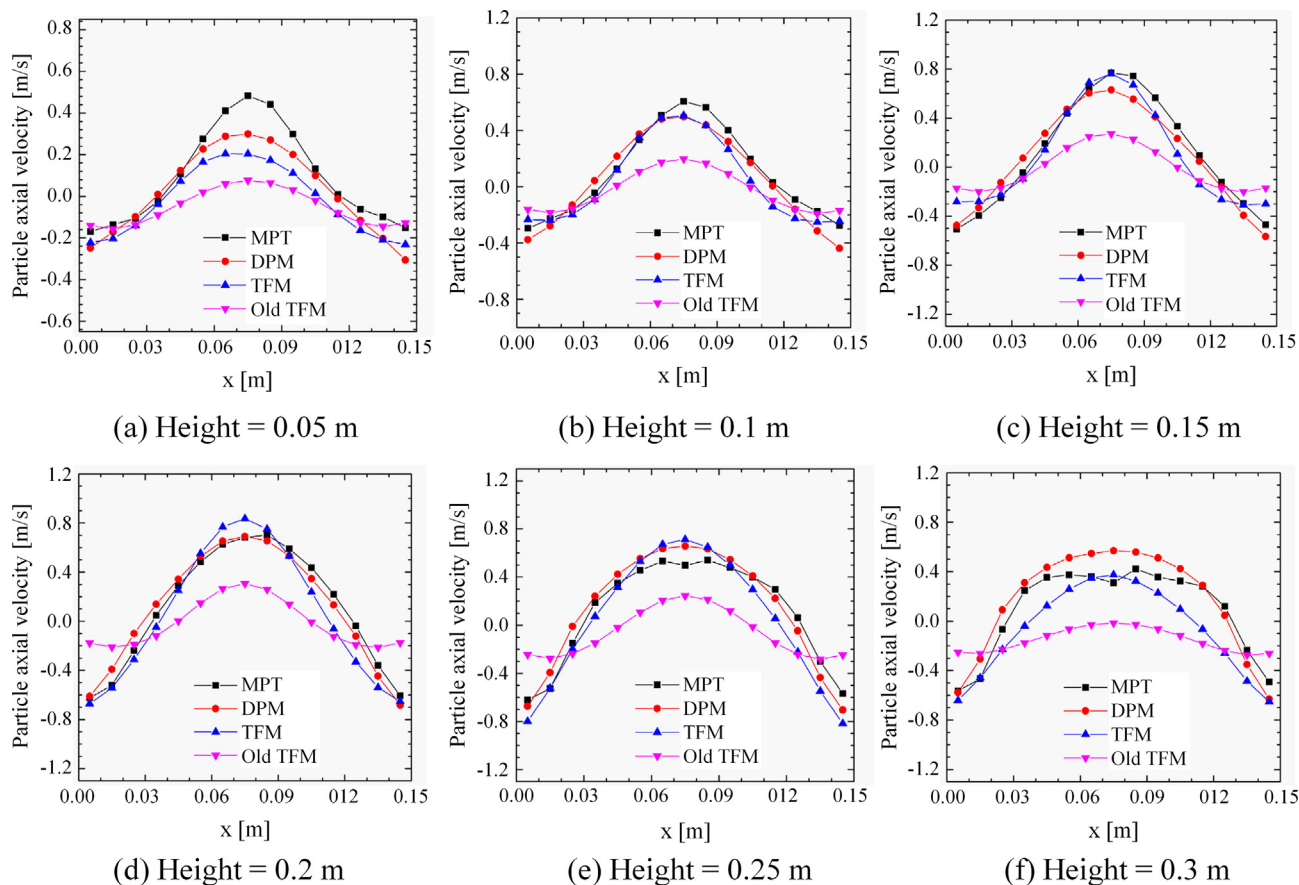


**Fig. 7.** Time-averaged solid axial velocity along the lateral ( $x$ ) direction: comparison between MPT (Magnetic Particle Tracking) experiments (black squares) and simulations (CFD-DEM: red circles; new TFM: blue up triangles; old TFM: magenta down triangles) at different heights in the pseudo-2D bed, for a superficial velocity  $U_g = 2.0U_{mf}$ . Reproduced from Yang, Padding, Buist, and et al. (2017). (For interpretation of the references to colour in this figure legend, the reader is referred to the Web version of this article.)

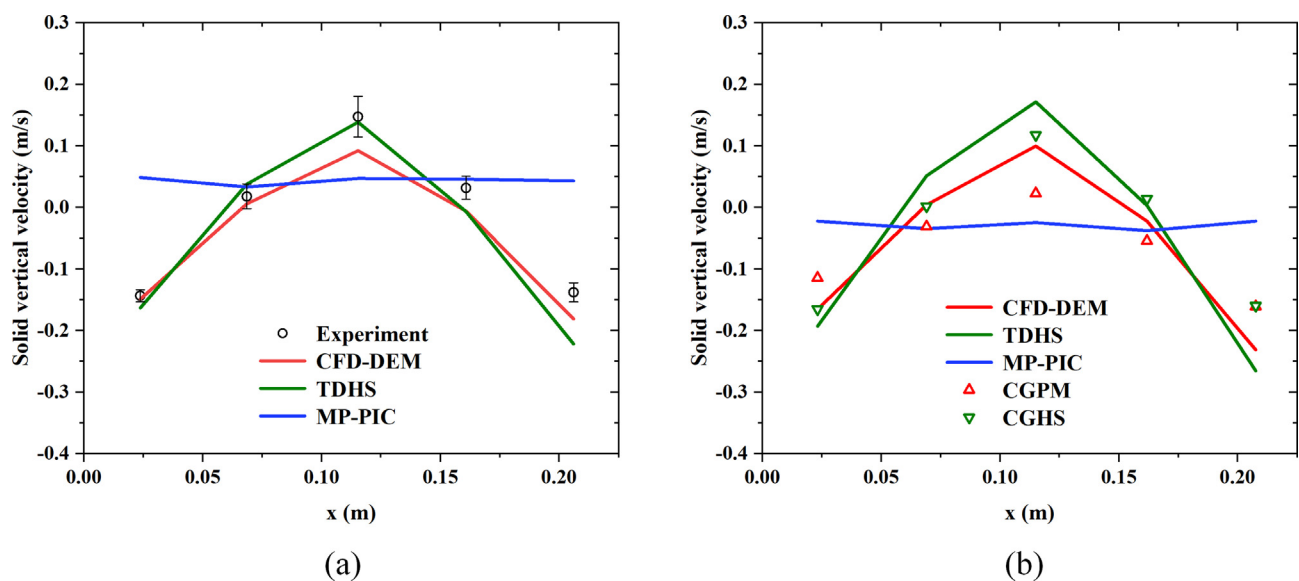


**Fig. 8.** Radial distribution of solid vertical velocity using different methods under a superficial gas velocity of 2.19 m/s. TDHS: time-driven hard-sphere; CGPM: coarse-grained particle method (soft sphere DEM); CGHS: coarse-grained hard-sphere. Reproduced from Lu, Benyahia, and Li (2017).

Table 2, it is noted that various hydrodynamics metrics exist for model validation. To ensure a rigorous and general examination of numerical methods, comprehensive validations should be

performed, not only using different metrics but also under different fluidization conditions.

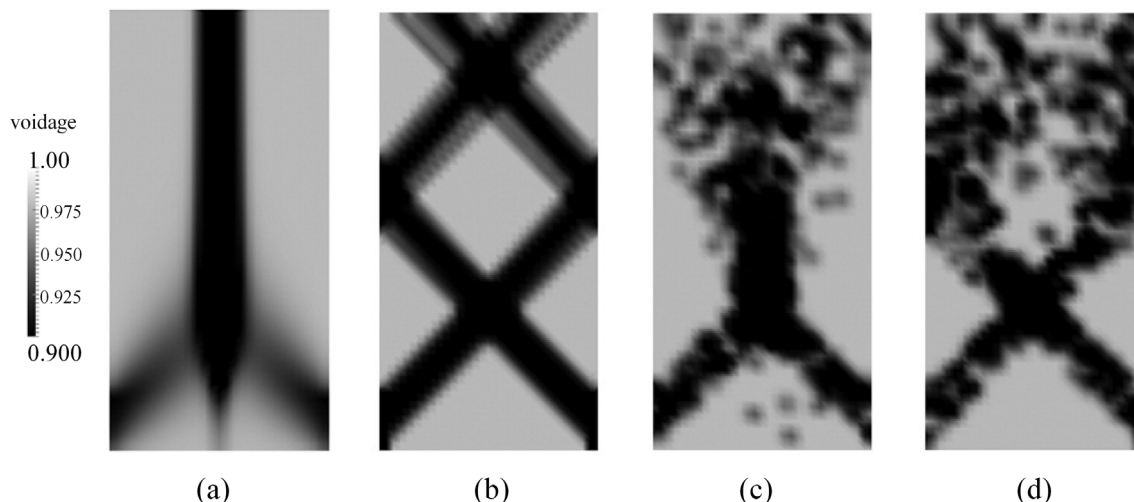


**Fig. 9.** Comparison of different methods to model impinging gas-solid flow, with a superficial gas velocity of 10 m/s and a solid volume fraction of 0.1: (a) TFM, (b) DDPM, (c) CFD-DEM ( $k_n = 1000$  N/m) and (d) CFD-DEM ( $k_n = 10$  N/m). The particles are injected from two opposite sides with  $45^\circ$  angles, and the gas flow is introduced from the bottom. Reproduced from [Chen and Wang \(2014\)](#).

3.1.2. Model validations in the CFB

[Table 3](#) summarizes typical model validations regarding dense gas-solid flow in CFBs. It is impractical to conduct validations of the PR-DNS due to the unaffordable computational costs. In contrast, the CFD-DEM has been widely validated towards CFBs within coarse particles (i.e., Geldart Group B and D particles), which was seldom validated towards CFBs within fine particles (i.e., Geldart Group A and small Geldart B particles) due to the limit of computational resources. [Luo et al. \(2015\)](#) simulated a lab-scale CFB within Geldart Group B particles using the CFD-DEM and correctly predicted the solid vertical velocity. [Xu et al. \(2018\)](#) comprehensively validated the CFD-DEM towards a lab-scale CFB within Geldart Group B particles. Reasonable agreement was achieved with a proper drag model in terms of the pressure drop, solid circulation rate, and inventory height. [Capecelatro et al. \(2014\)](#) validated the

CFD-DEM in 3D CFB riser regarding the solid volume fraction fluctuation, cluster descent velocity, and cluster solid concentration. [Carlos Varas et al. \(2017\)](#) simulated a pseudo-2D riser within Geldart Group D particles and they found that the simulation accuracy varied under different superficial gas velocities. At a superficial gas velocity of 6.74 m/s, the axial profile of solid concentration deviated from the experimental data significantly. At a superficial gas velocity of 5.95 m/s, the predicted cluster characteristics, e.g., cluster frequency, cluster volume fraction, and cluster aspect ratio agreed well with experimental data.

For the CFBs within coarse particles, the TFM can generally reproduce reasonable gas-solid hydrodynamics. [Jin et al. \(2010\)](#) conducted a 2D simulation of a high-flux CFB and obtained reasonable pressure gradient profiles by tuning collision parameters. [Li, Dietiker, and Shahnam \(2012\)](#) performed a TFM simulation

**Table 3**  
Validations of multi-scale methods in simulating CFBs.

Authors	Year	Method	Geldart Group	Bed geometry	Experiment	Comparison results
<a href="#">Luo et al. (2015)</a>	2016	CFD-DEM	B	Pseudo-2D	<a href="#">Muller et al. (2008)</a>	(1) $V_{sy}$ : $\pm$
<a href="#">Xu et al. (2018)</a>	2018	CFD-DEM	B	3D	<a href="#">Xu et al. (2018)</a>	(1) $\Delta p$ : $\pm$ ; (2) $G_{s,c}$ : -; (3) Standpipe inventory height: +
<a href="#">Varas et al. (2017)</a>	2017	CFD-DEM	B-D	Pseudo-2D	<a href="#">Varas et al. (2017)</a>	(1) $\epsilon_s$ : $\pm$ ; (2) $G_s$ : $\pm$ ; (3) $N_{cluster}$ : $\pm$ ; (4) $e_{cluster}$ : $\pm$ ; (5) $A_{cluster}$ : $\pm$ ; (6) $AR_{cluster}$ : $\pm$ ; (7) $U_{cluster}$ : $\pm$
<a href="#">Li, Dietiker, and Shahnam (2012)</a>	2012	TFM	B	3D	NETL CFB CP-iii	(1) pressure gradient profile: $\pm$ ; (2) $V_{sy}$ : $\pm$ ; (3) $G_s$ : $\pm$
<a href="#">Nikku et al. (2019)</a>	2019	TFM	B	3D	<a href="#">Nikku et al. (2019)</a>	(1) $\Delta p$ : $\pm$ ; (2) $\epsilon_s$ : $\pm$ ; (3) $V_{sy}$ : $\pm$ ; (4) $G_{s,c}$ : -
<a href="#">Yang et al. (2004)</a>	2004	TFM	A	2D	<a href="#">Li and Kwauk (1994)</a>	(1) $G_{s,c}$ : +; (2) $e_f$ (radial and axial): $\pm$
<a href="#">Gao et al. (2018)</a>	2018	TFM	A	3D	<a href="#">Wei et al. (1998)</a>	(1) $e_f$ (radial and axial): $\pm$
<a href="#">Yin et al. (2014)</a>	2014	MP-PIC	B/A	3D	<a href="#">Yin et al. (2012)</a> <a href="#">Richtberg et al. (2005)</a>	(1) $\Delta p$ : +; (2) $\epsilon_s$ : $\pm$
<a href="#">Wu et al. (2018)</a>	2018	MP-PIC	A	3D	<a href="#">Wang (2013)</a>	(1) $\epsilon_s$ : +; (2) $V_{sy}$ : $\pm$
<a href="#">Adamczyk et al. (2014)</a>	2014	DDPM	B	3D	<a href="#">Adamczyk et al. (2014)</a>	(1) $\Delta p$ : -; (2) $\epsilon_s$ : -
<a href="#">Adnan et al. (2018)</a>	2019	DDPM	A	3D	<a href="#">Herbert et al. (1999)</a>	(1) $G_{s,c}$ : +; (2) $\epsilon_s$ : $\pm$
<a href="#">Lu, Benyahia, and Li (2017)</a>	2017	CG-DEM	B	3D	NETL CFB CP-iii	(1) pressure gradient profile: $\pm$ ; (2) $V_{sy}$ : $\pm$ ; (3) $G_s$ : $\pm$

$V_{sy}$  solid vertical velocity,  $G_s$  solid flux,  $G_{s,c}$  solid circulation flux,  $e_f$  gas volume fraction,  $\epsilon_s$  solid volume fraction,  $A_{cluster}$  cluster size,  $AR_{cluster}$  aspect ratio of cluster,  $U_{cluster}$  cluster velocity,  $e_{cluster}$  cluster solids holdup,  $N_{cluster}$  cluster frequency,  $\Delta p$  pressure drop, NETL CFB CP-iii: The details of the experiment can be found in <https://mfix.netl.doe.gov/challenge-problem-iii-2010/>.  
+ good,  $\pm$  acceptable, - poor.

of a pilot-scale 3D CFB riser under three different operating conditions and gained good agreement regarding the pressure gradient and vertical solid velocity. However, it was found that the vertical solid mass flux deviated from the experimental data significantly for Case 3 (i.e., lowest gas velocity and solid circulation rate). Jalali et al. (2018) simulated a lab-scale 3D CFB riser and correctly predicted the pressure distribution. The solid circulation rate obtained from the simulation was 25% lower than the experimental measurements. Nikku et al. (2019) simulated a lab-scale 3D CFB riser and demonstrated only part of the quantities (e.g., axial pressure profile, radial solid velocity profile) could be well predicted.

For the CFBs within fine particles (i.e., Geldart Group A and small Geldart Group B particles), the TFM with the conventional drag models cannot reproduce gas-solid hydrodynamics and tends to overestimate the solid circulation rate (Agrawal et al., 2001; Yang et al., 2004). It stems from the inadequate grid resolution as pointed out by some researchers (Benyahia, 2012; Wang, 2008). However, Zhou et al. (2014) suggested it remained as an open question whether fine-grid TFM simulations could reproduce gas-solid hydrodynamics without a modification of drag force. Fullmer and Hrenya (2016) compared fine-grid TFM and CFD-DEM simulations of dense gas-solid flow in an unbounded fluidization system within Geldart Group A particles. Good agreement was achieved regarding the mean slip velocity with relative errors of less than 20% under different mean solid concentrations. Nevertheless, several simulations showed that although the high grid resolution improved TFM prediction, the agreement between simulations and experiments was still unsatisfactory (Hong et al., 2016; Lu et al., 2009). Hong et al. (2016) assessed the influence of grid size in the TFM simulation of a CFB within Geldart Group A particles. As shown in Fig. 10, the near-wall clusters can be captured with the decrease in grid size. However, the simulation cannot reproduce the “S” shape profile of solid concentration. Besides, the solid circulation flux is largely overestimated (e.g., 350% for the finest grid) as compared with the experimental data.

The failure of TFM in predicting CFBs within fine particles is generally attributed to unresolved heterogeneous structures. EMMS drag model has been widely used to account for heterogeneous structures to improve prediction accuracy. It gives rise to reasonable solid concentration distribution and solid circulation rate, as compared with the conventional drag models. For example, Yang et al. (2004) simulated dense gas-solid flow in a CFB riser within Geldart Group A particles by the EMMS drag model. As shown in Fig. 11, the EMMS drag model delivers a reasonable solid circulation rate while the Gidaspow drag model overestimates it considerably. Gao et al. (2018) demonstrated that the EMMS drag model could reproduce a more reasonable axial profile of voidage than the Gidaspow drag models when simulating a CFB riser. Dai et al. (2015) demonstrated that the EMMS drag model was also needed in the simulation of CFBs within small Geldart Group B particles to ensure prediction accuracy. More discussions on the drag models will be presented in the following section.

The MP-PIC and DDPM are incapable of accurately simulating dense gas-solid flow in BFBs due to the simplification of inter-particle collisions. In contrast, it is reasonable to use them to predict gas-solid flow in CFBs as the inter-particle collisions become insignificant under lower solid concentrations. Yin et al. (2014) simulated gas-solid flow in a pressurized high-flux CFB using the MP-PIC and achieved good predictions regarding the axial profile of pressure drop and radial distribution of solid volume fraction. Ma et al. (2018) also reported the MP-PIC simulation of a high-flux CFB and the predicted pressure profile across the full loop agreed well with experimental data. Adamczyk et al. (2014) compared the TFM and DDPM in simulating gas-solid flow in a pilot-scale CFB within Geldart Group B particles. The two methods predicted

comparable gas-solid hydrodynamics, but they all failed to predict pressure drop in the bottom region of the bed. The CG-DEM was also validated against CFB experiments. For example, Lu, Benyahia, and Li (2017) simulated gas-solid flow in a pilot-scale CFB riser within Geldart Group B particles using the CG-DEM and achieved reasonable prediction of pressure profiles, solid vertical velocity and solid flux. Similar to the TFM, the CG-DEM also needed the EMMS drag model to predict heterogeneous gas-solid flow in CFBs within fine particles (Song et al., 2018; Tu & Wang, 2018; Wu et al., 2018).

Gas-solid flow in 3D CFBs was commonly simulated by simplifying it into 2D ones in previous studies. However, 2D configuration was found to be unreliable to simulate the fully 3D CFB. Li et al. (2014) evaluated the difference between 2D and 3D simulations of gas-solid flow in CFBs. They demonstrated that the 2D simulation could not reproduce gas-solid hydrodynamics, as compared with experimental data and 3D simulation results. The 2D simulation restricted the intrinsic 3D gas-solid flow and could not obtain the angular movements of gas-solid flow. The inlet and outlet boundary conditions in the 2D simulations were not accurately accounted for. Capecelatro et al. (2014) also pointed out that the 2D simulation resulted in unphysical solid concentration and movements because particle motions were restricted to a plane. The effect of the 2D assumption may depend on the fluidization condition. For instance, Almuttahir and Taghipour (2008a) found that the 2D TFM simulation gave reasonable gas-solid flow patterns for a high-density CFB, but the prediction deviated significantly from the experimental data for a low-density CFB. Therefore, 3D configurations are more recommended for CFB simulations than 2D ones.

As shown in Table 3, several metrics, including the axial profile of pressure, radial profile of solid velocity and voidage profiles, are commonly employed to validate the TFM and CGM in modelling gas-solid flow in CFBs. However, the comparison of some crucial metrics has been seldom reported. For example, there are very limited comparisons regarding the cluster characteristics using the TFM and CGM (Fullmer et al., 2017; Wang, 2008). Lu, Benyahia, and Li (2017) evaluated the capability of the CFD-DEM and TFM to predict the cluster behaviours of Geldart Group A particles. The PR-DNS simulation was used as a benchmark. The results showed that the CFD-DEM could reasonably capture the cluster size, while the TFM could not correctly reproduce cluster characteristics. Both methods underpredicted the slip velocity and overpredicted the cluster aspect ratio. Thus, more comprehensive validations about gas-solid flow in CFBs using the TFM and CGM are needed.

### 3.1.3. Computational efficiency

It is necessary to conduct high-resolution simulations for analyzing gas-solid hydrodynamics in fluidized beds, but it suffers from high computational costs. Although the simulation can be efficiently accelerated by parallel computation, the modelling scales for different numerical methods still have upper limits. For comparison, some “large-scale” simulations under the corresponding numerical method are presented in Fig. 12.

For the PR-DNS, the major computation costs take place in the solution of governing equations of the fluid phase due to the huge grid number. Specifically, the grid resolution ( $\Delta/d_p$ ) of PR-DNS is typically lower than 1/10 (Esteghamatian et al., 2017; Luo et al., 2016). Hence, the PR-DNS can only simulate small-scale fluidized beds within a few thousand particles ( $O(\sim 10^3)$ ). Deen and Kuipers (2014) simulated a dense gas-solid system involving momentum and heat transfer using the PR-DNS. The system contained 663 suspended particles and the grid number was 24 million. Luo et al. (2016) reported a high-resolution PR-DNS simulation of a lab-scale BFB. The particle number was 9240 particles and the grid number was 58.6 million. It took approximately 162 days on 150 CPU

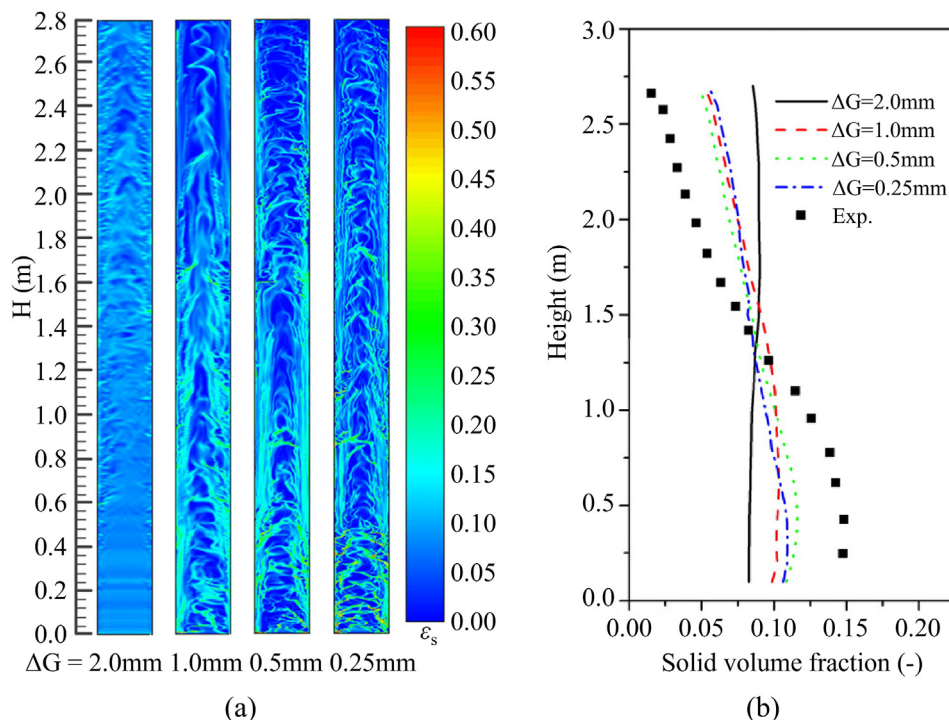


Fig. 10. (a) Instantaneous snapshots of solid volume fraction and (b) axial profiles of solid volume fraction, with  $\Delta G$  denoting the grid size. Reproduced from Hong et al. (2016).

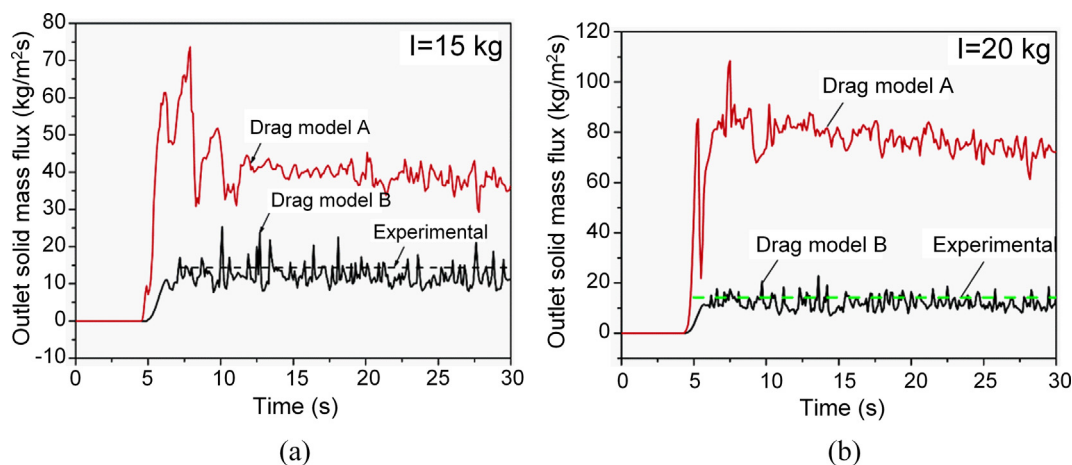


Fig. 11. Comparison of predicted outlet solid fluxes and experimental data, with drag model A denoting the Gidaspow drag model and model B denoting the EMMS drag model. Reproduced from Yang et al. (2004).

(Central Processing Unit) cores for a physical time of 2.7 s. Combining GPU (Graphics Processing Units) and LB method paves the way to speed up the PR-DNS. For example, Xiong et al. (2012) investigated gas-solid suspensions with about  $10^5$  particles in a 3D domain using the LB-based PR-DNS. Performance verification showed that the speedup of a GPU (Tesla C2050) to a single-core CPU (Intel E5520) was about 40.

In contrast, the grid resolution ( $\Delta/d_p$ ) (Peng et al., 2014) in the CFD-DEM simulation is typically 3–5, making it suitable to simulate large-scale fluidized beds within more than  $10^6$  particles. Accordingly, the bottleneck of the computational efficiency in the CFD-DEM simulation is the calculation of particle dynamics. Liu et al. (2014) demonstrated that the DEM solver takes approximately 90% of the total computation time. As shown in Fig. 12, the CFD-DEM can generally simulate millions of particles with a high-

efficient parallelization algorithm in lab-scale fluidized beds (Jajcevic et al., 2013; Tsuji et al., 2008; Wang, Luo, et al., 2017). One of the largest scales of the CFD-DEM simulations was conducted by Capecehatro and Desjardins (2013b), where 4,096 CPU cores were used to simulate a fluidized bed within 382 million particles using 200 million grids.

Featuring lower resolution but higher efficiency, the TFM and CGM have been commonly employed to simulate large-scale fluidized beds within more than  $10^9$  particles. In these simulations, coarse grids were used to reduce computational costs. Besides, the TFM and CGM are very efficient in modelling the solid phase. It is worth noting that the simulation of industrial-scale fluidized beds using fine grids is currently impractical, where the grid number may be in the order of  $10^{11}$ – $10^{13}$ . Using coarse grids causes severe discrepancies as the heterogeneous flow structures can not be well

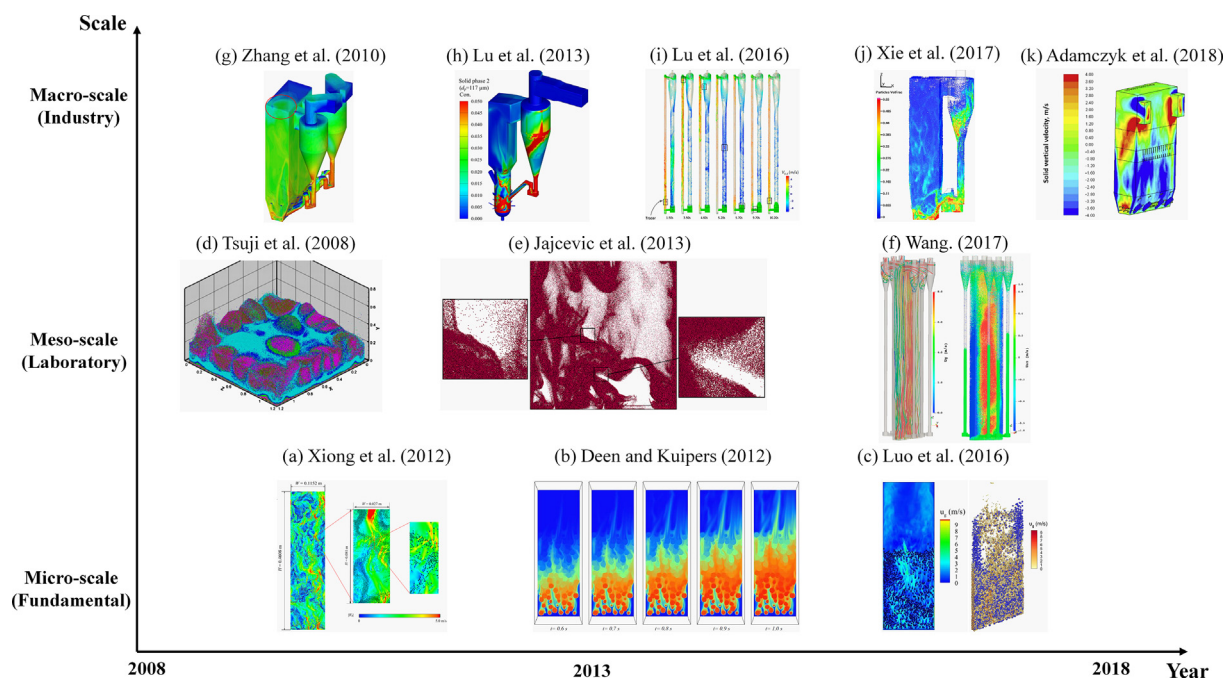


Fig. 12. Multi-scale simulations of fluidized beds in recent years.

captured (Agrawal et al., 2001). Therefore, sub-grid models considering the heterogeneous flow structures are needed to address the issue.

### 3.1.4. Discussions

As demonstrated by van der Hoef et al. (2008), a multi-scale modelling strategy can be employed to achieve a compromise between numerical resolution and computation costs. For instance, the PR-DNS resolves gas-solid flow in the highest fidelity among all numerical methods. Hence, the PR-DNS are often used to develop sub-models for coarse-scale methods (e.g., CFD-DEM, TFM). However, due to the highest computation costs, the PR-DNS is commonly applied to model small-scale fluidized beds within limited particles.

The CFD-DEM can gain a reasonable prediction of gas-solid flow in both BFBs and CFBs. However, discrepancies were still reported in some previous studies, which needs further identification of error sources. Besides, the CFD-DEM validation of gas-solid flow in fluidized beds within fine particles needs to be further conducted.

The TFM can also gain an acceptable prediction of gas-solid flow in most cases. However, the TFM often requires more model tuning than the CFD-DEM does, making it a less generalized method. Compared with the CFD-DEM, the TFM has several inherent limitations. Firstly, the TFM cannot track individual particles, making it impractical to obtain particle-scale information (e.g., particle residence time, particle rotation, and particle dispersion). Besides, the TFM is incapable to describe the size or shape change of the particle due to chemical reactions. Moreover, the TFM is difficult to depict polydisperse particles because each particle species needs to be modelled by a separated governing equation. Fortunately, several novel methods were proposed to achieve particle tracking in the TFM simulation (Ramkrishna, 2000). To account for the spatial and temporal evolutions of particle properties, the TFM is coupled with the population balance equation (PBE) (McGraw, 1997). One of the most crucial ways to solve PBE is the quadrature-based moment method (QBMM) (McGraw, 1997). With QBMM, the TFM can be applied to simulate gas-solid flow in fluidized beds with particle

agglomeration and breakage (Khadiilkar et al., 2014; Sun et al., 2017), heterogeneous chemical reactions (Li et al., 2013; Liu, LaMarche, et al., 2017), and so on.

The CGM can be regarded as an alternative to the TFM to speed up simulations. The MP-PIC treats inter-particle collisions in the most simplified way and special attention needs to be paid to collision-dominant regimes, such as the bubbling fluidization regime. For the CG-DEM (Chew et al., 2013; Kazari, 1995; Liu et al., 2013; Lu et al., 2016; Sakai et al., 2010), the similarity between real particle collisions and parcel collisions has not been proven analytically. Hence, more attention should be paid to the model development of the coarse-grained method.

Model validation is of primary importance for the simulation of gas-solid flow in fluidized beds under different fluidization regimes. Some discrepancies may result from experiment conditions (e.g., non-sphericity, polydispersity), measurement techniques, and post-processing treatment. On the other hand, tuning sub-models and their parameters is usually required to obtain reasonable predictions. It is significant to know the performance and sensitivity of various sub-models and parameters. Moreover, model validations should be conducted under multiple flow conditions and comprehensive metrics (e.g., velocity profiles at different heights, bubble or cluster characteristics).

### 3.2. Sensitivities of drag models

Drag force is a dominant interphase force in dense gas-solid flow and greatly affects the simulation results. A variety of drag models have been available in the literature, which can be generally divided into homogeneous drag models and heterogeneous drag models. The homogeneous drag models derived from experiments or PR-DNS are suitable for modelling fluidized beds within homogeneous solid distributions. Table 4 summarizes the commonly used homogeneous drag models.

The sub-grid solid distribution can be either homogenous or heterogeneous (see Fig. 13). Except for the PR-DNS, most simulations cannot capture the realistic sub-grid solid distribution,

leading to considerable discrepancies when modelling fluidized beds within heterogeneous flow structures. The heterogeneous drag model considering such a sub-grid effect (i.e., heterogeneous flow structures) can be obtained by multiplying a heterogeneous index  $H_d$  in the homogeneous drag model to account for the effect of sub-grid structures on the drag force:

$$\beta_{subgrid} = H_d \beta_{homogenous} \quad (51)$$

Heterogeneous drag models can be achieved in two ways, i.e., filtered drag model and EMMS drag model. The filtered drag model is established by filtering data generated from high-resolution TFM (Agrawal et al., 2001; Chu et al., 2016; Cloete et al., 2018; Igci & Sundaresan, 2011; Jiang et al., 2019; Milioli et al., 2013; Sarkar et al., 2016; Schneiderbauer & Pirker, 2014) or CFD-DEM (Radl & Sundaresan, 2014) simulations. Different parameters were employed as markers for constructing filtered drag models, including the filter size, solid volume fraction (Igci & Sundaresan,

**Table 4**  
Summary of commonly used homogeneous drag models.

No.	Model	Coefficient
A	Syamlal-O'Brien (Syamlal & O'Brien, 1987)	$\beta_{S-O} = \frac{3}{4} \frac{C_D \rho_f \epsilon_f \epsilon_p}{V_{rs}} \frac{ \mathbf{u}_f - \mathbf{v}_p }{d_p}$ $C_D = \left( 0.63 + \frac{4.8}{\sqrt{\text{Re}_p / V_{rs}}} \right)^2$ $V_{rs} = 0.5(A - 0.06\text{Re}_p + \sqrt{(0.06\text{Re}_p)^2 + 0.12\text{Re}_p(2B - A) + A^2})$ $A = \epsilon_f^{4.14}$ $B = \begin{cases} 0.8\epsilon_f^{1.28} & \epsilon_f \leq 0.85 \\ \epsilon_f^{2.65} & \epsilon_f > 0.85 \end{cases}$
B	Wen-Yu (Wen, 1966)	$\beta_{\text{Wen-Yu}} = \frac{3}{4} C_D \frac{\rho_f \epsilon_f \epsilon_p}{d_p} \frac{ \mathbf{u}_f - \mathbf{v}_p }{\epsilon_f^{-2.65}}$ $C_D = \begin{cases} \frac{24}{\text{Re}_p} (1 + 0.15\text{Re}_p^{0.687}) & \text{Re}_p < 1000 \\ 0.44 & \text{Re}_p \geq 1000 \end{cases}$
C	Gidaspow (Gidaspow, 1994)	$\beta_{\text{Gidaspow}} = \begin{cases} \frac{3}{4} C_D \frac{\rho_f \epsilon_f \epsilon_p}{d_p} \frac{ \mathbf{u}_f - \mathbf{v}_p }{\epsilon_f^{-2.65}} & \epsilon_f \geq 0.8 \\ \frac{150(1 - \epsilon_f)^2 \mu_f + 1.75\rho_f(1 - \epsilon_f)  \mathbf{u}_f - \mathbf{v}_p }{\epsilon_f d_p^2} & \epsilon_f < 0.8 \end{cases}$ $C_D = \begin{cases} \frac{24}{\text{Re}_p} (1 + 0.15\text{Re}_p^{0.687}) & \text{Re}_p < 1000 \\ 0.44 & \text{Re}_p \geq 1000 \end{cases}$
D	Hill-Koch-Ladd (Hill et al., 2001)	$\beta_{\text{HKL}} = \frac{18\mu_f \epsilon_f^2 \epsilon_p}{d_p^2} \left( F_0(\epsilon_p) + \frac{1}{2} F_3(\epsilon_p) \text{Re}_p \right)$ $F_0(\epsilon_p) = \begin{cases} \frac{1 + 3\sqrt{\frac{\epsilon_p}{2}} + \frac{135}{64}\epsilon_p \ln(\epsilon_p) + 16.14\epsilon_p}{1 + 0.681\epsilon_p - 8.48\epsilon_p^2 + 8.16\epsilon_p^3} & \epsilon_p < 0.4 \\ \frac{10\epsilon_p}{\epsilon_f^3} & \epsilon_p \geq 0.4 \end{cases}$ $F_3(\epsilon_p) = 0.0673 + 0.212\epsilon_p + \frac{0.0232}{\epsilon_f^5}$
E	Beetstra et al. (Beetstra et al., 2007a)	$\beta_{\text{Beetstra}} = \frac{18\mu_f \epsilon_f^2 \epsilon_p F_0}{d_p^2}$ $F_0 = 10 \frac{\epsilon_p}{\epsilon_f^2} + \epsilon_f^2 (1 + 1.5\sqrt{\epsilon_p}) + \frac{0.413\text{Re}_p}{24\epsilon_f^2} \left[ \frac{\epsilon_f^{-1} + 3\epsilon_p \epsilon_f + 8.4\text{Re}_p^{-0.343}}{1 + 10^3 \epsilon_p \text{Re}_p^{-(1+4\epsilon_p)/2}} \right]$
F	Di Felice (Di Felice, 1994)	$\beta_{\text{DiFelice}} = \frac{3}{4} C_D \frac{\rho_f \epsilon_p}{d_p} \frac{ \mathbf{u}_f - \mathbf{v}_p  f(\epsilon_f, \text{Re}_p)}{d_p}$ $C_D = \left( 0.63 + \frac{4.8}{\sqrt{\text{Re}_p}} \right)^2$ $f(\epsilon_f, \text{Re}_p) = \epsilon_f^{-\gamma}$ $\gamma = 3.7 - 0.65 \exp\left(\frac{-(1.5 - \log_{10}(\text{Re}_p))}{2}\right)$
G	Rong et al. (Rong et al., 2013)	$\beta_{\text{Rong}} = \frac{\pi}{8} C_D \rho_f  \mathbf{u}_f - \mathbf{v}_p  d_p^2 \epsilon_f^{(2-\alpha(\epsilon_f, \text{Re}_p))}$ $C_D = \left( 0.63 + \frac{4.8}{\sqrt{\text{Re}_p}} \right)^2$ $\alpha(\epsilon_f, \text{Re}_p) = 2.65(\epsilon_f + 1) - (5.3 - 3.5\epsilon_f)\epsilon_f^2 \exp\left(\frac{-(1.5 - \log \text{Re}_p)^2}{2}\right)$

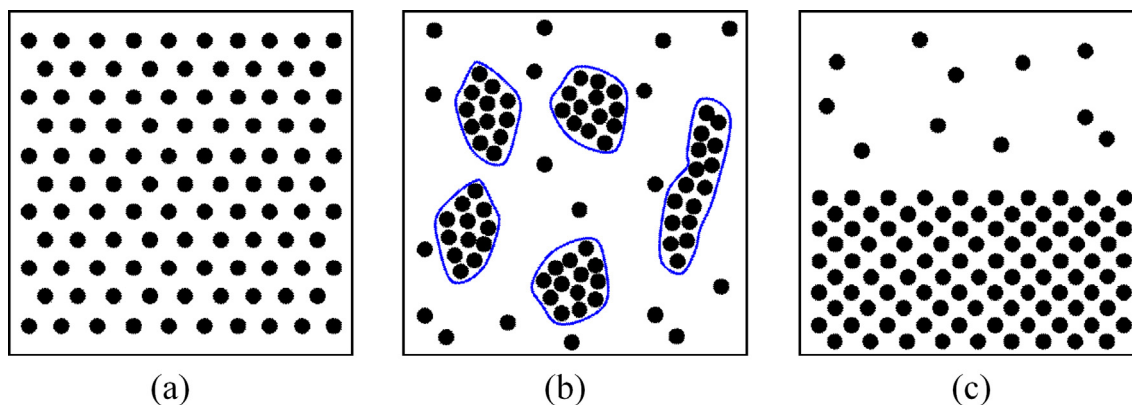


Fig. 13. Typical solid distributions within a computational grid: (a) homogeneous distribution; (b) heterogeneous structure A; (c) heterogeneous structure B.

2011; Parmentier et al., 2012; Radl & Sundaresan, 2014), slip velocity (Milioli et al., 2013; Sarkar et al., 2016; Schneiderbauer & Pirker, 2014), the variance of solid volume fraction (Schneiderbauer, 2017), etc. As the filtering process involves handling large data sets, machine learning techniques can be a promising way for model development. For example, Jiang et al. (Jiang et al., 2019) applied the neural network to derive a predictive model for sub-grid drift velocity and found that the solid volume fraction, slip velocity, and gas pressure gradient were important markers for estimating the drift velocity used in the filtered drag model. In contrast, the EMMS theory (Li & Kwauk, 1994) was proposed to describe the stability condition for heterogeneous flow structures. It demonstrated that the energy consumption for suspending and transporting particles per unit mass,  $N_{st}$ , tended to be minimal ( $N_{st} \rightarrow \min$ ). This theory was later extended to integrate with multi-scale numerical methods to quantify the effects of heterogeneous flow structures (Yang et al., 2003, 2004). The EMMS drag model regards the heterogeneous flow structures as two sub-systems (Fig. 13(b)), namely the dilute phase and dense (cluster) phase. In the EMMS drag model, the conservation equations for the dilute and dense phases, empirical cluster diameter correlation, and stability condition are solved to determine the drag force. Detailed information is documented in the literature (Chen et al., 2016; Shuai et al., 2014; Wang & Li, 2007). Compared with the homogeneous distribution, the presence of heterogeneous flow

structures leads to a reduced drag force. As shown in Fig. 14, the heterogeneity indices ( $H_d$ ) for the filtered drag model and EMMS drag model can be as low as  $\sim O(10^{-2})$  (Gao et al., 2018). Besides, the critical role of the local solid concentration gradient (Fig. 13(c)) in the interphase momentum exchange was also recognized, and the correction models were proposed to consider such heterogeneity (Li, Wang, et al., 2017; Su & Zhao, 2017; Zhu et al., 2018). The applicability of different drag models in simulating gas-solid flow in fluidized beds will be discussed in the following sections.

### 3.2.1. Bubbling fluidized bed

Homogeneous drag models are commonly used to simulate gas-solid flow in BFBs within coarse particles (Geldart Group B and D particles). Muller et al. (2008) compared the effects of different homogeneous drag models (i.e., Model C, E, and F in Table 4) in a BFB within Geldart Group D particles, and they found that the BVK drag model gave the best agreement with experimental data. Ku et al. (2013) also investigated the effects of three homogeneous drag models (i.e., Model C, modified Model D, and Model F in Table 4) in a BFB within Geldart Group D particles, and the results showed that the three drag models led to similar mean pressure profiles but different pressure fluctuations. Bakshi et al. (2015) compared the performance of Gidaspow and Syamlal-O'Brien drag models in modelling gas-solid flow in BFBs within Geldart Group B and D particles. They pointed out that the Gidaspow drag

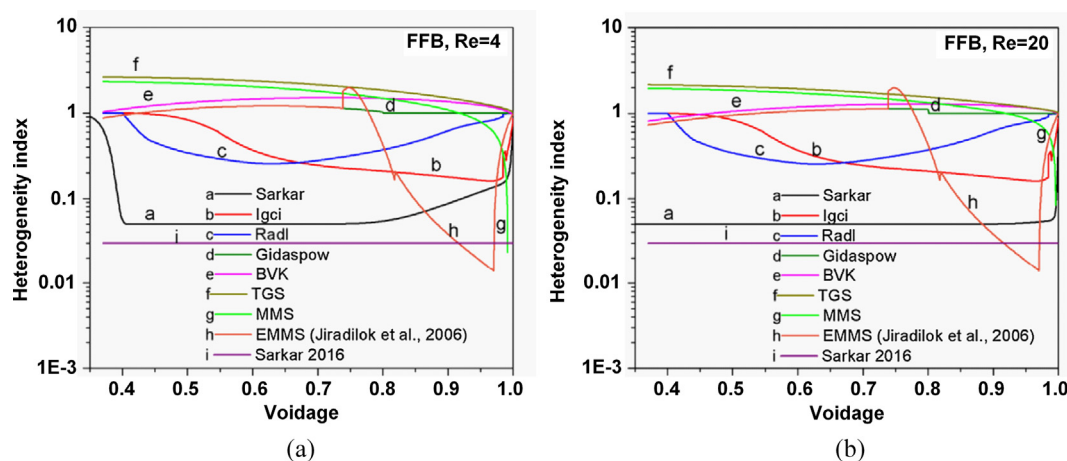


Fig. 14. Heterogeneity index ( $H_d$ ) of various drag models as a function of voidage at different Reynolds numbers (Re): (a) Re = 4; (b) Re = 20. Note that the drag models shown in the figures consist of: (i) homogenous drag models (Beetstra et al., 2007a; Gidaspow, 1994; Tenneti et al., 2011) (including Gidaspow, BVK, TGS). (ii) heterogeneous drag modes, including filtered drag models (Igci & Sundaresan, 2011; Radl & Sundaresan, 2014; Sarkar et al., 2016) (e.g., Sarkar, Igci, Radl, Sarkar), EMMS drag model (Yang et al., 2003) and MMS drag model (Mehrabadi et al., 2016). Reproduced from Gao et al. (2018).

model was more suitable for homogeneous bubbling fluidization regimes ( $U/U_{mf} < 4$ ) while the Syamlal-O'Brien drag model was only applicable for high gas velocity conditions ( $U/U_{mf} > 4$ ). A similar conclusion was also reported by Lungu et al. (2016).

The applicability assessment of several drag models was reported (Agrawal et al., 2018; Koralkar & Bose, 2016; Liu & van Wachem, 2019) based on the National Energy Technology Laboratory (NETL) BFB challenge problem (Geldart Group D particles) (Gopalan et al., 2016). Liu and van Wachem (2019) compared five homogenous drag models (i.e., Model A, B, C, E, and F in Table 4) in predicting gas-solid flow in the NETL BFB. The macroscopic flow characteristics (e.g., pressure drop, pressure fluctuation) predicted by the different drag models were qualitatively consistent. The BVK drag model could well capture the mean and root mean square (RMS) solid velocities under low gas velocity conditions. However, discrepancies between the prediction and experimental data in terms of several metrics (see Table 2) were still observed for all drag models. Agrawal et al. (2018) assessed various drag models (i.e., Model A, C, E, F, EMMS drag model, and Ayeni drag model (Ayeni et al., 2016)) in modelling gas-solid flow in the NETL BFB. The simulation results showed all drag models could not gain accurate prediction with experimental data for all fluidization conditions. Overall, the Di Felice drag model (Di Felice, 1994) and Ayeni drag model (Ayeni et al., 2016) gave a more reasonable prediction than the other drag models. Koralkar and Bose (2016) compared six drag models (i.e., Model A, B, C, D, E, and G) in modelling gas-solid flow in the NETL BFB, and the results showed that the Rong drag model gave the best prediction of pressure drop and RMS of solid velocity among all drag models.

For modelling gas-solid flow in BFBs within fine particles (Geldart Group A particles), the necessity of using heterogeneous drag models has been demonstrated by many studies based on the TFM (Feng et al., 2018; Hong et al., 2018; Li, Wang, et al., 2017; Li & Yang, 2017; Lv et al., 2014; Mckeen & Pugsley, 2003; Wang et al., 2016). Compared with homogenous drag models, the heterogeneous drag

models (e.g., EMMS drag model and filtered drag model) generally provide a better prediction of gas-solid flow in BFBs within fine particles. As shown in Fig. 15, Hong et al. (2018) found that the EMMS drag model correctly captured the radial profile of solid concentration, while the Gidaspow drag model led to a nearly uniform solid distribution with great discrepancies. It is worth noting that the heterogeneous drag models can be applicable for BFBs within small Geldart Group B particles. For example, Li and Yang (2017) investigated the effect of drag models on the flow hydrodynamics in five BFBs within small particles (65–350  $\mu\text{m}$ ). The results showed that the heterogeneous drag model yielded a more reasonable prediction than the Gidaspow drag model for both Geldart Group A and small Geldart Group B particles. However, both two drag models insignificantly affect gas-solid flow in BFBs within Geldart Group B particles.

### 3.2.2. Circulating fluidized bed

CFB has a lower solid concentration than BFB does, indicating the vital role of interphase interactions in modelling gas and solid hydrodynamics. In the CFB, the heterogeneous structures (i.e., cluster) significantly influence interphase interactions. Compared to the isolated particle, the gas-solid interactions, including the drag force (Helland et al., 2007; Shah et al., 2013) and mass transfer (Hou et al., 2013; Lu, Peters, & Kuipers, 2018; Wang, Luo, et al., 2017), are greatly reduced in the cluster. The effect of heterogeneous structures on gas-solid flow depends on the cluster size. Leckner (2017) pointed out that the cluster is much more pronounced for Geldart Group A particles and small Geldart Group B particles. The cluster nearly diminishes for Geldart Group D particles and large Geldart Group B particles. Lu et al. (2011) also found that the difference in prediction accuracy between the homogeneous and EMMS drag models diminished for large particles. A similar conclusion was also reported by Xie et al. (2018). Hence, the homogeneous drag model can yield reasonable gas-solid

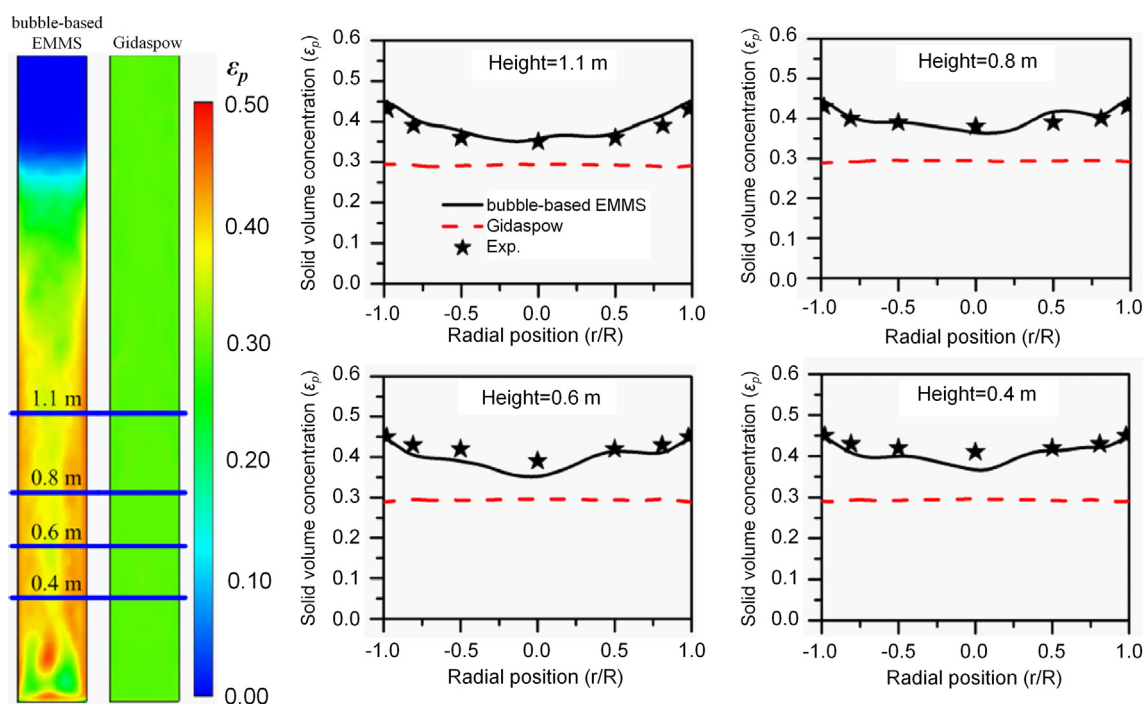


Fig. 15. Comparison of the predicted solid concentration distributions using the EMMS drag model and Gidaspow drag model for modelling gas-solid flow in BFB with Group A particles. Reproduced from Hong et al. (2018).

hydrodynamics when modelling CFBs within coarse particles (Li, Dietiker, & Shahnam, 2012; Luo et al., 2015; Xu et al., 2018).

On the other hand, many TFM or CGM studies showed that it was necessary to use heterogeneous drag models to simulate gas-solid flow in CFBs within fine particles (Dai et al., 2015; Li, Wang, et al., 2017; Shuai et al., 2014; Wang & Li, 2007; Yang et al., 2004). For instance, Xie et al. (2018) compared the effects of six homogenous drag models (Model A-E and Ergun-WenYu drag model), a filtered drag model (Sarkar drag model (Sarkar et al., 2016)) and three EMMS drag models (EMMS-Yang (Yang et al., 2003), EMMS-Matrix (Wang & Li, 2007) and EMMS-QL (Chen et al., 2016)) on the prediction accuracy of gas-solid flow in CFB risers. For the riser within Geldart Group A particles, the homogenous drag models extremely over-estimated the circulation flux by 350%. The EMMS-QL drag model provided the most accurate prediction of circulation flux estimation among all heterogeneous drag models with a relative error of 24%.

### 3.2.3. Discussions

It is hard to suggest which one is the best among all drag models for modelling gas-solid flow in all fluidization regimes. However, the assessment of available drag models still provides valuable principles for the selection of drag models in a specific fluidization regime. The heterogeneous drag models are unnecessary for modelling gas-solid flow in fluidized beds within coarse particles but are required for modelling gas-solid flow in fluidized beds within fine particles. Besides, the simulation accuracy of modelling gas-solid flow in fluidized beds within fine particles using heterogeneous drag models still needs to be improved. Specifically, the empirical cluster sub-models in the EMMS drag model play a vital role in prediction accuracy (Dai et al., 2015), but a general cluster-based sub-model is still lacking. As previously mentioned, the filtered drag model also needs further development to enhance generality and reliability (Gao et al., 2018).

In essence, the drag force combines the effects of voidage (also solid volume fraction) and slip velocity. Thus, the calculation of the voidage highly determines the drag force. Taking the CFD-DEM as an example, the fluid quantities need to be interpolated to the position of each particle and vice versa for calculating interphase momentum exchanges. The solid volume fraction in a specific cell is given by:

$$\varepsilon_s = \frac{1}{V_{cell}} \sum_{i=1}^n W_{interp,i} V_{p,i} \quad (52)$$

where  $V_{cell}$  is the cell volume and  $W_{interp,i}$  is the interpolation weight. In the CFD-DEM, the continuous gas phase and discrete particles are modelled under different frameworks. A bridge linking the two sides together is significant for calculating interphase momentum exchanges. As illustrated in Fig. 16(a), the particle needs the information of its local gas field quantities as its boundary conditions, and the effect of the presence of the particle should be transferred back to the governing equations of the gas phase through a source term. The interpolation from discrete particles to the continuum field is often termed backward interpolation or mapping. The interpolation from the continuum field to the particle position is termed forward interpolation. The calculation of voidage ( $\varepsilon_f$ ) and mapping of quantities ( $\phi$ ) from the discrete particles to the continuum field is achieved by several methods, as shown in Fig. 16(b) (Clarke et al., 2018). The simplest mapping scheme is the particle-centroid method (PCM), where a particle belongs to the cell within the particle centroid ( $W_{interp,i} \in [0, 1]$ ). Another commonly used mapping method is the divided particle volume method (DPVM). The interpolation weight is calculated based on the fraction of the particle volume occupied by nearby cells. In the

statistical kernel method, the interpolation weight is obtained based on the kernel function (e.g., Gaussian distribution), where a particle can influence a region 3–5 times larger than its diameter. The satellite point method employs multiple points to represent a particle, and the interpolation weight can then be determined by summing the satellite points. Different mapping methods lead to distinct local volume fractions. Clarke et al. (2018) demonstrated that the PCM was not suitable for the fine grid ( $\Delta/d_p = 1.6$ ), and the DPVM gave the best agreement with experimental data. Wang et al. (2019) demonstrated that the influence of more surrounding cells should be considered to accurately capture the drag force when the grid size was comparable to particle size ( $h/d_p \approx 1$ ). The results showed that the statistical kernel method provided a promising way to handle the scenario where the grid size approaches particle diameter.

### 3.3. Sensitivities of collision models

In addition to the interphase momentum exchange, an accurate simulation also relies on the proper selection of interparticle collision models. In general, particle collisions include particle-particle collisions and particle-wall collisions, both critical to the simulation of gas-solid flow in fluidized beds. The collision procedure can be fully resolved by the DEM while it is simplified and described by a solid stress term in the TFM based on the kinetic theory of granular flow. Note that the collision is oversimplified in the MP-PIC and DDPM. Hence, we mainly focus on the CFD-DEM and TFM in this section.

Collision parameters (e.g., restitution coefficient, friction coefficient) are used in both the CFD-DEM and TFM. In the CFD-DEM, the friction coefficient consists of the sliding friction coefficient and rolling friction coefficient. The friction coefficient in the following sections refers to the sliding friction coefficient for convenience unless specific definition. Besides, the repulsive force during the particle collision is linearly dependent on the spring constant. A higher spring constant leads to a shorter collision time. A small solid time step is usually required to capture particle collisions accurately when a high spring constant is used. Hence, a small spring constant is often used to reduce the computation cost. These parameters are the physical properties of the particle, but it is still challenging to obtain them through experimental measurements. As a result, the tuning of collision parameters is inevitable in practice to achieve a successful fluidized bed simulation.

#### 3.3.1. Bubbling fluidized bed

Some typical numerical studies of the collision models and parameters are summarized in Table 5. In general, the modelling of gas-solid flow in BFBs is found to be sensitive to collision models and parameters due to the relatively high solid concentration. The restitution coefficient characterizes the energy loss or retention during particle collisions, and a higher restitution coefficient corresponds to less energy loss. Several studies claimed that the simulation results were insensitive to the restitution coefficient as long as some routes of energy dissipation were provided (Li, Dietiker, & Shahnam, 2012; Müller et al., 2009), while many other studies demonstrated that the restitution coefficient played a vital role in reproducing fluidization dynamics (Goldschmidt et al., 2001; Reuge et al., 2008). Wang, Chao, and Jakobsen (2010) demonstrated that the restitution coefficient greatly influenced solid circulation patterns. Several studies showed that increasing the restitution coefficient led to fewer bubbles, and the perfect elastic collision ( $e = 1.0$ ) caused bubble elimination (Fede et al., 2016; Goldschmidt et al., 2001; Loha et al., 2014; Reuge et al., 2008; Verma et al., 2013; Zhao, Lu, & Zhong, 2015). In other words, the homogeneity of gas-solid flow is intensified with the

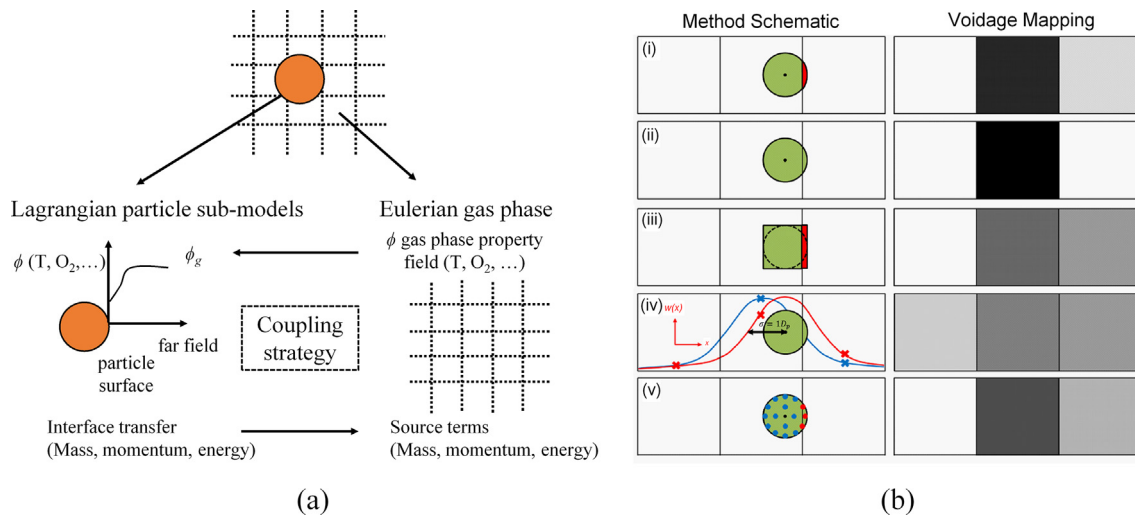


**Fig. 16.** (a) Interpolation between continuum field and discrete particles (Zhang et al., 2020); (b) Different backward interpolation/mapping methods of the voidage: (i) analytical method, (ii) particle centroid method (PCM), (iii) divided particle volume method (DPVM), (iv) statistical kernel method, and (v) satellite point method. Reproduced from Clarke et al. (2018).

**Table 5**  
Evaluations of the collision models and parameters.

Method	Models and Parameters	Literature
BFB Parameters	Restitution coefficient	DEM: Goldschmidt et al. (2001); Li and Kuipers (2007); Müller et al. (2009); He et al. (2012); Ku et al. (2013); Bakshi, Altantzis, et al. (2018); TFM: Reuge et al. (2008); Wang, Chao, and Jakobsen (2010); Li et al. (2010); Verma et al. (2013); Loha et al. (2014); Zhao, Zhou, et al. (2015); Fede et al. (2016); Geng et al. (2016); Yang, Padding, Buist, and et al. (2017)
	Friction coefficient	DEM: Li and Kuipers (2007); Müller et al. (2009); Ku et al. (2013); Bakshi, Altantzis, et al. (2018); Hamidouche et al. (2019)
	Specularity coefficient	TFM: Li et al. (2010); Li and Benyahia (2012); Loha et al. (2013); Altantzis et al. (2015); Bakshi et al. (2015); Fede et al. (2016); Geng et al. (2016)
Models	Solid stress model	TFM: Patil et al. (2010); Reuge et al. (2008); Verma et al. (2013); Farzaneh et al. (2015); Geng et al. (2016); Yang et al. (2016); Lungu et al. (2016); Kia and Aminian (2017); Haghgoo et al. (2018)
	Solid boundary model	TFM: Reuge et al. (2008); Fede et al. (2016); Geng et al. (2016); Yang, Padding, Buist, and et al. (2017); Haghgoo et al. (2018)
CFB Parameters	Restitution coefficient	DEM: Zhang et al. (2008); Han et al. (2015); Liu, Papadikis, et al. (2017) TFM: Almuttahir and Taghipour (2008b); Jin et al. (2010); Cloete et al. (2011); Benyahia (2012); Kong et al. (2014); Upadhyay and Park (2015); Cloete et al. (2016)
	Friction coefficient	DEM: Zhang et al. (2008); Han et al. (2015); Liu, Papadikis, et al. (2017)
	Specularity coefficient	TFM: Jin et al. (2010); Cloete et al. (2011); Benyahia (2012); Kong et al. (2014); Upadhyay and Park (2015); Cloete et al. (2016)
Models	Solid stress model	TFM: Cloete et al. (2011); Upadhyay and Park (2015); Qiu et al. (2017)
	Solid boundary model	TFM: Almuttahir and Taghipour (2008a); Kong et al. (2014); Upadhyay and Park (2015); Cloete et al. (2016)

increased restitution coefficient. However, conclusions about the influence of the restitution coefficient on bed height can be controversial. Some studies demonstrated that increasing the restitution coefficient led to a higher bed height (Bakshi, Altantzis, et al., 2018; Fede et al., 2016; Reuge et al., 2008; Verma et al., 2013). Loha et al. (2014) and Li and Benyahia (2012) pointed out that the bed height increased with the decrease in the restitution coefficient. Zhao, Zhou, et al. (2015) demonstrated that the solid translational kinetic energy was doubled when the restitution coefficient was reduced from 0.97 to 0.6. It was interesting to find that increasing the restitution coefficient resulted in a lower solid kinetic energy. It is noted that several studies of the spouted bed also demonstrated that increasing the restitution coefficient restrained translational particle movements (Hu et al., 2019a, 2019b; van Buijtenen et al., 2009; Yang et al., 2014a). Specifically, Hu et al. (2019a, 2019b) demonstrated that increasing the restitution coefficient led to an intensified particle-wall interaction, which

in turn restrained the translational particle movements. For the BFB, further efforts are required to clarify the comprehensive influence of the restitution coefficient.

The friction coefficient is used to determine the sliding effect of the collision in the tangential direction. During the collision procedure, the energy loss tends to increase at the increased friction coefficient. However, controversies still exist about the influence of the friction coefficient on bed hydrodynamics. Müller et al. (2009) found that the friction coefficient showed a minor effect on voidage distributions. Based on the CFD-DEM, Bakshi, Altantzis, et al. (2018) pointed out that increasing the friction coefficient reduced bed height. Nevertheless, the TFM simulations conducted by Yang, Padding, Buist, and et al. (2017) and Zhao, Zhou, et al. (2015) suggested that increasing friction coefficient led to more vigorous solid movements and more considerable bed expansion. Further investigations are still needed to clarify the influence of the friction coefficient. The above discussions are about the sliding friction

coefficient, and special attention needs to be paid to the rolling friction coefficient. The rolling torque is generated from the rolling friction that is related to the rolling friction coefficient. [Goniva et al. \(2012\)](#) numerically studied the effect of the rolling friction coefficient on the particle velocity in a pseudo-2D spout-fluidized bed where a dilute phase is in the spout region while a dense phase is in the annulus region. The results demonstrated that increasing the rolling friction coefficient from 0 to 0.125 improved the prediction accuracy in the annulus region where the particle-particle/wall collision force is dominant. However, the rolling friction coefficient has a negligible influence in the spout region where gas-solid drag force is dominant (see [Fig. 17](#)). This conclusion was also convinced by [Yang et al. \(2016b\)](#), who found that further elevating the rolling friction coefficient from 0.125 to 0.35 insignificantly improved prediction accuracy. The above conclusions indicate that the rolling friction coefficient is necessary for modelling collision-dominated dense gas-solid flow in BFBs but is expected to be unnecessary in modelling drag-dominated dilute gas-solid flow in CFBs.

In the CFD-DEM, the particle-particle/wall collisions are commonly modelled using the soft-sphere contact model based on a linear spring-dashpot (LSD) assumption or a non-linear Hertzian assumption. The rebound feature of the colliding particles is described by the spring constant and Young's modulus, respectively. Most researchers continue to use the LSD model due to its simplicity, and reasonable accuracy for different applications ([Bakshi, Altantzis, et al., 2018](#); [Di Renzo & Di Maio, 2004](#)). In the LSD model, the spring represents the rebound off the colliding particles and the dashpot mimics energy dissipation arising from inelastic particle deformation. Due to the difficulties in the measurement of impact properties, the spring constant is often estimated based on different analytical and semiempirical approaches. Tangential-normal spring stiffness ratio  $k_t/k_n$  depends on the structural properties and is approximately  $2/3$  for most materials ([Silbert et al., 2001](#)). For non-cohesive particles, the choice of spring stiffness is shown to have little impact on bubbling dynamics ([Gu et al., 2016](#); [Kaneko et al., 1999](#); [Moreno-Atanasio et al., 2007](#)) while other studies indicate severe consequences on particle velocities ([Lommen et al., 2014](#); [Paulick et al., 2015](#)). Recently, via identifying critical model parameters in CFD-DEM simulations of 3D fluidized beds through multivariate sensitivity analysis, [Bakshi, Altantzis, et al. \(2018\)](#) pointed out that an extremely low spring constant ( $k_n = 10$  N/m) led to unrealistic gas-solid dynamics. They suggested

the spring constant in modelling low-velocity (10–30 m/s) fluidized beds should be larger than 100 N/m. [Lungu et al. \(2022\)](#) demonstrated that the CG-DEM was sensitive to the value of the spring constant specified, unlike the conventional CFD-DEM. Increasing the spring constant by a factor of 10 from 80 N/m to 8000 N/m gradually altered the fluidization dynamics from slugging/bubbling to a flow structure resembling fast fluidization for all operating conditions. The influence of spring constant on bed hydrodynamics needs to be further assessed.

The non-linear Hertzian model has been increasingly applied in DEM simulations with the rapid development of computer hardware because this model is time-expensive to resolve the collision procedure by integrating overlap displacements between two particles ([Horabik & Molenda, 2016](#)). In the non-linear Hertzian model, Young's modulus is a mechanical property that measures the tensile or compressive stiffness of a solid material when the force is applied lengthwise, which quantifies the relationship between tensile/compressive stress and axial strain in the linear elastic region. In the DEM simulation, Young's modulus with several orders smaller (1–100 MPa) than the original one (1–100 GPa) is commonly used as a general practice, so bigger time steps can be taken for simulations to reduce computational costs ([Qi, 2017](#)). The contact radius is overestimated with the smaller Young's modulus in the DEM model which results in an over-prediction of the conductive heat transfer rate. A coefficient  $c (= (Y^*/Y_0)^{1/5})$  is incorporated to correct the overestimated contact radius ([Zhou et al., 2008](#)), which is related to the value of Young's modulus used in the DEM model  $Y^*$  and the real value of Young's modulus of the materials. Moreover, according to the sensitivity study of the particle properties in the CFD-DEM simulation ([Yang et al., 2014b](#)), Young's modulus in the range of  $10^7$ – $10^{10}$  Pa insignificantly affects simulation results.

[Zhao, Zhou, et al. \(2015\)](#) simulated gas-solid flow in a pseudo-2D BFB using the TFM, and they found that the particle-wall friction coefficient was the most important parameter, followed by the normal restitution coefficient for inter-particle collision. The inter-particle friction coefficient, tangential restitution coefficient, and normal particle-wall restitution coefficient showed minor effects. [Yang, Padding, Buist, et al. \(2017\)](#) investigated the influences of collision parameters in modelling a pseudo-2D BFB, and they found that the inter-particle friction coefficient significantly affected the solid movements while the inter-particle restitution coefficient had an insignificant impact. [Bakshi, Altantzis, et al. \(2018\)](#)

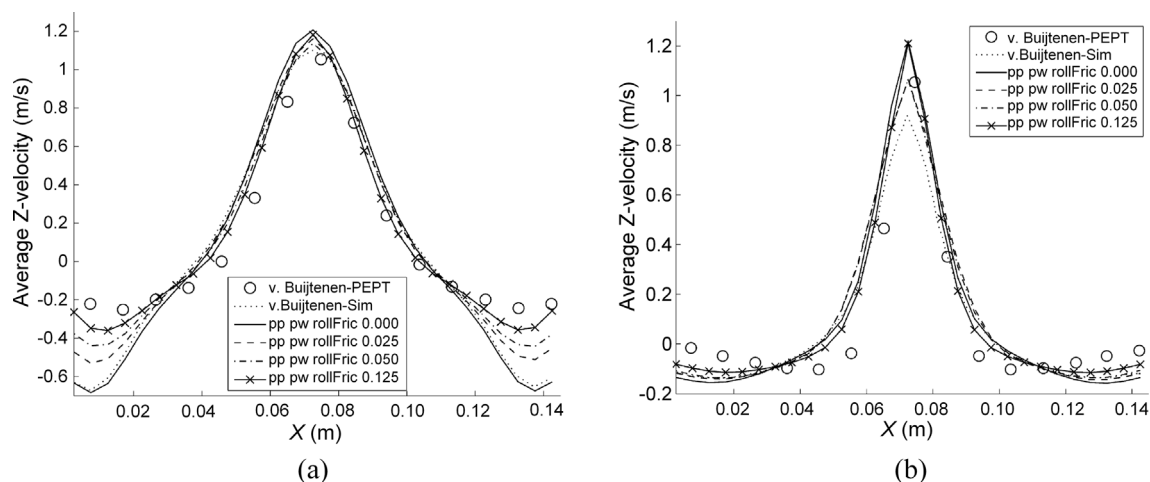


**Fig. 17.** Profiles at the height  $z = 0.1$  m (a) and  $z = 0.05$  m (b) of time-averaged vertical particle velocity for varying particle-particle rolling friction, with the present results being compared to data obtained with PEPT and simulation both by [van Buijtenen et al. \(2011\)](#). Reproduced from [Goniva et al. \(2012\)](#).

comprehensively analyzed the sensitivity of collision parameters in simulating gas-solid flow in a pseudo-2D fluidized bed. Four metrics were used for evaluation, i.e., bubble size, lateral bubble position, particle root mean square (RMS) velocity, and average particle height. As shown in Fig. 18 regarding the quantification of sensitivity using a Morris-One-At-a-Time (MOAT) method, the most influential parameters were found to be the inter-particle friction coefficient, inter-particle restitution coefficient, particle-wall restitution coefficient, and inter-particle tangential-normal damping ratio. Besides, the particle RMS velocity, average bubble size, and average height increased when the lower-energy-dissipation parameters were adopted, i.e., a larger restitution coefficient and a smaller friction coefficient. Moreover, the effects of the restitution coefficient, friction coefficient, and tangential damping strongly interacted with each other. For instance, the sensitivity to the normal restitution coefficient decreased with the increase in friction coefficient. Thus, uncertainty quantification could be an essential tool to evaluate the influence of collision parameters. Other parameters (e.g., operating conditions and bed geometry) will also perform an interactive effect on the collision parameters, which requires further studies.

As pointed out by Wu et al. (2019), the solid stress model continues to be a major challenge for the TFM modelling of fluidized

beds, especially BFBs within the dense gas-solid flow. The solid stress tensor is generally divided into two components, i.e., (a) kinetic-collisional stress and (b) frictional stress. For a BFB, frequent collisions between particles require a consideration of the stress caused by the Coulomb friction. Table 6 summarizes the commonly used frictional stress models, which are critical for the accurate simulation of gas-solid flow in BFBs (Wu et al., 2019). Several models were developed from the critical theory of soil mechanics, e.g., Johnson and Jackson (Johnson & Jackson, 1987), Schaeffer (Schaeffer, 1987) and Srivastava-Sundaresan (Srivastava & Sundaresan, 2003) models. Jop et al. (2006) developed a frictional stress model based on local rheological principles. Farzaneh et al. (2015) compared the three frictional models (Model I, II, and III in Table 6) and they demonstrated that the model proposed by Jop et al. (2006) showed the best agreement with experimental data when simulating gas-solid flow in a BFB. The Schaeffer model (Schaeffer, 1987) and Srivastava-Sundaresan model (Srivastava & Sundaresan, 2003) led to the unrealistic movements of fuel particles and significantly underestimated the circulation time of fuel particles. Yang et al. (2016) compared the Jenkins-Zhang model and their newly proposed KTGF for rough spheres in modelling gas-solid flow in a BFB within Geldart Group D particles. They pointed out that the KTGF model considering rough spheres gave a

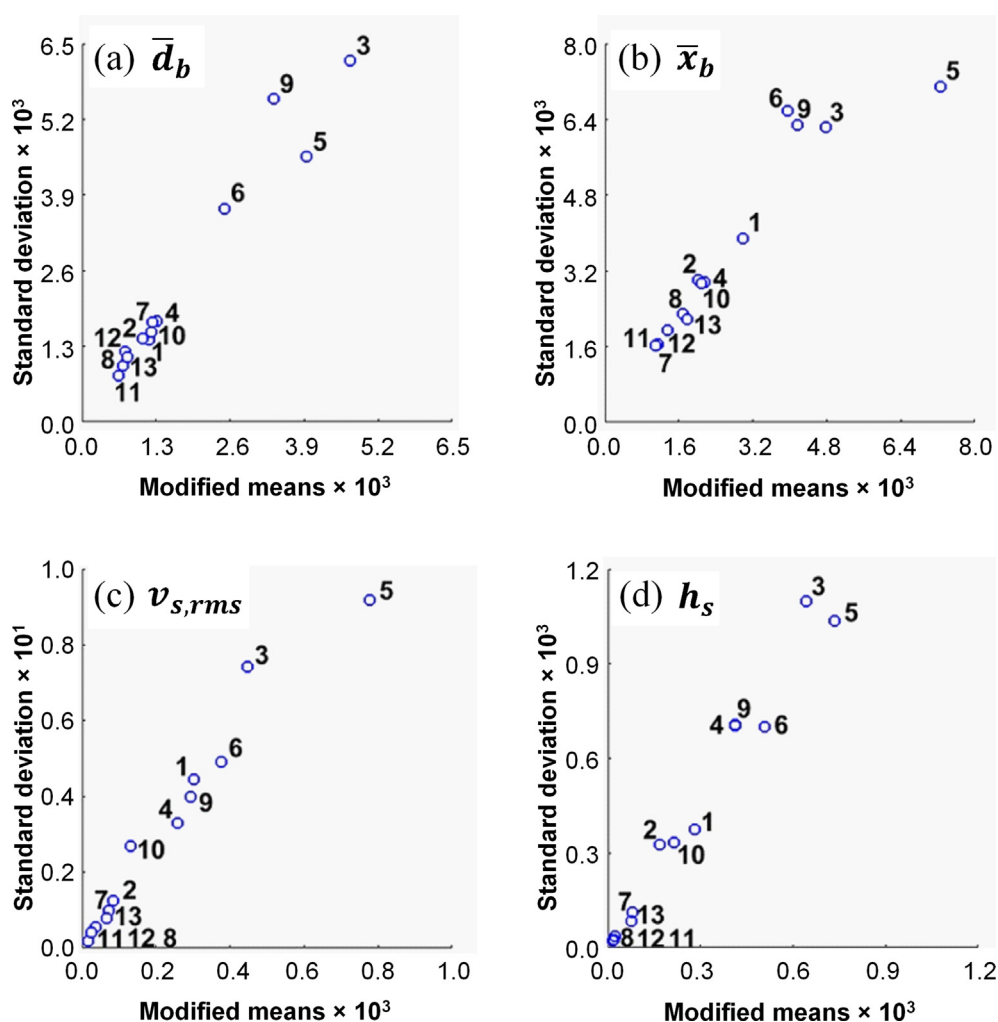


**Fig. 18.** The sensitivities of (a) bubble size, (b) lateral bubble location, (c) root mean square (RMS) velocity and (d) average particle height to various parameters. The most influential parameters P3, P4, P5, P6, and P9 refer to the inter-particle friction coefficient, particle-wall friction coefficient, inter-particle restitution coefficient, particle-wall restitution coefficient and inter-particle tangential-normal damping ratio, respectively. Reproduced from Bakshi, Altantzis, et al. (2018).

**Table 6**  
Summary of typical used frictional stress models in the TFM.

No.	Model	Coefficient
I	Schaeffer (Schaeffer, 1987)	$\tau_{s,f} = -P_{s,f}\mathbf{I} + 2\mu_{s,f}\mathbf{S}_s$ $p_{s,f} = \begin{cases} 10^{25}(\epsilon_s - \epsilon_s^{\max})^{10} & \epsilon_s > \epsilon_s^{\max} \\ 0 & \epsilon_s < \epsilon_s^{\max} \end{cases}$ $\mu_{s,f} = \begin{cases} \frac{\sqrt{2}p_{s,f} \sin(\phi)}{2\sqrt{\mathbf{S}_s : \mathbf{S}_s}} & \epsilon_s > \epsilon_s^{\max} \\ 0 & \epsilon_s < \epsilon_s^{\max} \end{cases}$ $\mathbf{S}_s = \frac{1}{2}[\nabla\mathbf{u}_s + (\nabla\mathbf{u}_s)^T] - \frac{1}{3}(\nabla \cdot \mathbf{u}_s)\mathbf{I}$
II	Srivastava-Sundaresan (Srivastava & Sundaresan, 2003) (ie., Princeton model)	$\tau_{s,f} = -P_{s,f}\mathbf{I} + 2\mu_{s,f}\mathbf{S}_s$ $p_{c,f} = \begin{cases} 10^{25}(\epsilon_s - \epsilon_s^{\max})^{10} & \epsilon_s \geq \epsilon_s^{\max} \\ \text{Fr} \frac{(\epsilon_s - \epsilon_s^{\min})^r}{(\epsilon_s^{\max} - \epsilon_s)^s} & \epsilon_s^{\max} > \epsilon_s \geq \epsilon_s^{\min} \\ 0 & \epsilon_s^{\min} > \epsilon_s \end{cases}$ $\text{Fr} = 0.5, r = 2 \text{ and } s = 5$ $\frac{p_{s,f}}{p_{c,f}} = \left(1 - \frac{\nabla \cdot \mathbf{u}_s}{n\sqrt{2}\sin(\phi)\sqrt{\mathbf{S}_s : \mathbf{S}_s + \Theta/d_p^2}}\right)^{n-1}$ $\mu_{s,f} = \frac{\sqrt{2}p_{s,f} \sin(\phi)}{\sqrt{\mathbf{S}_s : \mathbf{S}_s + \Theta/d_p^2}} \left[ n - (n-1) \left(\frac{p_{s,f}}{p_{c,f}}\right)^{\frac{1}{n-1}} \right]$ $n = \begin{cases} \frac{\sqrt{3}}{2\sin(\phi)} & \nabla \cdot \mathbf{u}_{sm} \geq 0 \\ 1.03 & \nabla \cdot \mathbf{u}_{sm} < 0 \end{cases}$ $\mathbf{S}_s = \frac{1}{2}[\nabla\mathbf{u}_s + (\nabla\mathbf{u}_s)^T] - \frac{1}{3}(\nabla \cdot \mathbf{u}_s)\mathbf{I}$
III	Jop (Jop et al., 2006)	$\tau_{s,f} = \begin{cases} -P_{iso}\mathbf{I} - 2\mu_{s,f}(I)\frac{\mathbf{\Gamma}}{ \mathbf{\Gamma} } & \epsilon_s \geq \epsilon_s^{\min} \\ 0 & \epsilon_s < \epsilon_s^{\max} \end{cases}$ $\mu_{s,f}(I) = \mu_1 + \frac{\mu_2 - \mu_1}{I_0/I + 1}$ $\mathbf{\Gamma} = \nabla\mathbf{u}_s + (\nabla\mathbf{u}_s)^T$ $I = \frac{d_p \mathbf{\Gamma} }{(P_{iso}/\rho_s)^{0.5}}$ $I_0 = 0.279, \mu_1 = \tan(20.9) \text{ and } \mu_2 = \tan(32.76)$
IV	Jenkins-Zhang (Jenkins & Zhang, 2002)	$e_{eff} = e - \frac{1}{2}a_1 + \frac{1}{2}a_2\frac{b_1}{b_2}$ $a_1 = \frac{\mu}{\mu_0} \left[ \pi\mu_0 \left(1 - \frac{2}{\pi} \arctan \mu_0\right) + \frac{2\mu_0^2}{1 + \mu_0^2} \left(1 - 2\frac{\mu}{\mu_0}\right) \right]$ $a_2 = \frac{5\mu}{2\mu_0} \left[ \frac{\pi}{2}\mu_0 \left(1 - \frac{2}{\pi} \arctan \mu_0\right) + \frac{\mu_0^2 - \mu_0^4}{(1 + \mu_0^2)^2} \right]$ $b_1 = \left(\frac{\mu}{\mu_0}\right)^2 \frac{\mu_0^2}{1 + \mu_0^2}$ $b_2 = \frac{\mu}{2\mu_0} \left[ \frac{\pi}{2}\mu_0 \left(1 - \frac{2}{\pi} \arctan \mu_0\right) + \frac{\mu_0^2}{1 + \mu_0^2} \right]$ $\mu_0 = \frac{7\mu(1+e)}{1+\beta_0}$

better prediction of solid velocity and volume fraction than the traditional KTGf model.

The description of particle-wall collisions, i.e., the solid boundary model, also plays a vital role in the TFM simulation of BFBs. In the previous studies (Bakshi et al., 2015; Li et al., 2010; Loha et al., 2013), the model proposed by Johnson and Jackson (1987) was most used, in which the specularity coefficient is introduced to characterize the momentum exchange between the particle and wall in the tangential direction. Compared with collision parameters (e.g., restitution coefficient and friction coefficient), the specularity coefficient is unavailable from the experimental measurements but specified according to the given condition. In general, increasing the specularity coefficient results in a more

significant wall hindrance. Several studies demonstrated that the specularity coefficient was an important parameter that significantly affected the overall solid behaviours in pseudo-2D fluidized bed systems (Bakshi et al., 2015; Li et al., 2010; Loha et al., 2013). For instance, Altantzis et al. (2015) investigated the influence of the specularity coefficient on bed hydrodynamics in a thin rectangular gas-solid fluidized bed, and found that the specularity coefficient significantly affected bubble characteristics (see Fig. 19). Specifically, increasing the specularity coefficient causes more bubbles with smaller bubble sizes and the resultant lower solid circulation fluxes. Nevertheless, Bakshi et al. (2015) pointed out that the gas-solid hydrodynamics was insensitive to the specularity coefficient in the simulation of 3D BFBs. The specularity coefficient was

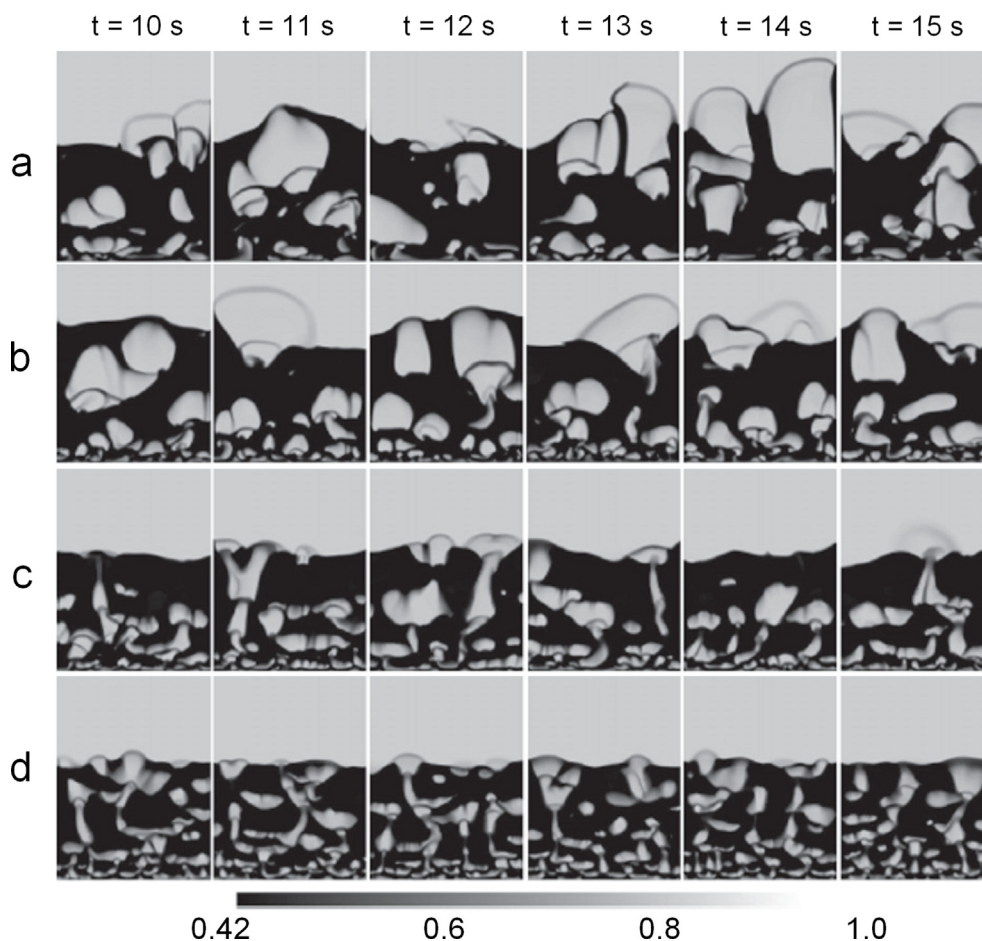


**Fig. 19.** Instantaneous solid volume fraction distributions in a thin BFB at  $U = 1.75U_{mf}$  with different specular coefficients ( $\phi$ ): (a)  $\phi = 0.0005$ , (b)  $\phi = 0.005$ , (c)  $\phi = 0.05$  and (d)  $\phi = 0.5$ . Reproduced from Altantzis et al. (2015).

suggested to be specified as 0.01–0.3. The particle-wall interaction insignificantly influenced bed hydrodynamics in large-scale 3D systems than in small-scale 3D or pseudo-2D systems. Besides, researchers proposed various specular coefficient models which quantitatively correlated the specular coefficient with the particle-wall restitution coefficient and friction coefficient (Li & Benyahia, 2012; Zhao et al., 2016). In addition to the Johnson-Jackson boundary model, novel solid boundary models were proposed considering both sliding and non-sliding scenarios (Schneiderbauer et al., 2012) and rotational granular temperature (Yang, Padding, Buist, & et al., 2017; Zhao et al., 2014).

### 3.3.2. Circulating fluidized bed

Compared with the BFB, the CFB operated under a fast fluidization regime weakens the role of inter-particle collisions in gas-solid hydrodynamics. Upadhyay and Park (2015) reported a TFM simulation of gas-solid flow in a 2D CFB riser, and they found a higher inter-particle restitution coefficient resulted in a lower solid concentration in the bottom and near-wall regions. Jin et al. (2010) also investigated the effect of the inter-particle restitution coefficient based on the 2D TFM simulation and found that the solid concentration showed a similar trend (Upadhyay & Park, 2015). Besides, the effect of the restitution coefficient was enhanced for large particles ( $d_p = 300 \mu\text{m}$ ), as compared with small particles ( $d_p = 60 \mu\text{m}$ ). This finding was further evidenced by Benyahia (2012) and Wang et al. (2012). They reported that the restitution coefficient performed a minor effect on the bed hydrodynamics in

CFB risers within small particles. Han et al. (2015) investigated the liquid-solid flow hydrodynamics in a 3D CFB riser using the CFD-DEM method and found the collision parameters showed a minor effect on the mean residence time.

Upadhyay and Park (2015) demonstrated that the stress model proposed by Syamlal et al. (1993) gave a good agreement with experimental data for predicting solid concentration in the middle and top regions of the bed, while the model proposed by Gidaspow (1994) well-captured flow structures in the bottom part of the bed. Nonetheless, Qiu et al. (2017) suggested that solid stress played a minor role in predicting bed hydrodynamics in a 3D CFB. They compared the simplified TFM that neglected the solid stress term with the standard TFM. The prediction from these two models showed slight differences.

Several studies showed that the particle-wall restitution coefficient insignificantly influenced bed hydrodynamics (Almuttahir & Taghipour, 2008b; Jin et al., 2010; Kong et al., 2014; Wang, Chao, & Jakobsen, 2010). In contrast, the specular coefficient was found to have a profound effect. Jin et al. (2010) demonstrated that the specular coefficient significantly affected the solid concentration distribution. Cloete et al. (2016) pointed out that the Schneiderbauer boundary model (Schneiderbauer et al., 2012) could better reproduce the experimental data than the Johnson-Jackson boundary model (Johnson & Jackson, 1987).

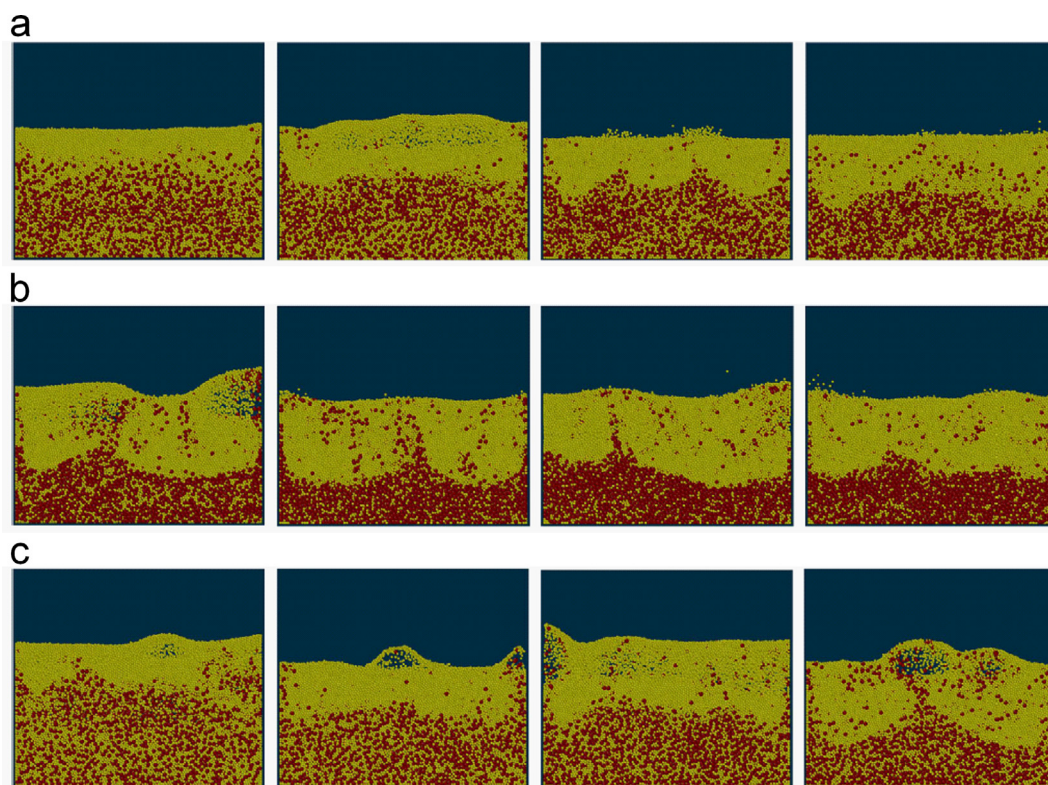


**Fig. 20.** CFD-DEM simulations of binary fluidized beds at 15 s, 30 s, 45 s and 60 s respectively using: (a) the Beetstra et al. drag model with polydisperse correction, (b) the Ergun drag model and (c) the Ergun model with polydisperse correction. The yellow and red particles are 1.5 mm and 2.5 mm in diameter. Reproduced from [Olaofe et al. \(2014\)](#). (For interpretation of the references to colour in this figure legend, the reader is referred to the Web version of this article.)

### 3.3.3. Polydisperse fluidized bed

Polydisperse particles are commonly practised in fluidized bed applications. Most previous studies focused on monodisperse particles while little attention was paid to polydisperse particles. One of the research topics of polydisperse particles in the BFB is segregation. The experiment about the BFB with binary particles by [Goldschmidt et al. \(2003\)](#) was frequently employed for model validation. Various drag models have been proposed considering the polydispersity effect ([Beetstra et al., 2007b](#); [Cello et al., 2010](#); [Holloway et al., 2010](#); [Rong et al., 2014](#)). The segregation behaviour was found to be sensitive to the drag models ([Beetstra et al., 2007b](#); [Jiang et al., 2018](#); [Olaofe et al., 2014](#); [Zhang et al., 2017](#)). In general, polydisperse drag models can reproduce more realistic segregation behaviour than monodisperse drag models. For instance, [Olaofe et al. \(2014\)](#) compared three drag models in predicting binary fluidized beds within Geldart Group D particles. As shown in [Fig. 20](#), the Ergun drag model resulted in a fast segregation behaviour that fine and coarse particles are separated more completely. The polydisperse drag models agreed better with experimental data than the Ergun drag model. Nonetheless, the polydisperse drag models could not reasonably capture the segregation behaviour in fluidized beds with a high initial bed height.

As pointed out by [Gera et al. \(2004\)](#), the TFM tended to over-predict the segregation rate of BFBs within binary particles. Accordingly, several researchers investigated the particle-particle drag model, which accounts for the friction force between different solid phases ([Chao et al., 2012](#); [Fan & Fox, 2008](#); [Gera et al., 2004](#); [Syamlal & O'Brien, 1987](#)). The particle-particle drag model was found to slow down the segregation process. Empirical parameters were employed in these models for tuning purposes, inhibiting their universal applications. The commonly used KTGF model was feasible for monodisperse particles. Some researchers

also proposed novel KTGF models suitable for polydisperse particles ([Chao et al., 2011](#); [Garzo et al., 2007](#); [Huilin et al., 2010](#); [Iddir & Arastoopour, 2005](#); [Jenkins & Mancini, 1987](#); [van Sint Annaland et al., 2009a](#)). [van Sint Annaland et al. \(2009b\)](#) assessed the performance of different KTGF models and found that the segregation rate predicted by the polydisperse KTGF model was approximately half of the conventional KTGF model. Moreover, the former gained a better prediction of experimental data than the latter did.

Fewer studies were reported in terms of the CGM to predict the segregation behaviours in BFBs. [O'Rourke and Snider \(2014\)](#) pointed out that the MP-PIC overpredicted the segregation rate and proposed a blended acceleration model to slow down the segregation process. The MP-PIC fails to predict polydisperse fluidized beds, which results from the over-simplification of inter-particle collisions. Particle friction that significantly affects segregation behaviours is usually neglected in the MP-PIC. Moreover, [Lu, Peters, and Kuipers \(2018\)](#) used the CG-DEM to simulate a fluidized bed within binary particles and achieved a reasonable prediction of the segregation rate.

Employing an extended KTGF model considering binary particles, [Lu, Peters, and Kuipers \(2018\)](#) simulated a CFB riser within binary particles based on the experiment conducted by [Mathiesen et al. \(1999\)](#). The predicted solid concentration, mean particle diameter, and solid velocity agreed well with experimental data. Based on the KTGF model proposed by [Chao et al. \(2011\)](#) and the EMMS drag model, [Qin and Wang \(2019\)](#) simulated two CFB risers within binary particles. A good agreement between simulation results and experimental data was achieved regarding the distributions of pressure drop and solid flux. [Zhou and Wang \(2015\)](#) evaluated the influences of the KTGF model and particle-particle drag model for simulating a CFB riser within binary particles.

They suggested that both models should be employed to obtain a reasonable prediction.

#### 4. Summary and conclusions

The applicability of multi-scale numerical methods (e.g., PR-DNS, CFD-DEM, and TFM) in predicting gas-solid flow in fluidized beds at specific fluidization regimes (e.g., bubbling fluidization region, fast fluidization regime) is comprehensively assessed in this state-of-the-art review, with a focus on the inter-particle collision models, inter-phase interaction models, collision parameters, and polydispersity effect. The conclusion are drawn as below.

- (1) A mutual restriction exists between resolution and efficiency. Higher-resolution methods (e.g., PR-DNS) need more computational resources and thus are suitable for smaller-scale simulations to provide a database for closure development. Lower-resolution methods (e.g., TFM) require fewer computational resources and thus underpin large-scale simulations to explore macro-scale phenomena. With the introduction of the parcel concept and solid stress model into the CFD-DEM framework, the coarse-grained method including CG-DEM, MP-PIC, and DDPM achieves a compromise between the resolution and efficiency.
- (2) The PR-DNS provides the most accurate prediction of gas-solid flow in BFBs but is incapable of simulating gas-solid flow in CFBs due to unaffordable computational costs. The CFD-DEM reasonably predicts gas-solid flow in BFBs and CFBs but needs further validations for fluidized beds within fine particles. The TFM requires more model tuning than the other methods and is difficult in obtaining particle-scale information (e.g., shrinkage, polydispersity). The MP-PIC is suitable for modelling CFBs within drag-dominated flow but deviates significantly in modelling BFBs within the collision-dominated flow. Model validations need to be further conducted under multiple flow conditions and comprehensive metrics (e.g., velocity profiles at different heights, bubbles, or cluster characteristics).
- (3) The homogeneous drag models (e.g., Gidaspow drag model) are feasible for modelling gas-solid flow in BFBs within coarse particles but are difficult to reproduce gas-solid flow in CFBs within clusters or BFBs within fine particles. The incapability of the homogeneous drag models can be overcome by heterogeneous drag models which include the filtered drag model and EMMS drag model. A general cluster-based sub-model needs to be developed to improve the generality of the EMMS drag model. The DPVM allows the grid size to be slightly larger than the particle diameter, providing a better prediction of gas-solid flow in fluidized beds than the traditionally used PCM. The grid-independent statistical kernel method shows potential in the future development of the CFD-DEM with a balance between accuracy and efficiency.
- (4) In the CFD-DEM, the rolling friction coefficient is necessary for modelling collision-dominated flow in BFBs but is expected to be unnecessary in modelling drag-dominated flow in CFBs. An extremely low spring constant ( $k_n = 10 \text{ N/m}$ ) causes unrealistic gas-solid dynamics, which should be larger than  $100 \text{ N/m}$  in modelling low-velocity ( $10\text{--}30 \text{ m/s}$ ) fluidized beds. Young's modulus with several orders smaller ( $1\text{--}100 \text{ MPa}$ ) than the original one ( $1\text{--}100 \text{ GPa}$ ) is commonly used as a general practice, allowing bigger time steps in simulations to reduce computational costs. Uncertainty quantification is expected to be an essential tool to evaluate the influence of collision parameters. In the TFM, frictional

stress models and specular coefficient are critical for the accurate simulation of gas-solid flow in BFBs. The restitution coefficient shows a more significant influence on predicting gas-solid flow in CFBs within large particles than that within small particles. Sub-models considering the polydispersity effect improve the prediction of key phenomena (e.g., segregation) in fluidized beds.

Overall, the challenges of the simulation of gas-solid flow in fluidized beds lie in two aspects: (i) the interconnection of sub-models and parameters; (ii) the interconnection of operating parameters, solid properties, geometrical configurations, polydispersity, and multi-physics forces. More validations need to be carried out for further improvement of the applicability of each numerical method.

#### Declaration of competing interest

The authors declare that they have no known competing financial interests or personal relationships that could have appeared to influence the work reported in this paper.

#### Acknowledgements

This work was supported by the National Natural Science Foundation of China (No. 51925603) and the Fundamental Research Funds for the Central Universities (No. 2022ZFJH004).

#### References

- Acosta-Iborra, A., Sobrino, C., Hernandez-Jimenez, F., et al. (2011). Experimental and computational study on the bubble behavior in a 3-D fluidized bed. *Chemical Engineering Science*, 66(15), 3499–3512.
- Adamczyk, W. P., Klimanek, A., Bialecki, R. A., et al. (2014). Comparison of the standard Euler-Euler and hybrid Euler-Lagrange approaches for modeling particle transport in a pilot-scale circulating fluidized bed. *Particology*, 15, 129–137.
- Adams, M. (1987). Forces between particles in continuous and discrete liquid media. *Tribology in Particle Technology*, 154.
- Adnan, M., Zhang, N., Sun, F., et al. (2018). Numerical simulation of a semi-industrial scale CFB riser using coarse-grained DDPM-EMMS modelling. *Canadian Journal of Chemical Engineering*, 96(6), 1403–1416.
- Agrawal, K., Loezos, P. N., Syamlal, M., et al. (2001). The role of meso-scale structures in rapid gas-solid flows. *Journal of Fluid Mechanics*, 445, 151.
- Agrawal, V., Shinde, Y., Shah, M. T., et al. (2018). Effect of drag models on CFD-DEM predictions of bubbling fluidized beds with Geldart D particles. *Advanced Powder Technology*, 29(11), 2658–2669.
- Ai, J., Chen, J., Rotter, J. M., et al. (2011). Assessment of rolling resistance models in discrete element simulations. *Powder Technology*, 206(3), 269–282.
- Almuthahar, A., & Taghipour, F. (2008). Computational fluid dynamics of a circulating fluidized bed under various fluidization conditions. *Chemical Engineering Science*, 63(6), 1696–1709.
- Almuthahar, A., & Taghipour, F. (2008). Computational fluid dynamics of high density circulating fluidized bed riser: Study of modeling parameters. *Powder Technology*, 185(1), 11–23.
- Altantzis, C., Bates, R. B., & Ghoniem, A. F. (2015). 3D Eulerian modeling of thin rectangular gas-solid fluidized beds: Estimation of the specular coefficient and its effects on bubbling dynamics and circulation times. *Powder Technology*, 270, 256–270.
- Ayeni, O. O., Wu, C. L., Nandakumar, K., et al. (2016). Development and validation of a new drag law using mechanical energy balance approach for DEM-CFD simulation of gas-solid fluidized bed. *Chemical Engineering Journal*, 302, 395–405.
- Bakshi, A., Altantzis, C., Bates, R. B., et al. (2015). Eulerian-Lulerian simulation of dense solid-gas cylindrical fluidized beds: Impact of wall boundary condition and drag model on fluidization. *Powder Technology*, 277, 47–62.
- Bakshi, A., Altantzis, C., Bershanska, A., et al. (2018). On the limitations of 2D CFD for thin-rectangular fluidized bed simulations. *Powder Technology*, 332, 114–119.
- Bakshi, A., Shahnam, M., Gel, A., et al. (2018). Comprehensive multivariate sensitivity analysis of CFD-DEM simulations: Critical model parameters and their impact on fluidization hydrodynamics. *Powder Technology*, 338, 519–537.
- Baltussen, M. W., Buist, K. A., Peters, E. A., et al. (2018). *Multiscale modelling of dense gas-particle flows*. Elsevier.
- Beetstra, R., van der Hoef, M. A., & Kuipers, J. (2007). Drag force of intermediate Reynolds number flow past mono-and bidisperse arrays of spheres. *AIChE Journal*, 53(2), 489–501.

- Beetstra, R., van der Hoef, M. A., & Kuipers, J. (2007). Numerical study of segregation using a new drag force correlation for polydisperse systems derived from lattice-Boltzmann simulations. *Chemical Engineering Science*, 62(1–2), 246–255.
- Benyahia, S. (2012). Fine-grid simulations of gas-solids flow in a circulating fluidized bed. *AIChE Journal*, 58, NETL-PUB-2.
- Bi, H. T., & Grace, J. R. (1995). Flow regime diagrams for gas-solid fluidization and upward transport. *International Journal of Multiphase Flow*, 21(6), 1229–1236.
- van Buijtenen, M. S., Deen, N. G., Heinrich, S., et al. (2009). Discrete particle simulation study on the influence of the restitution coefficient on spout fluidized-bed dynamics. *Chemical Engineering & Technology*, 32(3), 454–462.
- van Buijtenen, M. S., van Dijk, W., Deen, N. G., et al. (2011). Numerical and experimental study on multiple-spout fluidized beds. *Chemical Engineering Science*, 66(11), 2368–2376.
- Campbell, C. S., & Brennen, C. E. (1985). Computer simulation of granular shear flows. *Journal of Fluid Mechanics*, 151, 167–188.
- Capecelatro, J., & Desjardins, O. (2013). An Euler–Lagrange strategy for simulating particle-laden flows. *Journal of Computational Physics*, 238, 1–31.
- Capecelatro, J., & Desjardins, O. (2013). An Euler–Lagrange strategy for simulating particle-laden flows. *Journal of Computational Physics*, 238, 1–31.
- Capecelatro, J., Pepiot, P., & Desjardins, O. (2014). Numerical characterization and modeling of particle clustering in wall-bounded vertical risers. *Chemical Engineering Journal*, 245, 295–310.
- Cello, F., Di Renzo, A., & Di Maio, F. P. (2010). A semi-empirical model for the drag force and fluid-particle interaction in polydisperse suspensions. *Chemical Engineering Science*, 65(10), 3128–3139.
- Chao, Z., Wang, Y., Jakobsen, J. P., et al. (2011). Derivation and validation of a binary multi-fluid Eulerian model for fluidized beds. *Chemical Engineering Science*, 66(16), 3605–3616.
- Chao, Z., Wang, Y., Jakobsen, J. P., et al. (2012). Investigation of the particle-particle drag in a dense binary fluidized bed. *Powder Technology*, 224, 311–322.
- Chen, C., Dai, Q., & Qi, H. (2016). Improvement of EMMS drag model for heterogeneous gas-solid flows based on cluster modeling. *Chemical Engineering Science*, 141, 8–16.
- Chen, X., & Wang, J. (2014). A comparison of two-fluid model, dense discrete particle model and CFD-DEM method for modeling impinging gas-solid flows. *Powder Technology*, 254, 94–102.
- Chew, J. W., Parker, D. M., & Hrenya, C. M. (2013). Elutriation and species segregation characteristics of polydisperse mixtures of group B particles in a dilute CFB riser. *AIChE Journal*, 59(1), 84–95.
- Chu, K., Chen, J., & Yu, A. (2016). Applicability of a coarse-grained CFD-DEM model on dense medium cyclone. *Minerals Engineering*, 90, 43–54.
- Clarke, D. A., Sederman, A. J., Gladden, L. F., et al. (2018). Investigation of void fraction schemes for use with CFD-DEM simulations of fluidized beds. *Industrial & Engineering Chemistry Research*, 57(8), 3002–3013.
- Cloete, S., Amini, S., Johansen, S. T., et al. (2011). *Evaluation of a Lagrangian discrete phase modeling approach for application to industrial scale bubbling fluidized beds*.
- Cloete, J. H., Cloete, S., Muncicchi, F., et al. (2018). Development and verification of anisotropic drag closures for filtered Two Fluid Models. *Chemical Engineering Science*, 192, 930–954.
- Cloete, J. H., Cloete, S., Radl, S., et al. (2016). Evaluation of wall friction models for riser flow. *Powder Technology*, 303, 156–167.
- Cundall, P. A., & Strack, O. D. (1979). A discrete numerical model for granular assemblies. *Géotechnique*, 29(1), 47–65.
- Dai, Q., Chen, C., & Qi, H. (2015). A generalized drag Law for heterogeneous gas-solid flows in fluidized beds. *Powder Technology*, 283, 120–127.
- Deen, N. G., & Kuipers, J. (2014). Direct numerical simulation of fluid flow accompanied by coupled mass and heat transfer in dense fluid-particle systems. *Chemical Engineering Science*, 116, 645–656.
- Derjaguin, B. V., Muller, V. M., & Toporov, Y. P. (1975). Effect of contact deformations on the adhesion of particles. *Journal of Colloid and Interface Science*, 53(2), 314–326.
- Di Felice, R. (1994). The voidage function for fluid-particle interaction systems. *International Journal of Multiphase Flow*, 20(1), 153–159.
- Di Renzo, A., & Di Maio, F. P. (2004). Comparison of contact-force models for the simulation of collisions in DEM-based granular flow codes. *Chemical Engineering Science*, 59(3), 525–541.
- Ding, J., & Gidaspow, D. (1990). A bubbling fluidization model using kinetic theory of granular flow. *AIChE Journal*, 36(4), 523–538.
- Dubrawski, K., Tebianian, S., Bi, H. T., et al. (2013). Traveling column for comparison of invasive and non-invasive fluidization voidage measurement techniques. *Powder Technology*, 235, 203–220.
- Ergun, S. (1952). Fluid flow through packed columns. *Chemical Engineering Progress*, 48, 89–94.
- Ergun, S., & Orning, A. A. (1949). Fluid flow through randomly packed columns and fluidized beds. *Industrial & Engineering Chemistry*, 41(6), 1179–1184.
- Esteghamatian, A., Hammouti, A., Lance, M., et al. (2017). Particle resolved simulations of liquid/solid and gas/solid fluidized beds. *Physics of Fluids*, 29(3), Article 33302.
- Fan, R., & Fox, R. O. (2008). Segregation in polydisperse fluidized beds: Validation of a multi-fluid model. *Chemical Engineering Science*, 63(1), 272–285.
- Farzaneh, M., Almstedt, A., Johnsson, F., et al. (2015). The crucial role of frictional stress models for simulation of bubbling fluidized beds. *Powder Technology*, 270, 68–82.
- Fede, P., Simonin, O., & Ingram, A. (2016). 3D numerical simulation of a lab-scale pressurized dense fluidized bed focussing on the effect of the particle-particle restitution coefficient and particle-wall boundary conditions. *Chemical Engineering Science*, 142, 215–235.
- Feng, M., Li, F., Wang, W., et al. (2018). Parametric study for MP-PIC simulation of bubbling fluidized beds with Geldart A particles. *Powder Technology*, 328, 215–226.
- Fullmer, W. D., & Hrenya, C. M. (2016). Quantitative assessment of fine-grid kinetic-theory-based predictions of mean-slip in unbounded fluidization. *AIChE Journal*, 62(1), 11–17.
- Fullmer, W. D., Liu, G., Yin, X., et al. (2017). Clustering instabilities in sedimenting fluid-solid systems: Critical assessment of kinetic-theory-based predictions using direct numerical simulation data. *Journal of Fluid Mechanics*, 823, 433.
- Galvin, J. E., & Benyahia, S. (2014). The effect of cohesive forces on the fluidization of aeratable powders. *AIChE Journal*, 60(2), 473–484.
- Gao, X., Li, T., Sarkar, A., et al. (2018). Development and validation of an enhanced filtered drag model for simulating gas-solid fluidization of Geldart A particles in all flow regimes. *Chemical Engineering Science*, 184, 33–51.
- Garzo, V., Dufty, J. W., & Hrenya, C. M. (2007). Enskog theory for polydisperse granular mixtures. I. Navier-Stokes order transport. *Physical Review E*, 76(3), Article 31303.
- Geng, S., Jia, Z., Zhan, J., et al. (2016). CFD modeling the hydrodynamics of binary particle mixture in pseudo-2D bubbling fluidized bed: Effect of model parameters. *Powder Technology*, 302(NOV), 384–395.
- Gera, D., Syamlal, M., & O'Brien, T. J. (2004). Hydrodynamics of particle segregation in fluidized beds. *International Journal of Multiphase Flow*, 30(4), 419–428.
- Gidaspow, D. (1994). *Multiphase flow and fluidization: Continuum and kinetic theory descriptions*. Academic press.
- Goldschmidt, M., Beetstra, R., & Kuipers, J. (2004). Hydrodynamic modelling of dense gas-fluidized beds: Comparison and validation of 3D discrete particle and continuum models. *Powder Technology*, 142(1), 23–47.
- Goldschmidt, M., Kuipers, J., & van Swaaij, W. P. M. (2001). Hydrodynamic modelling of dense gas-fluidized beds using the kinetic theory of granular flow: Effect of coefficient of restitution on bed dynamics. *Chemical Engineering Science*, 56(2), 571–578.
- Goldschmidt, M., Link, J. M., Mellema, S., et al. (2003). Digital image analysis measurements of bed expansion and segregation dynamics in dense gas-fluidized beds. *Powder Technology*, 138(2–3), 135–159.
- Gomez-Barea, A., & Leckner, B. (2010). Modeling of biomass gasification in fluidized bed. *Progress in Energy and Combustion Science*, 36(4), 444–509.
- Goniva, C., Kloss, C., Deen, N. G., et al. (2012). Influence of rolling friction on single spout fluidized bed simulation. *Particology*, 10(5), 582–591.
- Gopalan, B., Shahnam, M., Panday, R., et al. (2016). Measurements of pressure drop and particle velocity in a pseudo 2-D rectangular bed with Geldart Group D particles. *Powder Technology*, 291, 299–310.
- Gu, Y., Ozel, A., & Sundaresan, S. (2016). A modified cohesion model for CFD-DEM simulations of fluidization. *Powder Technology*, 296, 7–28.
- Hager, A. (2014). *CFD-DEM on multiple scales - an extensive investigation of particle-fluid interactions*.
- Haghgo, M. R., Bergstrom, D. J., & Spiteri, R. J. (2018). Effect of particle stress tensor in simulations of dense gas-particle flows in fluidized beds. *Particology*. S2108435246X.
- Hamidouche, Z., Dufresne, Y., Pierson, J., et al. (2019). DEM/CFD simulations of a pseudo-2D fluidized bed: Comparison with experiments. *Fluids*, 4(1), 51.
- Han, Q., Yang, N., Zhu, J., et al. (2015). Onset velocity of circulating fluidization and particle residence time distribution: A CFD-DEM study. *Particology*, 21, 187–195.
- Harris, S. E., & Crighton, D. G. (1994). Solitons, solitary waves, and voidage disturbances in gas-fluidized beds. *Journal of Fluid Mechanics*, 266, 243–276.
- Helland, E., Bournot, H., Occelli, R., et al. (2007). Drag reduction and cluster formation in a circulating fluidized bed. *Chemical Engineering Science*, 62(1–2), 148–158.
- Herbert, P., Nicolai, R., & Reh, L. (1999). The ETH experience: Experimental database and results from the past 8 years. In *AIChE symposium series*. New York, NY: American Institute of chemical Engineers, 1971-c2002 (pp. 61–66).
- Hernandez-Jimenez, F., Ssnchez-Delgado, S., Gamez-Garcia, A., et al. (2011). Comparison between two-fluid model simulations and particle image analysis & velocimetry (PIV) results for a two-dimensional gas-solid fluidized bed. *Chemical Engineering Science*, 66(17), 3753–3772.
- He, Y., Wang, T., Deen, N., et al. (2012). Discrete particle modeling of granular temperature distribution in a bubbling fluidized bed. *Particology*.
- Hill, R. J., Koch, D. L., & Ladd, A. J. (2001). The first effects of fluid inertia on flows in ordered and random arrays of spheres. *Journal of Fluid Mechanics*, 448, 213.
- van der Hoef, M. A., van Sint Annaland, M., Deen, N. G., et al. (2008). Numerical simulation of dense gas-solid fluidized beds: A multiscale modeling strategy. *Annual Review of Fluid Mechanics*, 40, 47–70.
- Holloway, W., Yin, X., & Sundaresan, S. (2010). Fluid-particle drag in inertial polydisperse gas-solid suspensions. *AIChE Journal*, 56(8), 1995–2004.
- Hong, K., Chen, S., Wang, W., et al. (2016). Fine-grid two-fluid modeling of fluidization of Geldart A particles. *Powder Technology*, 296, 2–16.
- Hong, K., Gao, Y., Ullah, A., et al. (2018). Multi-scale CFD modeling of gas-solid bubbling fluidization accounting for sub-grid information. *Advanced Powder Technology*, 29(3), 488–498.
- Horabik, J., & Molenda, M. (2016). Parameters and contact models for DEM simulations of agricultural granular materials: A review. *Biosystems Engineering*, 147, 206–225.

- Hou, B., Tang, H., Zhang, H., et al. (2013). Experimental and theoretical investigation of mass transfer in a circulating fluidized bed. *Chemical Engineering Science*, 102, 354–364.
- Huillin, L., Shuyan, W., Jianxiang, Z., et al. (2010). Numerical simulation of flow behavior of agglomerates in gas-cohesive particles fluidized beds using agglomerates-based approach. *Chemical Engineering Science*, 65(4), 1462–1473.
- Hu, C., Luo, K., Wang, S., et al. (2019). Influences of operating parameters on the fluidized bed coal gasification process: A coarse-grained CFD-DEM study. *Chemical Engineering Science*, 195, 693–706.
- Hu, C., Luo, K., Wang, S., et al. (2019). The effects of collisional parameters on the hydrodynamics and heat transfer in spouted bed: A CFD-DEM study. *Powder Technology*, 353, 132–144.
- Iddir, H., & Arastoopour, H. (2005). Modeling of multitype particle flow using the kinetic theory approach. *AIChE Journal*, 51(6), 1620–1632.
- Igci, Y., & Sundaresan, S. (2011). Constitutive models for filtered two-fluid models of fluidized gas-particle flows. *Industrial & Engineering Chemistry Research*, 50(23), 13190–13201.
- Jajcevic, D., Siegmann, E., Radeke, C., et al. (2013). Large-scale CFD-DEM simulations of fluidized granular systems. *Chemical Engineering Science*, 98, 298–310.
- Jalali, P., Nikku, M., Ritvanen, J., et al. (2018). Flow characteristics of circulating fluidized beds near terminal velocity: Eulerian model of a lab-scale apparatus. *Powder Technology*, 339, 569–584.
- Jenkins, J. T., & Mancini, F. (1987). *Balance laws and constitutive relations for plane flows of a dense, binary mixture of smooth, nearly elastic, circular disks*.
- Jenkins, J. T., & Zhang, C. (2002). Kinetic theory for identical, frictional, nearly elastic spheres. *Physics of Fluids*, 14(3), 1228–1235.
- Jiang, Z., Hagemeyer, T., Buck, A., et al. (2018). Color-PTV measurement and CFD-DEM simulation of the dynamics of poly-disperse particle systems in a pseudo-2D fluidized bed. *Chemical Engineering Science*, 179, 115–132.
- Jiang, Y., Kolehmainen, J., Gu, Y., et al. (2019). Neural-network-based filtered drag model for gas-particle flows. *Powder Technology*, 346, 403–413.
- Jin, B., Wang, X., Zhong, W., et al. (2010). Modeling on high-flux circulating fluidized bed with Geldart group B particles by kinetic theory of granular flow. *Energy & Fuels*, 24(5), 3159–3172.
- Johnson, R. W. (2016). *Handbook of fluid dynamics*. Crc Press.
- Johnson, P. C., & Jackson, R. (1987). Frictional-collisional constitutive relations for granular materials, with application to plane shearing. *Journal of Fluid Mechanics*, 176, 67–93.
- Johnson, K. L., Kendall, K., & Roberts, A. (1971). Surface energy and the contact of elastic solids. *Proceedings of the royal society of London. A, mathematical and physical sciences*, 324(1558), 301–313.
- Jop, P., Forterre, Y., & Pouliquen, O. (2006). A constitutive law for dense granular flows. *Nature*, 441(7094), 727–730.
- Kaneko, Y., Shiojima, T., & Horio, M. (1999). DEM simulation of fluidized beds for gas-phase olefin polymerization. *Chemical Engineering Science*, 54(24), 5809–5821.
- Karimipour, S., & Pugsley, T. (2012). Application of the particle in cell approach for the simulation of bubbling fluidized beds of Geldart A particles. *Powder Technology*, 220, 63–69.
- Kazari, M. (1995). A study on conditions for similarity of particle motion in numerical simulation of dense gas-solid two phase flow. In *Proceedings of the 2nd International conference on multiphase Flow'95, Kyoto*.
- Khadilkar, A., Rozelle, P. L., & Pisupati, S. V. (2014). Models of agglomerate growth in fluidized bed reactors: Critical review, status and applications. *Powder Technology*, 264, 216–228.
- Kia, S. A., & Aminian, J. (2017). Hydrodynamic modeling strategy for dense to dilute gas-solid fluidized beds. *Particuology*, 31, 105–116, 002.
- Kobayashi, T., Tanaka, T., Shimada, N., et al. (2013). DEM-DFD analysis of fluidization behavior of Geldart Group A particles using a dynamic adhesion force model. *Powder Technology*, 248, 143–152.
- Kong, L., Zhang, C., & Zhu, J. (2014). Evaluation of the effect of wall boundary conditions on numerical simulations of circulating fluidized beds. *Particuology*, 13, 114–123.
- Koralkar, N. V., & Bose, M. (2016). Performance of drag models for simulation of fluidized beds with Geldart D particles. *Advanced Powder Technology*, 27(6), 2377–2398.
- Kriebitzsch, S., Van der Hoef, M. A., & Kuipers, J. (2013). Fully resolved simulation of a gas-fluidized bed: A critical test of DEM models. *Chemical Engineering Science*, 91, 1–4.
- Ku, X., Li, T., & Lovas, T. (2013). Influence of drag force correlations on periodic fluidization behavior in Eulerian-Lagrangian simulation of a bubbling fluidized bed. *Chemical Engineering Science*, 95, 94–106.
- Kunii, D., & Levenspiel, O. (2013). *Fluidization engineering*. Elsevier.
- Leckner, B. (2017). Regimes of large-scale fluidized beds for solid fuel conversion. *Powder Technology*, 308, 362–367.
- Liang, Y., Zhang, Y., Li, T., et al. (2014). A critical validation study on CPFD model in simulating gas-solid bubbling fluidized beds. *Powder Technology*, 263, 121–134.
- Li, T., & Benyahia, S. (2012). Revisiting Johnson and Jackson boundary conditions for granular flows. *AIChE Journal*, 58(7), 2058–2068.
- Li, T., Dietiker, J., Rogers, W., et al. (2016). Investigation of CO<sub>2</sub> capture using solid sorbents in a fluidized bed reactor: Cold flow hydrodynamics. *Powder Technology*, 301, 1130–1143.
- Li, T., Dietiker, J., & Shahnam, M. (2012). MFX simulation of NETL/PSRI challenge problem of circulating fluidized bed. *Chemical Engineering Science*, 84, 746–760.
- Li, T., Garg, R., Galvin, J., et al. (2012). Open-source MFX-DEM software for gas-solids flows: Part II-validation studies. *Powder Technology*, 220, 138–150.
- Li, T., Grace, J., & Bi, X. (2010). Study of wall boundary condition in numerical simulations of bubbling fluidized beds. *Powder Technology*, 203(3), 447–457.
- Li, J., & Kuipers, J. (2007). Effect of competition between particle-particle and gas-particle interactions on flow patterns in dense gas-fluidized beds. *Chemical Engineering Science*, 62(13), 3429–3442.
- Li, J., & Kwauk, M. (1994). *Particle-fluid two-phase flow: The energy-minimization multi-scale method; minimization multi-scale method; metallurg*. Beijing: Industry Press.
- Li, J., Luo, Z., Lan, X., et al. (2013). Numerical simulation of the turbulent gas-solid flow and reaction in a polydisperse FCC riser reactor. *Powder Technology*, 237, 569–580.
- Li, T., Pannala, S., & Shahnam, M. (2014). CFD simulations of circulating fluidized bed risers, part II, evaluation of differences between 2D and 3D simulations. *Powder Technology*, 254, 115–124.
- Li, T., Rabha, S., Verma, V., et al. (2017). Experimental study and discrete element method simulation of Geldart Group A particles in a small-scale fluidized bed. *Advanced Powder Technology*, 28(11), 2961–2973.
- Li, J., Tian, X., & Yang, B. (2017). Hydromechanical simulation of a bubbling fluidized bed using an extended bubble-based EMMS model. *Powder Technology*, 313, 369–381.
- Liu, P., LaMarche, C. Q., Kellogg, K. M., et al. (2017). Dense versus dilute fluidization of cohesive particles: Reverse sensitivity to friction and restitution coefficient. *Physical Review Fluids*, 2(5), Article 54302.
- Liu, B., Papadakis, K., Gu, S., et al. (2017). CFD modelling of particle shrinkage in a fluidized bed for biomass fast pyrolysis with quadrature method of moment. *Fuel Processing Technology*, 164, 51–68.
- Liu, Z., Suda, T., Tsuji, T., et al. (2013). *Use of similarities in CFD-DEM simulation of fluidized bed*.
- Liu, H., Tafti, D. K., & Li, T. (2014). Hybrid parallelism in MFX CFD-DEM using OpenMP. *Powder Technology*, 259, 22–29.
- Liu, D., & van Wachem, B. (2019). Comprehensive assessment of the accuracy of CFD-DEM simulations of bubbling fluidized beds. *Powder Technology*, 343, 145–158.
- Li, T., Wang, L., Rogers, W., et al. (2017). An approach for drag correction based on the local heterogeneity for gas-solid flows. *AIChE Journal*, 63(4), 1203–1212.
- Li, J., & Yang, B. (2017). CFD simulation of bubbling fluidized beds using a local-structure-dependent drag model. *Chemical Engineering Journal*, 329, 100–115.
- Loha, C., Chattopadhyay, H., & Chatterjee, P. K. (2013). Euler-Euler CFD modeling of fluidized bed: Influence of specular coefficient on hydrodynamic behavior. *Particuology*, 11(6), 673–680.
- Loha, C., Chattopadhyay, H., & Chatterjee, P. K. (2014). Effect of coefficient of restitution in Euler-Euler CFD simulation of fluidized-bed hydrodynamics. *Particuology*, 15, 170–177.
- Lommen, S., Schott, D., & Lodewijks, G. (2014). DEM speedup: Stiffness effects on behavior of bulk material. *Particuology*, 12, 107–112.
- Loth, E., & Dorgan, A. J. (2009). An equation of motion for particles of finite Reynolds number and size. *Environmental Fluid Mechanics*, 9(2), 187–206.
- Lu, L., Benyahia, S., & Li, T. (2017). An efficient and reliable predictive method for fluidized bed simulation. *AIChE Journal*, 63(12), 5320–5334.
- Lu, L., Gopalan, B., & Benyahia, S. (2017). Assessment of different discrete particle methods ability to predict gas-particle flow in a small-scale fluidized bed. *Industrial & Engineering Chemistry Research*, 56(27), 7865–7876.
- Lu, Y., Huang, J., & Zheng, P. (2015). A CFD-DEM study of bubble dynamics in fluidized bed using flood fill method. *Chemical Engineering Journal*, 274, 123–131.
- Lu, L., Liu, X., Li, T., et al. (2017). Assessing the capability of continuum and discrete particle methods to simulate gas-solids flow using DNS predictions as a benchmark. *Powder Technology*, 321, 301–309.
- Lungu, M., Siame, J., & Mukosha, L. (2022). Coarse-grained CFD-DEM simulations of fluidization with large particles. *Powder Technology*, 402, Article 117344.
- Lungu, M., Wang, H., Wang, J., et al. (2016). Two-fluid model simulations of the national energy technology laboratory bubbling fluidized bed challenge problem. *Industrial & Engineering Chemistry Research*, 55(17), 5063–5077.
- Lun, C., Savage, S. B., Jeffrey, D. J., et al. (1984). Kinetic theories for granular flow: Inelastic particles in Couette flow and slightly inelastic particles in a general flowfield. *Journal of Fluid Mechanics*, 140, 223–256.
- Luo, K., Hu, C., Wu, F., et al. (2017). Direct numerical simulation of turbulent boundary layer with fully resolved particles at low volume fraction. *Physics of Fluids*, 29(5), Article 53301.
- Luo, K., Tan, J., Wang, Z., et al. (2016). Particle-resolved direct numerical simulation of gas-solid dynamics in experimental fluidized beds. *AIChE Journal*, 62(6), 1917–1932.
- Luo, K., Wang, Z., Li, D., et al. (2017). Fully resolved simulations of turbulence modulation by high-inertia particles in an isotropic turbulent flow. *Physics of Fluids*, 29(11), Article 113301.
- Luo, K., Wu, F., Yang, S., et al. (2015). High-fidelity simulation of the 3-D full-loop gas-solid flow characteristics in the circulating fluidized bed. *Chemical Engineering Science*, 123, 22–38.
- Lu, J., Peters, E. A., & Kuipers, J. A. (2018). Direct numerical simulation of fluid flow and mass transfer in particle clusters. *Industrial & Engineering Chemistry Research*, 57(13), 4664–4679.
- Lu, B., Wang, W., & Li, J. (2009). Searching for a mesh-independent sub-grid model for CFD simulation of gas-solid riser flows. *Chemical Engineering Science*, 64(15), 3437–3447.

- Lu, B., Wang, W., & Li, J. (2011). Eulerian simulation of gas-solid flows with particles of Geldart groups A, B and D using EMMS-based meso-scale model. *Chemical Engineering Science*, 66(20), 4624–4635.
- Lu, L., Xu, J., Ge, W., et al. (2016). Computer virtual experiment on fluidized beds using a coarse-grained discrete particle method-EMMS-DPM. *Chemical Engineering Science*, 155(NOV), 314–337.
- Lu, L., Xu, Y., Li, T., et al. (2018). Assessment of different coarse graining strategies to simulate polydisperse gas-solids flow. *Chemical Engineering Science*, 179, 53–63.
- Lv, X., Li, H., & Zhu, Q. (2014). Simulation of gas-solid flow in 2D/3D bubbling fluidized beds by combining the two-fluid model with structure-based drag model. *Chemical Engineering Journal*, 236, 149–157.
- Ma, Q., Lei, F., & Xiao, Y. (2018). Numerical analysis of operating conditions for establishing high-density circulating fluidized bed by CPFD method. *Powder Technology*, 338, 446–457.
- Mathiesen, V., Solberg, T., Arastoopour, H., et al. (1999). Experimental and computational study of multiphase gas/particle flow in a CFB riser. *AIChE Journal*, 45(12), 2503–2518.
- McGraw, R. (1997). Description of aerosol dynamics by the quadrature method of moments. *Aerosol Science and Technology*, 27(2), 255–265.
- McKeen, T., & Pugsley, T. (2003). Simulation and experimental validation of a freely bubbling bed of FCC catalyst. *Powder Technology*, 129(1–3), 139–152.
- McLaughlin, J. B. (1991). Inertial migration of a small sphere in linear shear flows. *Journal of Fluid Mechanics*, 224, 261–274.
- Mehrabadi, M., Murphy, E., & Subramaniam, S. (2016). Development of a gas-solid drag law for clustered particles using particle-resolved direct numerical simulation. *Chemical Engineering Science*, 152, 199–212.
- Mei, R. (1992). An approximate expression for the shear lift force on a spherical particle at finite Reynolds number. *International Journal of Multiphase Flow*, 18(1), 145–147.
- Mikami, T., Kamiya, H., & Horio, M. (1998). Numerical simulation of cohesive powder behavior in a fluidized bed. *Chemical Engineering Science*, 53(10), 1927–1940.
- Milioli, C. C., Milioli, F. E., Holloway, W., et al. (2013). Filtered two-fluid models of fluidized gas-particle flows: New constitutive relations. *AIChE Journal*, 59(9), 3265–3275.
- Moreno-Atanasio, R., Xu, B. H., & Ghadiri, M. (2007). Computer simulation of the effect of contact stiffness and adhesion on the fluidization behaviour of powders. *Chemical Engineering Science*, 62(1–2), 184–194.
- Muller, C. R., Holland, D. J., Sederman, A. J., et al. (2008). Granular temperature: Comparison of magnetic resonance measurements with discrete element model simulations. *Powder Technology*, 184(2), 241–253.
- Müller, C. R., Scott, S. A., Holland, D. J., et al. (2009). Validation of a discrete element model using magnetic resonance measurements. *Particuology*, 7(4), 297–306.
- Nikku, M., Daikeler, A., Stroh, A., et al. (2019). Comparison of solid phase closure models in Eulerian-Eulerian simulations of a circulating fluidized bed riser. *Chemical Engineering Science*, 195, 39–50.
- O'Rourke, P. J., & Snider, D. M. (2014). A new blended acceleration model for the particle contact forces induced by an interstitial fluid in dense particle/fluid flows. *Powder Technology*, 256, 39–51.
- Olaofe, O. O., Patil, A. V., Deen, N. G., et al. (2014). Simulation of particle mixing and segregation in bidisperse gas fluidized beds. *Chemical Engineering Science*, 108, 258–269.
- Ostermeier, P., DeYoung, S., Vandersickel, A., et al. (2019). Comprehensive investigation and comparison of TFM, DenseDPM and CFD-DEM for dense fluidized beds. *Chemical Engineering Science*, 196, 291–309.
- Parmentier, J., Simonin, O., & Delsart, O. (2012). A functional subgrid drift velocity model for filtered drag prediction in dense fluidized bed. *AIChE Journal*, 58(4), 1084–1098.
- Patil, D. J., Smit, J., Annaland, M. V. S., et al. (2010). Wall-to-bed heat transfer in gas-solid bubbling fluidized beds. *AIChE Journal*, 52(1), 58–74.
- Paulick, M., Morgeneyer, M., & Kwade, A. (2015). Review on the influence of elastic particle properties on DEM simulation results. *Powder Technology*, 283, 66–76.
- Peng, Z., Doroodchi, E., Luo, C., et al. (2014). Influence of void fraction calculation on fidelity of CFD-DEM simulation of gas-solid bubbling fluidized beds. *AIChE Journal*, 60(6), 2000–2018.
- Pepiot, P., & Desjardins, O. (2012). Numerical analysis of the dynamics of two-and three-dimensional fluidized bed reactors using an Euler-Lagrange approach. *Powder Technology*, 220, 104–121.
- Popoff, B., & Braun, M. (2007). *A Lagrangian approach to dense particulate flows*. Leipzig, Germany: International Conference on Multiphase Flow.
- Qi, F. (2017). *Discrete element method modeling of biomass fast pyrolysis granular flows*. Iowa State University.
- Qin, Z., & Wang, J. (2019). Coarse grid simulation of the hydrodynamics of binary gas-solid flow in CFB risers. *Canadian Journal of Chemical Engineering*, 97(3), 793–807.
- Qiu, X., Wang, L., Yang, N., et al. (2017). A simplified two-fluid model coupled with EMMS drag for gas-solid flows. *Powder Technology*, 314, 299–314.
- Radl, S., Gonzales, B. C., Goniva, C., et al. (2015). *State of the art in mapping schemes for dilute and dense Euler-Lagrange simulations*.
- Radl, S., & Sundaresan, S. (2014). A drag model for filtered Euler-Lagrange simulations of clustered gas-particle suspensions. *Chemical Engineering Science*, 117, 416–425.
- Ramkrishna, D. (2000). *Population balances: Theory and applications to particulate systems in engineering*. Elsevier.
- Reuge, N., Cadoret, L., Coufort-Saudejaud, C., et al. (2008). Multifluid Eulerian modeling of dense gas-solids fluidized bed hydrodynamics: Influence of the dissipation parameters. *Chemical Engineering Science*, 63(22), 5540–5551.
- Richtberg, M., Richter, R., & Wirth, K. (2005). Characterization of the flow patterns in a pressurized circulating fluidized bed. *Powder Technology*, 155(2), 145–152.
- Rong, L. W., Dong, K. J., & Yu, A. B. (2013). Lattice-Boltzmann simulation of fluid flow through packed beds of uniform spheres: Effect of porosity. *Chemical Engineering Science*, 99, 44–58.
- Rong, L. W., Dong, K. J., & Yu, A. B. (2014). Lattice-Boltzmann simulation of fluid flow through packed beds of spheres: Effect of particle size distribution. *Chemical Engineering Science*, 116, 508–523.
- Saffman, P. G. (1965). The lift on a small sphere in a slow shear flow. *Journal of Fluid Mechanics*, 22(2), 385–400.
- Sakai, M., Abe, M., Shigeto, Y., et al. (2014). Verification and validation of a coarse grain model of the DEM in a bubbling fluidized bed. *Chemical Engineering Journal*, 244, 33–43.
- Sakai, M., Yamada, Y., Shigeto, Y., et al. (2010). Large-scale discrete element modeling in a fluidized bed. *International Journal for Numerical Methods in Fluids*, 64(10–12), 1319–1335.
- Sanchez-Delgado, S., Marugan-Cruz, C., Soria-Verdugo, A., et al. (2013). Estimation and experimental validation of the circulation time in a 2D gas-solid fluidized beds. *Powder Technology*, 235, 669–676.
- Sande, P. C., & Ray, S. (2014). Mesh size effect on CFD simulation of gas-fluidized Geldart A particles. *Powder Technology*, 264, 43–53.
- Sarkar, A., Milioli, F. E., Ozarkar, S., et al. (2016). Filtered sub-grid constitutive models for fluidized gas-particle flows constructed from 3-D simulations. *Chemical Engineering Science*, 152, 443–456.
- Schaeffer, D. G. (1987). Instability in the evolution equations describing incompressible granular flow. *Journal of Differential Equations*, 66(1), 19–50.
- Schneiderbauer, S. (2017). A spatially-averaged two-fluid model for dense large-scale gas-solid flows. *AIChE Journal*, 63(8), 3544–3562.
- Schneiderbauer, S., & Pirker, S. (2014). Filtered and heterogeneity-based subgrid modifications for gas-solid drag and solid stresses in bubbling fluidized beds. *AIChE Journal*, 60(3), 839–854.
- Schneiderbauer, S., Schellander, D., Loderer, A., et al. (2012). Non-steady state boundary conditions for collisional granular flows at flat frictional moving walls. *International Journal of Multiphase Flow*, 43, 149–156.
- Shah, M. T., Utikar, R. P., Tade, M. O., et al. (2013). Effect of a cluster on gas-solid drag from lattice Boltzmann simulations. *Chemical Engineering Science*, 102, 365–372.
- Shi, Z., Wang, W., & Li, J. (2011). A bubble-based EMMS model for gas-solid bubbling fluidization. *Chemical Engineering Science*, 66(22), 5541–5555.
- Shuai, W., Guangbo, Z., Guodong, L., et al. (2014). Hydrodynamics of gas-solid risers using cluster structure-dependent drag model. *Powder Technology*, 254, 214–227.
- Silbert, L. E., Ertas, D., Grest, G. S., et al. (2001). Granular flow down an inclined plane: Bagnold scaling and rheology. *Physical Review E*, 64(5), Article 51302.
- van Sint Annaland, M., Bokkers, G. A., Goldschmidt, M., et al. (2009). Development of a multi-fluid model for poly-disperse dense gas-solid fluidised beds, Part I: Model derivation and numerical implementation. *Chemical Engineering Science*, 64(20), 4222–4236.
- van Sint Annaland, M., Bokkers, G. A., Goldschmidt, M., et al. (2009). Development of a multi-fluid model for poly-disperse dense gas-solid fluidised beds, Part II: Segregation in binary particle mixtures. *Chemical Engineering Science*, 64(20), 4237–4246.
- Smuts, E. M. (2015). *A methodology for coupled CFD-DEM modeling of particulate suspension rheology*.
- Snider, D. M. (2001). An incompressible three-dimensional multiphase particle-in-cell model for dense particle flows. *Journal of Computational Physics*, 170(2), 523–549.
- Song, F., Li, F., Wang, W., et al. (2018). A sub-grid EMMS drag for multiphase particle-in-cell simulation of fluidization. *Powder Technology*, 327, 420–429.
- Srivastava, A., & Sundaresan, S. (2003). Analysis of a frictional-kinetic model for gas-particle flow. *Powder Technology*, 129(1–3), 72–85.
- Stanly, R., & Shoeff, G. (2018). Detailed analysis of recent drag models using multiple cases of mono-disperse fluidized beds with Geldart-B and Geldart-D particles. *Chemical Engineering Science*, 188, 132–149.
- Sundaresan, S., Ozel, A., & Kolehmainen, J. (2018). Toward constitutive models for momentum, species, and energy transport in gas-particle flows. *Annual Review of Chemical and Biomolecular Engineering*, 9, 61–81.
- Sun, L., Luo, K., & Fan, J. (2017). Population balance equation of cohesive particle flow in a circulating fluidized bed. *Chemical Engineering & Technology*, 40(9), 1544–1551.
- Sun, R., & Xiao, H. (2015). Diffusion-based coarse graining in hybrid continuum-discrete solvers: Applications in CFD-DEM. *International Journal of Multiphase Flow*, 77.
- Su, M., & Zhao, H. (2017). Modifying the inter-phase drag via solid volume fraction gradient for CFD simulation of fast fluidized beds. *AIChE Journal*, 63(7), 2588–2598.
- Syamlal, M., & Bissett, L. A. (1992). *METC gasifier advanced simulation (MGAS) model*. WV (United States): USDOE Morgantown Energy Technology Center.
- Syamlal, M., & O'Brien, T. J. (1987). *The derivation of a drag coefficient formula from velocity-voidage correlations*. NETL, Morgantown, WV: Technical Note, US Department of energy, Office of Fossil Energy.

- Syamlal, M., & O'Brien, T. J. (1988). Simulation of granular layer inversion in liquid fluidized beds. *International Journal of Multiphase Flow*, 14(4), 473–481.
- Syamlal, M., Rogers, W., & O'Brien, T. J. (1993). *MFIIX documentation theory guide*. WV (United States): USDOE Morgantown Energy Technology Center.
- Tang, Y., Lau, Y. M., Deen, N. G., et al. (2016). Direct numerical simulations and experiments of a pseudo-2D gas-fluidized bed. *Chemical Engineering Science*, 143, 166–180.
- Tenneti, S., Garg, R., & Subramaniam, S. (2011). Drag law for monodisperse gas-solid systems using particle-resolved direct numerical simulation of flow past fixed assemblies of spheres. *International Journal of Multiphase Flow*, 37(9), 1072–1092.
- Tenneti, S., & Subramaniam, S. (2014). Particle-resolved direct numerical simulation for gas-solid flow model development. *Annual Review of Fluid Mechanics*, 46, 199–230.
- Third, J. R., Chen, Y., & Muller, C. R. (2016). Comparison between finite volume and lattice-Boltzmann method simulations of gas-fluidized beds: Bed expansion and particle-fluid interaction force. *Computational Particle Mechanics*, 3(3), 373–381.
- Tseng, Y., & Ferziger, J. H. (2003). A ghost-cell immersed boundary method for flow in complex geometry. *Journal of Computational Physics*, 192(2), 593–623.
- Tsuji, T., Yabumoto, K., & Tanaka, T. (2008). Spontaneous structures in three-dimensional bubbling gas-fluidized bed by parallel DEM-CFD coupling simulation. *Powder Technology*, 184(2), 132–140.
- Tu, Q., & Wang, H. (2018). CPFD study of a full-loop three-dimensional pilot-scale circulating fluidized bed based on EMMS drag model. *Powder Technology*, 323, 534–547.
- Uhlmann, M. (2005). An immersed boundary method with direct forcing for the simulation of particulate flows. *Journal of Computational Physics*, 209(2), 448–476.
- Uhlmann, M., & Chouippe, A. (2017). Clustering and preferential concentration of finite-size particles in forced homogeneous-isotropic turbulence. *Journal of Fluid Mechanics*, 812, 991–1023.
- Upadhyay, M., & Park, J. (2015). CFD simulation via conventional Two-Fluid Model of a circulating fluidized bed riser: Influence of models and model parameters on hydrodynamic behavior. *Powder Technology*, 272, 260–268.
- Van Wachem, B., & Sasic, S. (2008). Derivation, simulation and validation of a cohesive particle flow CFD model. *AIChE Journal*, 54(1), 9–19.
- Varas, A. C., Peters, E., & Kuipers, J. (2017). CFD-DEM simulations and experimental validation of clustering phenomena and riser hydrodynamics. *Chemical Engineering Science*, 169, 246–258.
- Verma, V., Deen, N. G., Padding, J. T., et al. (2013). Two-fluid modeling of three-dimensional cylindrical gas-solid fluidized beds using the kinetic theory of granular flow. *Chemical Engineering Science*, 102, 227–245.
- Verma, V., & Padding, J. T. (2020). A novel approach to MP-PIC: Continuum particle model for dense particle flows in fluidized beds. *Chemical Engineering Science: X*, 6, Article 100053.
- Verma, V., Padding, J. T., Deen, N. G., et al. (2014). Bubble dynamics in a 3D gas-solid fluidized bed using ultrafast electron beam X-ray tomography and two-fluid model. *AIChE Journal*, 60(5), 1632–1644.
- Wang, J. (2008). High-resolution Eulerian simulation of RMS of solid volume fraction fluctuation and particle clustering characteristics in a CFB riser. *Chemical Engineering Science*, 63(13), 3341–3347.
- Wang, C. (2013). *High density gas-solids circulating fluidized bed riser and downer reactors*.
- Wang, Y., Chao, Z., & Jakobsen, H. A. (2010). A Sensitivity Study of the Two-Fluid Model Closure Parameters ( $\beta, \epsilon$ ) Determining the Main Gas/Solid Flow Pattern Characteristics. *Industrial & Engineering Chemistry Research*, 49(7), 3433–3441.
- Wang, S., Chen, J., Wang, Q., et al. (2016). Evaluation of a bubble-structure dependent drag model for the simulation of bubbling fluidization with Geldart A particles. *Powder Technology*, 289, 44–51.
- Wang, Z., Fan, J., & Luo, K. (2008). Combined multi-direct forcing and immersed boundary method for simulating flows with moving particles. *International Journal of Multiphase Flow*, 34(3), 283–302.
- Wang, X., Jin, B., Zhong, W., et al. (2010). Modeling on the hydrodynamics of a high-flux circulating fluidized bed with Geldart group A particles by kinetic theory of granular flow. *Energy & Fuels*, 24(2), 1242–1259.
- Wang, W., & Li, J. (2007). Simulation of gas-solid two-phase flow by a multi-scale CFD approach-of the EMMS model to the sub-grid level. *Chemical Engineering Science*, 62(1–2), 208–231.
- Wang, Z., & Liu, M. (2020). Semi-resolved CFD-DEM for thermal particulate flows with applications to fluidized beds. *International Journal of Heat and Mass Transfer*, 159, Article 120150.
- Wang, S., Liu, G., Lu, H., et al. (2012). Computational fluid dynamics of riser using kinetic theory of rough spheres. *Powder Technology*, 228, 56–68.
- Wang, S., Luo, K., Hu, C., et al. (2017). CFD-DEM study of the effect of cyclone arrangements on the gas-solid flow dynamics in the full-loop circulating fluidized bed. *Chemical Engineering Science*, 172, 199–215.
- Wang, Z., Teng, Y., & Liu, M. (2019). A semi-resolved CFD-DEM approach for particulate flows with kernel based approximation and Hilbert curve based searching strategy. *Journal of Computational Physics*, 384, 151–169.
- Wang, J. W., Van der Hoef, M. A., & Kuipers, J. (2010). The role of particle-particle interactions in bubbling gas-fluidized beds of Geldart A particles: A discrete particle study. In *AIP conference proceedings*. American Institute of physics (pp. 766–768).
- Wang, J., Van der Hoef, M. A., & Kuipers, J. (2011). The role of scale resolution versus inter-particle cohesive forces in two-fluid modeling of bubbling fluidization of Geldart A particles. *Chemical Engineering Science*, 66(18), 4229–4240.
- Wang, L., Wu, C., & Ge, W. (2017). Effect of particle clusters on mass transfer between gas and particles in gas-solid flows. *Powder Technology*, 319, 221–227.
- Wei, F., Lin, H., Cheng, Y., et al. (1998). Profiles of particle velocity and solids fraction in a high-density riser. *Powder Technology*, 100(2–3), 183–189.
- Wen, C. Y. (1966). *Mechanics of fluidization*.
- Wu, K., de Martin, L., & Coppens, M. (2017). Pattern formation in pulsed gas-solid fluidized beds-The role of granular solid mechanics. *Chemical Engineering Journal*, 329, 4–14.
- Wu, K., de Martin, L., Mazzei, L., et al. (2016). Pattern formation in fluidized beds as a tool for model validation: A two-fluid model based study. *Powder Technology*, 295, 35–42.
- Wu, K., Francia, V., & Coppens, M. O. (2019). Dynamic viscoplastic granular flows: A persistent challenge in gas-solid fluidization. *Powder Technology*.
- Wu, Y., Peng, L., Qin, L., et al. (2018). Validation and application of CPFD models in simulating hydrodynamics and reactions in riser reactor with Geldart A particles. *Powder Technology*, 323, 269–283.
- Xie, J., Zhong, W., & Yu, A. (2018). MP-PIC modeling of CFB risers with homogeneous and heterogeneous drag models. *Advanced Powder Technology*, 29(11), 2859–2871.
- Xiong, Q., Li, B., Zhou, G., et al. (2012). Large-scale DNS of gas-solid flows on Mole-8.5. *Chemical Engineering Science*, 71, 422–430.
- Xu, Y., Musser, J., Li, T., et al. (2018). Numerical simulation and experimental study of the gas-solid flow behavior inside a full-loop circulating fluidized bed: Evaluation of different drag models. *Industrial & Engineering Chemistry Research*, 57(2), 740–750.
- Yang, S., Luo, K., Fan, J., et al. (2014). Particle-scale investigation of the solid dispersion and residence properties in a 3D spout-fluid bed. *AIChE Journal*, 60(8), 2788–2804.
- Yang, S., Luo, K., Fan, J., et al. (2014). Particle-scale investigation of the solid dispersion and residence properties in a 3-D spout-fluid bed. *AIChE Journal*, 60(8), 2788–2804.
- Yang, L., Padding, J. T., Buist, K. A., et al. (2017). Three-dimensional fluidized beds with rough spheres: Validation of a two fluid model by magnetic particle tracking and discrete particle simulations. *Chemical Engineering Science*, 174, 238–258.
- Yang, L. L., Padding, J. J., & Kuipers, J. H. (2016). Modification of kinetic theory of granular flow for frictional spheres, part I: Two-fluid model derivation and numerical implementation. *Chemical Engineering Science*, 152, 767–782.
- Yang, L., Padding, J. J., & Kuipers, J. H. (2017). Investigation of collisional parameters for rough spheres in fluidized beds. *Powder Technology*, 316, 256–264.
- Yang, L., Padding, J. T., & Kuipers, J. (2017). Partial slip boundary conditions for collisional granular flows at flat frictional walls. *AIChE Journal*, 63(6), 1853–1871.
- Yang, S., Sun, Y., Zhang, L., et al. (2016). Numerical investigation on the effect of draft plates on spouting stability and gas-solid characteristics in a spout-fluid bed. *Chemical Engineering Science*, 148, 108–125.
- Yang, S., Sun, Y., Zhang, L., et al. (2016). Numerical investigation on the effect of draft plates on spouting stability and gas-solid characteristics in a spout-fluid bed. *Chemical Engineering Science*, 148, 108–125.
- Yang, N., Wang, W., Ge, W., et al. (2003). CFD simulation of concurrent-up gas-solid flow in circulating fluidized beds with structure-dependent drag coefficient. *Chemical Engineering Journal*, 96(1–3), 71–80.
- Yang, N., Wang, W., Ge, W., et al. (2004). Simulation of heterogeneous structure in a circulating fluidized-bed riser by combining the two-fluid model with the EMMS approach. *Industrial & Engineering Chemistry Research*, 43(18), 5548–5561.
- Yin, S., Jin, B., Zhong, W., et al. (2012). Solids holdup of high flux circulating fluidized bed at elevated pressure. *Chemical Engineering & Technology*, 35(5), 904–910.
- Yin, S., Zhong, W., Jin, B., et al. (2014). Modeling on the hydrodynamics of pressurized high-flux circulating fluidized beds (PHFCFBs) by Eulerian-Lagrangian approach. *Powder Technology*, 259, 52–64.
- Zhang, M. H., Chu, K. W., Wei, F., et al. (2008). A CFD-DEM study of the cluster behavior in riser and downer reactors. *Powder Technology*, 184(2), 151–165.
- Zhang, J., Li, T., Ström, H., et al. (2020). Grid-independent Eulerian-Lagrangian approaches for simulations of solid fuel particle combustion. *Chemical engineering journal (Lausanne, Switzerland : 1996)*, 387, Article 123964.
- Zhang, Y., Zhao, Y., Lu, L., et al. (2017). Assessment of polydisperse drag models for the size segregation in a bubbling fluidized bed using discrete particle method. *Chemical Engineering Science*, 160, 106–112.
- Zhao, Y., Ding, T., Zhu, L., et al. (2016). A specular coefficient model and its application to dense particulate flow simulations. *Industrial & Engineering Chemistry Research*, 55(5), 1439–1448.

- Zhao, Y., Lu, B., & Zhong, Y. (2015). Influence of collisional parameters for rough particles on simulation of a gas-fluidized bed using a two-fluid model. *International Journal of Multiphase Flow*, 71, 1–13.
- Zhao, Y., Zhong, Y., He, Y., et al. (2014). Boundary conditions for collisional granular flows of frictional and rotational particles at flat walls. *AIChE Journal*, 60(12), 4065–4075.
- Zhao, B., Zhou, Q., Wang, J., et al. (2015). CFD study of exit effect of high-density CFB risers with EMMS-based two-fluid model. *Chemical Engineering Science*, 134, 477–488.
- Zhou, Q., & Wang, J. (2015). CFD study of mixing and segregation in CFB risers: Extension of EMMS drag model to binary gas-solid flow. *Chemical Engineering Science*, 122, 637–651.
- Zhou, G., Xiong, Q., Wang, L., et al. (2014). Structure-dependent drag in gas-solid flows studied with direct numerical simulation. *Chemical Engineering Science*, 116, 9–22.
- Zhou, J. H., Yu, A. B., & Horio, M. (2008). Finite element modeling of the transient heat conduction between colliding particles. *Chemical Engineering Journal*, 139(3), 510–516.
- Zhu, L., Liu, Y., & Luo, Z. (2018). An effective three-marker drag model via sub-grid modeling for turbulent fluidization. *Chemical Engineering Science*, 192, 759–773.
- Zhu, G., Zhao, Y., Wang, Z., et al. (2022). Semi-resolved CFD-DEM simulation of fine particle migration with heat transfer in heterogeneous porous media. *International Journal of Heat and Mass Transfer*, 197, Article 123349.
- Zhu, H. P., Zhou, Z. Y., Yang, R. Y., et al. (2007). Discrete particle simulation of particulate systems: Theoretical developments. *Chemical Engineering Science*, 62(13), 3378–3396.
- Zhu, H. P., Zhou, Z. Y., Yang, R. Y., et al. (2008). Discrete particle simulation of particulate systems: A review of major applications and findings. *Chemical Engineering Science*, 63(23), 5728–5770.
- Zimmermann, S., & Taghipour, F. (2005). CFD modeling of the hydrodynamics and reaction kinetics of FCC fluidized-bed reactors. *Industrial & Engineering Chemistry Research*, 44(26), 9818–9827.